UNIVERSITÀ DEGLI STUDI DI PADOVA

DIPARTIMENTO DI INGEGNERIA INDUSTRIALE

CORSO DI LAUREA MAGISTRALE

IN INGEGNERIA CHIMICA E DEI PROCESSI INDUSTRIALI

Tesi di Laurea Magistrale
in Ingegneria Chimica e dei Processi Industriali

HYDROGEN PRODUCTION VIA AMMONIA DECOMPOSITION IN MEMBRANE REACTOR: A KINETIC STUDY AND AN EXPERIMENTAL INVESTIGATION ON Pd-BASED MEMBRANE

Relatrice: Prof. Martina Roso
Correlatori: Prof. Fausto Gallucci, Ing. Valentina Cechetto

Laureando: LEONARDO PASE

ANNO ACCADEMICO 2021 - 2022

Abstract

Ammonia represents the more valuable chemicals able to transport hydrogen through its chemical bonds, and hence to provide a chemical storage for energy. However, the ammonia decomposition is presently the bottleneck of the process. A possible solution is to exploit catalytic membrane reactor, which enables process intensification and higher energy efficiency.

The specific issue indagated in this Thesis, collocated within the European project *Arenha*, is to improve the performance of the reactor configuration. A kinetic study on Ru/γ-Al_2O_3 (2 wt%) catalyst has been performed in a packed bed reactor in the range of 400-500°C and 1-4.5 bar. The reaction has proof to follow Temkin's kinetic, where k_0 = 23305.41 mol·Pa^{β}/min/g_{CAT}, E_{att} = 80.7324 kJ/mol, β = 0.2206 with a R^2 coefficient 0.94. A catalyst dilution with inert γ-Al_2O_3 has been carried out in lab-scale membrane reactor keeping constant the membrane area covered by the packed bed. A catalyst excess has been demonstrated for high temperature (475°C), but a fine tuning is still missing to minimize the cost associated at the future development of this technology. Further the Pd-based membrane *Arenha-5* used has showed improvements respect the previous prototypes, reaching a hydrogen recovery of 94.90% at 475°C and 5 bar, independent on the catalyst concentration and inlet reactant flowrate studied.

Riassunto esteso

Lo sviluppo delle infrastrutture per sfruttare a pieno il potenziale delle energie rinnovabili ha un ruolo fondamentale nella lotta contro i cambiamenti climatici. In questo campo, lo stoccaggio di gradi quantità di energia risulta essere un aspetto cruciale per compensare l'intermittenza e la stagionalità di molte fonti rinnovabili. Una possibile soluzione è lo stoccaggio chimico, dove l'elettricità viene utilizzata per la sintesi di specie chimiche che fungono da carrier di energia. In particolare, l'idrogeno rappresenta una possibile alternativa ai combustibili fossili perché il suo utilizzo nelle celle combustibili permette una conversione efficace in elettricità senza l'emissione di gas ad effetto serra. La sua volatilità e bassa densità energetica per volume rendono il traporto e lo stoccaggio delle fasi critiche. Questo ha motivato lo studio per la produzione di idrogeno on-site attraverso l'uso di carrier energetici, tra cui l'ammoniaca. La sua decomposizione on-site rappresenta la fase critica di questo processo a causa delle alte temperature (maggiori di 500°C) e della difficoltà di eliminare le tracce di ammoniaca che risultano incompatibili con l'utilizzo nelle celle a combustibili. Per questo motivo è stato proposto l'utilizzo di reattori a membrana che permettono di intensificare il processo e di abbassare le temperature di esercizio.

Questa Tesi si è sviluppata all'interno del progetto europeo *Arenha* con lo scopo di migliorare la fattibilità della decomposizione di ammoniaca in reattore a membrana. In particolare, il focus riguarda l'utilizzo del catalizzatore a base di rutenio, scelto in quanto risulta essere il più cataliticamente attivo per la decomposizione dell'ammoniaca sebbene il suo elevato costo.

Un approccio sperimentale è stato preferito alla simulazione numerica del sistema, ma il punto di partenza non è cambiato: uno studio cinetico sul catalizzatore a base di rutenio (2 wt%) depositato su pellet di γ-Al_2O_3 è stato performato in un reattore a letto impaccato. Le condizioni investigate rispecchiano quelle utilizzate nel reattore a membrana: temperatura nel range tra 400 e 500°C, pressione tra 1 e 4.5 bar, tempo di residenza, presenza di azoto e idrogeno in alimentazione. Appropriati test in laboratorio hanno escluso la presenza di limitazioni dovute al trasporto di massa tra gas e solido e all'interno del solido stesso. Tramite i risultati sperimentali si è confermato che il catalizzatore segue la cinetica descritta dal modello di Temkin, nel quale alte pressioni e la presenza di idrogeno inibiscono la reazione. I parametri cinetici ottenuti tramite il fitting di 39 test con il software *Matlab 2021b*, hanno dato come risultati: k_0=23305.41 mol·Pa^{β}/min/g_{CAT}, E_{att} = 80.7324 kJ/mol, β = 0.2206 con un coefficiente di correlazione del 94%.

L'analisi del reattore a membrana è stata condotta prima analizzando separatamente membrana e reattore impaccato, e solo poi il sistema nel suo complesso. Per quanto riguarda la membrana, codificata come *Arenha-5*, si è determinata la permeazione (2.18e-6 mol/m^2/s/$Pa^{0.5}$) e la perm-selettiva (1.03e5) attraverso test a gas singoli (idrogeno e azoto), i quali hanno registrato dei progressi rispetto ai precedenti prototipi all'interno del progetto.

Nel reattore a letto impaccato i pellet di catalizzatore sono stati utilizzati per evitar perdite di pressione. La conversione di ammoniaca è stata investigata comparando i risultati sperimentali con un modello sviluppato utilizzando la cinetica precedentemente determinata e senza tenere in

considerazioni limitazioni di trasferimento di massa. Una forte diminuzione delle performance del catalizzatore si sono registrate analizzando un letto composto da 125 g di catalizzatore, indice di forti limitazioni nel trasferimento di massa.

Infine più test di reazione sono stati eseguiti con il reattore a membrana. La sequenza di analisi ha previsto la diminuzione della quantità di catalizzatore nei diversi esperimenti tramite diluzione con pellet di γ-Al_2O_3 per mantenere la superficie attiva della membrana totalmente circondata dal letto catalitico. I dati riguardanti la conversione di ammoniaca e il recupero di idrogeno nel permeato hanno confermato la presenza di un eccesso di catalizzatore nel reattore: questi indici di performance sono rimasti invariati diminuendo da 250 g a 62.5 g la quantità di catalizzatore presente nel letto impaccato lavorando alla temperatura di 475°C. Inoltre la presenza dell'inerte ha permesso un miglior controllo termico all'interno del sistema, dato che si tratta di una reazione endotermica.

Il reattore a membrana investigato ha evidenziato un miglioramento rispetto agli altri prototipi di laboratorio in termini di recupero di idrogeno nel permeato pari al 94.90% con una conversione intorno al 98% a 475°C e 5 bar di pressione nel retentato, indipendentemente dalla portata in entrata di ammoniaca investigata. Infatti, la quantità di catalizzatore presente nel reattore risulta ancora in eccesso e un ulteriore diluzione è possibile.

Per la ricerca delle condizioni ottimali di reazione nel reattore a membrana studiato, lo sviluppo di un modello che descrivi il sistema risulta necessario. Con i dati raccolti in laboratorio sarà possibile validare il modello e ottenere così ulteriori miglioramenti nell'utilizzo del catalizzatore. I fenomeni più rilevanti da modellare sono le limitazioni al trasferimento di massa sia all'interno del catalizzatore poroso che all'esterno, il modello di flusso e la presenza di inerte nel letto. Sia la cinetica di reazione che le caratteristiche della membrana sono state già ricavate durante questo lavoro.

Table of Contents

Introduction

In the current context of global momentum in favour of renewable energy, higher storage capacities are required to provide a portfolio of grid services for the decarbonization of industrial and transport sectors. For this purpose, hydrogen produced through water electrolysis exploiting clean energy is a key pathway to unlock the full potential of renewables and to resolve the problem of the relating seasonal storage of large quantities. Indeed, hydrogen can provide high efficiency for energy conversion when employed as feedstock in fuel cells with the only emission of water as by-product.

However, hydrogen is the lightest element in nature, hence large volumes of this gas are necessary to meet identical energy demand compared with oil-based fuels. A solution to the hydrogen storage problem is the conversion into a liquid chemical: ammonia represents the best candidate as carbon-free and dispatchable hydrogen carrier.

Nevertheless, the use of ammonia has so far been limited by the high temperatures (larger than 500°C) required in its decomposition carried out in conventional packed bed reactor and by the additional separation system to reach the tight hydrogen purity (0.1 ppm of NH_3). A possible solution to overcome these problems is represented by the catalytic membrane reactor, which is expected to simultaneously perform ammonia decomposition and high-purity H_2 separation within the same integrated unit. The reaction temperature required is thus lowered (increase of efficiency), while the downstream separation is not required (decrease of capital costs).

This work aims to make a step forward toward the feasibility of ammonia decomposition carried out in membrane reactor decreasing the capital costs linked to the catalyst. The starting point are the achievements reached within the European project *Arenha*, where the reactor design is based on the use of a Pd-based membrane surrounded by 250 g of catalyst pellet made of 2 wt% ruthenium deposited on γ-Al_2O_3. Analysing the previous data collected, it has been discovered that the reaction performances are slightly influenced by both the temperature and the inlet flowrate. This observation leads to the central idea of this work: the presence of a catalyst overload in the reaction system.

The aim of the study is to demonstrate the feasibility of a catalyst reduction by means of a dilution with inert pellets inside a lab-scale membrane reactor.

The Thesis is structured in 5 chapters.

In Chapter 1 the background of ammonia as energy carrier has been described with the focus on the final step of H_2 recovering through the dehydrogenation reaction carried out in packed bed membrane reactor. The main information about ammonia decomposition thermodynamic and kinetics, the state-of-the-art of the metallic membranes have been provided.

In Chapter 2 the technical choices followed to carry out the kinetic study with the available set-up at the Technical University of Eindhoven have been explained together with a catalyst and

inert characterization.

In Chapter 3 the kinetic study results have been showed up: the kinetic has been individualized between the main ones adopted in literature for ammonia decomposition proposed by Temkin and Tamaru. The kinetic description of the Ru-based catalyst has been used as starting point to preliminary estimate the catalyst quantity to adopt in in the packed bed membrane reactor.

Then in Chapters 4 and 5 the focus has shifted on the packed bed membrane reactor, in which a catalyst excess aims to be demonstrated. The work has been approached through an experimental way rather than a modelling one.

Chapter 4 contains the methodologies applied in laboratory: preliminary the Pd-based membrane and a simple packed bed reactor have been studied, only later the packed bed membrane reactor. The last one is built up with different catalyst concentrations in the packed bed, which kept in any case constant the total mass of solid balancing with an inert (γ-Al_2O_3) in order to ensure the total coverage of membrane area.

Chapter 5 contains a discussion supported by the collected data about the possible impacts of mass transfer limitations and catalyst dilution in packed bed membrane reactor.

Chapter 1

Background

An overview of the field in which this work is focus is given in this chapter. Starting from the concept of hydrogen economy, the description of how ammonia can be exploited as energy carrier follows. The key challenges of ammonia decomposition, subsequent separation and purification are investigated focusing on the solutions proposed in this work to make the process reliable, energy-efficient, and scalable at commercial level.

1.1 Prospect and challenges of hydrogen

Mitigating climate change is one of the most critical challenges that nowadays facing our society.

In this context, the United Nations Climate Change Conference of Parties has established four primary goals to prevent catastrophic consequences on the Earth (COP26 Goals - UN Climate Change Conference Glasgow, 2021):

- secure global net zero greenhouse emission by mid-century and keep global warming at 1.5°C within reach though the acceleration of coal phase-out, the curtail of deforestation, the speeding up of switch to electric vehicles and encouraging investment in renewables.
- protect communities and natural habitats since the climate is already changing.
- as regards developed countries, make good on their promise to mobilise $100bn USD/year in climate finance.
- team working as the way to address the big challenges of climate crisis.

Gaies et al. (2022) state the condition to meet the first goal: halve the emission of CO_2 by the end of 2050, meanwhile the population growth and projected economy will require to deliver roughly twice as much energy as today. An unprecedented undertaking thinking that nowadays fossil fuels are the main energy sources and energy carriers in the word (Rosen and Koohi-Fayegh, 2016). Indeed, the energy production is more than 80% based on fossil fuel and no progress has been made in the last decade since around 85% of the global energy used increment has been still fossil-based.

Renewable energies will play an important role in reducing these emissions and addressing the transition towards a decarbonized society. However, all the foreseeable future energy sources (falling water, solar radiation, wind, uranium, etc.) cannot act as energy carriers for the provision of end-use services: indeed, they are capable to producing, for the most part, just one energy carrier: electricity (Rahman et al., 2012). The world's societies cannot operate

effectively with energy provided only in the form of electricity, as they need also chemical fuels and feedstocks (Rosen and Koohi-Fayegh, 2016).
Moreover, the inherent intermittency and stochastic fluctuation problems of renewables are challenges to overcome for cover the mismatch between energy supply and energy demand. In this field, energy storage is a crucial aspect: batteries may not be the best solution due to cost, safety, and environmental issues, while pumped-storage hydroelectricity and compressed energy storage suffer from geological constraints for their deployment.
A suitable solution is the use of chemical energy carriers through the so-called "Power-to-X" technologies: they guarantee flexibility and large quantities storage over long time and in any location. As the name implies, the concept evolves around converting power (electricity) to chemicals (X), which could be very diversified hence the utilization of the "X": examples are power-to-CH_4, power-to-Chemicals (methanol, formic acid, formaldehyde), power-to-liquid (Alkanes, diesel, jet-fuel).
Hydrogen represents the ideal energy carrier: it can be stored and transported, and it can be used as a carbon-free fuel or converted to electricity in such a device as fuel cells.
There are many reasons why hydrogen is a logical and appropriate choice as a chemical fuel to replace fossil fuels (Rosen and Koohi-Fayegh, 2016):

- it represents a complementary carrier to electricity; both are necessary to satisfy the entire range of energy demand.
- it is a clean alternative, since water is the only product generated to produce energy.
- it can be stored in a large quantity , unlike electricity, and in a variety of forms depending on the applications.
- it can be transported in road, rail, ship or through pipelines with losses significantly lower than those associated with high-voltage electrical lines.

This molecule is not available in pure state in the environment and required to be synthesized. The main pathway currently employed at industrial scale for hydrogen production is catalytic steam methane reforming; however, since it represents a carbon intensive process, electrolysis of water exploiting sustainable electricity may be regarded in the future as a green alternative.
Moreover, hydrogen has also some undesirable characteristics derived from the fact that it is a gas: it requires severe conditions to condensate, and its density is low. So, despite a high energy density by mass with a lower heating value of 119.7 MJ/kg at 25°C and 1 bar (more than two times higher than the methane one), when dealing with volume it decreases to 8.96 GJ/m^3 referred as hydrogen in liquid state (Lucentini et al., 2021).
Moreover, the process of storing H_2 is inherently inefficient and challenging: nowadays it is commonly stored at room temperature as compressed gas (about 700 bar), but it can be stored also as a liquid at higher volumetric density (-253°C and 1 bar) or by cryo-compression that apply conditions in between the previous ones.

There are others two problems of secondary importance when dealing with hydrogen: the first one being related to safety during handling and the second one to the fact that action needs to be taken against the metal's embrittled occurring in the storage vessels or pipelines. In regard to the former problem, many studies demonstrate that the dangers of hydrogen do not seem worse than those of gasoline, natural gas, or any other fuel, but are merely different (Rosen and Koohi-Fayegh, 2016).

1.2 Ammonia as possible energy carrier

In this H_2-based energy paradigm shift, the storage and transportation of hydrogen play a very important role in the overall supply chain. To overcome these challenges chemical storage is proposed as an alternative. Specifically, the most promising alternatives are hydrogen absorption/desorption on solid materials and hydrogen storage in the chemical bonds of liquid H_2 carriers (Byun et al., 2022).
The former alternative requires a solid with a large surface area and adequate pore size such as carbon nanotubes, structures based on metal-organic frameworks or metal hydrides. In any case H_2 absorption/desorption on solids has limited practical applications since it leads to an increase in transportation weight and the regeneration cycles are still limited (Byun et al., 2022).
The second option of the chemical storage involves an exothermic hydrogenation reaction in which an H_2-rich compound is synthetized. That species is supposed to be easily transported in liquid phase and on-site H_2 is released through an endothermic dehydrogenation reaction. Different options are compared in Figure 1.1 respect their volumetric energy density, a fundamental property to discriminate the more convenient chemical carrier. NH_3 has an energy density about 3.5 kWh/l, which is less than but comparable with other hydrocarbons.
Moreover, it can be utilised directly as a fuel in gas turbine or engine, exploiting its high-octane number, even if the technology is still in the prototype stage (Lucentini et al., 2021).
Summarizing, ammonia has been recognized as a promising alternative hydrogen provider given the following advantages (Sun et al., 2022):

- high hydrogen content (17.8% by weight) and a volumetric density of 121 kg H_2/m^3 at 10 bar.
- no CO_x by-products from ammonia decomposition, which both eliminate the polluted aspect of energy production and it is also beneficial for the following steps of separation and purification.
- readily transport since NH_3 is easily liquefied both at atmospheric pressure and -33°C or at ambient temperature and 10 bar.
- high selectivity since the only product are H_2 and stoichiometric N_2, different from the other liquid hydrogen carrier.

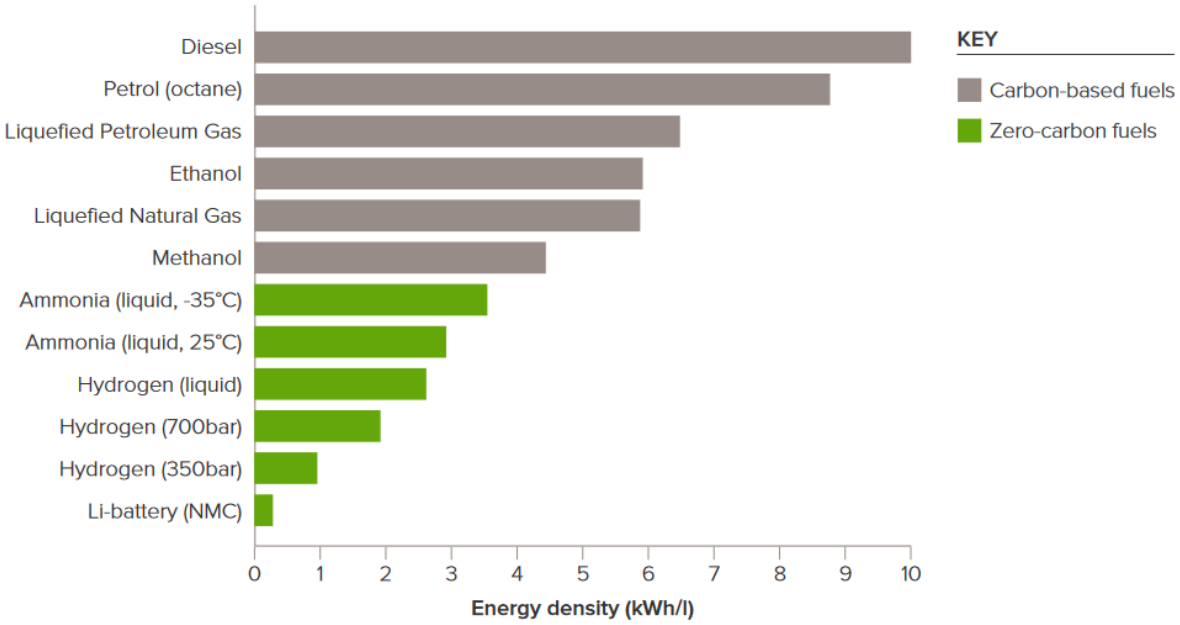

Figure 1.1. *Volumetric energy density of a range of fuel options.*

Ammonia is the second more widely produced chemical with a world's production of 150 Mt/year and an installed capacity soon reaching 250 Mt/year. The market of reference is the fertilizer manufacturing, which cover 88% of ammonia produced (Lamb et al., 2019a).

Almost all the ammonia is produced by the so-called Haber-Bosch process, which used Fe-based catalysts with promoters, temperature around 400-600°C and pressure between 100-400 bar. Ammonia synthesis is one of the most energy efficient processes implemented in industry: the production nowadays reaches an efficiency of about 70% (7.9 MWh to produce 5.6 MWh of chemical energy) (Lamb et al., 2019a).

Nevertheless, ammonia production consumes about 2% of the world's energy supply and it releases more than 400 Mt CO_2 for year, the equivalent of 1.6% of total global emissions (Green ammonia | Royal Society). The greatest contribution to the total cost of the process is given by the raw materials: both H_2 and N_2 are produced using almost exclusively energy from fossil fuels. Therefore, several attempts have been made to decarbonize the process through the concept of "blue ammonia" production using carbon capture systems, and "green ammonia" using hydrogen produced from electrolysis of water fed with sustainable electricity, instead of steam reforming. However, Haber-Bosh process is still the more convenient option nowadays (Schüth et al., 2012).

1.3 State-of-the-art of NH_3 infrastructure

The steps to produce hydrogen from ammonia are in order: ammonia storage and transport, decomposition, separation and purification and final hydrogen use (Lamb et al., 2019b).

In regard to storage and transportation, they are well developed at different scales. Ammonia can in fact be shipped in trucks, railroad cars, ships, and pipelines. Storage is possible under

pressure for smaller scale, while large scale is mostly done in cryo-vessels. Adapting such infrastructure to even larger scale seems feasible; instead for small scale mobile applications, the solid-state storage in metal ammines would probably be used (Schüth et al., 2012).
The ammonia decomposition and hydrogen purification steps are on the other hand less developed at commercial scale and more challenging. A major portion of energy cost, indeed, is derived from the recovery of H_2 mainly due to the need of high temperatures to reach conversion close to 100%, and further energy input is required to maintain the reaction conditions due to the intrinsic endothermicity of the reaction (Sun et al., 2022). As these two steps are the bottleneck of the ammonia-to-hydrogen process, this work focuses on these arguments, which are treated more precisely in §1.5 and §1.6.
The use of H_2 is mainly addressed to proton-exchange membrane fuel cell (PEMFCs), where it acts as a fuel to produce electricity (Rosen and Koohi-Fayegh, 2016). A fuel cell is an energy conversion device that continually converts the chemical energy of a fuel into electricity, as long as the fuel and the oxidant are available. It exhibits advantageous characteristics exceeding conventional combustion-based technologies for a higher efficiency combined with lower emissions; water is the only product of the power generation process in hydrogen fuel cells.
PEMFC works at low temperature (70-80°C) with platinum as catalyst in both anode and cathode, where respectively hydrogen oxidation and oxygen reduction take place. The distinctive advantages of rapid start-up time, wild operative temperatures (from -40°C to 90°C) and high specific energy have made PEMFCs stand out from all the other types of fuel cell. This device can be wildly used both in vehicles and stationary applications (Fan et al., 2021).
However, there is a restricted requirement of reactant quality for hydrogen, while oxygen can be taken directly from air. Indeed, the presence of NH_3 in the hydrogen feed is detrimental for the device's life. Ammonia is a poison for the catalyst and moreover it damages the protonic membrane. The composition requirements for fuel cells are set out by the International Organization for Standardization (ISO). For road vehicles the hydrogen quality is regulated by ISO14687-2:2012 at 99.97% v/v, so the maximum concentration of impurities is 300 μmol/mol: for N_2 the limit is the maximum, while for NH_3 the limit is more severe, namely 0.1 μmol/mol. Instead, ISO14687-3:2012 regulates the stationary appliances of fuel cells and it states the fuel quality at the boundary point between the storage and supply at a minimum concentration of 50% mol, with the NH_3 tolerance as before. The standards have been reviewed due to the remarkable progress of the technology; however ISO14687:2019 does not modify the points of our interest (ISO - Standards).
As direct consequences the steps of ammonia decomposition and purification become more critical: for sure the closer to 100% conversion is, the less effort in separation is required. However, traces of ammonia are inevitable present, so an efficient separation step seems mandatory.

1.4 Ammonia decomposition

An initial analysis on the reaction thermodynamic is performed to quantify heat effects in the reacting system and enable the calculation of the equilibrium conversion. The more probable reaction mechanisms are then described in detail, and finally the catalyst formulations that have obtained better results in literature are reported.

1.4.1 Reaction thermodynamics

The decomposition of ammonia (Eqn. 1.1) is the reverse reaction of ammonia synthesis:

$$2\,NH_3 \leftrightarrows 3\,H_2 + N_2 \qquad \Delta H^0_{f,298K} = 46.19\ kJ/mol_{NH_3}\,. \qquad (1.1)$$

The reaction is mildly endothermic and proceeds with an increase in number of moles, suggesting that the process is thermodynamically enhanced by high temperatures and low pressures.

The reaction can be carried out in presence of a catalyst (catalytic cracking) or without a catalyst (thermal decomposition), but its presence is advisable as it allows for a decrease of the operative temperature, with consequent reduction of energy cost.

Taking in consideration the future practical applications, such catalyst is going to operate mainly with pure ammonia or in a mixture with other inert gasses, so no side reactions will occur leading to a selectivity of 100%. Further consequence is an easier reactor design and control(Sun et al., 2022).

Thermodynamic equilibrium calculations have been performed using NASA software to provide an idea of the theoretically obtainable conversion: as calculated in Table 1.1 and in agree with Sun et al. (2022), the equilibrium conversion overcomes 99.5% at 400°C and ambient pressure considering an inlet flow composed only of ammonia.

Table 1.6.1.1. *Trend of equilibrium conversion as function of temperature and pressure calculated with NASA software.*

P	T	200°C	250°C	350°C	400°C	450°C	500°C	550°C
1 bar	$\mathbf{X_{NH3}}$ **[%]**	85.23%	94.58%	99.09%	99.57%	99.77%	99.87%	99.92%
3 bar		70.06%	86.43%	97.37%	98.72%	99.32%	99.62%	99.77%
5 bar		61.52%	80.42%	95.77%	97.90%	98.88%	99.36%	99.62%

However, current ammonia decomposition reaction needs to operate at higher temperature due to exclusively kinetic limitations, since thermodynamics is not more a constrain as shown above 400°C. For example, industrial applications in annealing metals and galvanization are adopting temperatures around 800°C (Lucentini et al., 2021), while in the research field of hydrogen

economy, temperature higher than 500°C is applied with the most active catalyst (Guo & Chen, 2017).

The reaction applications place the highest demand on the catalyst activity, since high temperatures are very unfeasible for on-board hydrogen generation in cars, and even for stationary decomposition units, for instance in hydrogen fuelling stations.

1.4.2 Reaction kinetics

As proposed by Temkin (Lucentini et al., 2021), the mechanism considered for ammonia decomposition occurs following the opposite steps of ammonia synthesis (Eqn. 1.2-1.7): it starts with the adsorption of ammonia on the catalyst surface active sites, followed by three subsequent dehydrogenation steps, then nitrogen and hydrogen atoms desorb as their corresponding molecules leaving free the catalyst active sites.

$$NH_{3(g)} + s \leftrightarrows NH_{3(a)}, \tag{1.2}$$

$$NH_{3(a)} + s \leftrightarrows NH_{2(a)} + H_{(a)}, \tag{1.3}$$

$$NH_{2(a)} + s \leftrightarrows NH_{(a)} + H_{(a)}, \tag{1.4}$$

$$NH_{(a)} + s \leftrightarrows N_{(a)} + H_{(a)}, \tag{1.5}$$

$$2N_{(a)} \leftrightarrows N_2 + 2s, \tag{1.6}$$

$$2H_{(a)} \leftrightarrows H_2 + 2s, \tag{1.7}$$

where s represents a free active site on catalyst surface, while the subscriptions (a) and (g) refer to species adsorbed on the solid phase and free in gaseous phase.

The modus operandi to study the kinetics and to understand the reaction mechanism during the years has been the quasi-equilibrium approach: testing different kinetic expressions obtained by alternatively assuming each elementary step of the reaction as the rate limiting one, while considering all the other steps in equilibrium.

Historically the first analyses on the different catalysts tested were based on the assumption that the recombinative desorption of nitrogen (Eqn. 1.6) is the slowest step between the elementary reaction's chain. The proposal was based on the knowledge about the reverse reaction, the ammonia synthesis, where the limiting step is the cleavage of the N-N bond of nitrogen molecule.

Actually, the decomposition kinetic depends not only on the composition of the catalyst, but on many other factors such as the catalyst synthesis method (architecture of the active sites, support-type, etc.), the active metal content and the reaction conditions (temperature, pressure, gas composition). Indeed, varying the conditions in which the reaction is taking place, the applicable kinetic model might change because the rate determining step on which the reaction mechanism is based on changes (Lucentini et al., 2021).

Tamaru (1988) has been observed that at moderate low temperatures the decomposition reaction rate depends on the hydrogen partial pressure, and a transition from one kinetic regime to another is present.

At lower temperature and higher hydrogen partial pressure, the model of Temkin-Pyzhev is the more probable to describe the kinetic of ammonia decomposition (Eqn. 1.8)(Gobina et al., 1995):

$$-r_{NH3} = k_0 \cdot exp\left(\frac{-E_{att}}{R \cdot T}\right) \cdot \left[\left(\frac{P_{NH3}^2}{P_{H2}^3}\right)^{1-\beta} - \frac{P_{N2}}{{K_{eq}}^2} \cdot \left(\frac{P_{H2}^3}{P_{NH3}^2}\right)^{\beta}\right], \quad (1.8)$$

where P_{NH3}, P_{H2}, P_{N2} are the chemical species partial pressures (Pa), k_0 the pre-exponential factor (mol·Pa$^{\beta}$/m^3/s), E_{att} the activation energy (J/mol), β a dimensionless model parameter, $-r_{NH3}$ the ammonia reaction rate (mol/ m^3/s). The first term between the brackets is the rate of ammonia decomposition, while the contribution of ammonia synthesis by re-hydrogenation is in the second term. The kinetic constant is of the Arrhenius-type as explicitly reported in Eqn. 1.8, while β can assume a value between 0 and 1. As regard the equilibrium constant K_{eq} used, it is reported in Eqn. 1.9 as function of temperature T (K) (Gobina et al., 1995).

$$\log\frac{1}{K_{eq}} = \frac{2250.322}{T} - 0.8534 - 1.51049\log(T) - 25.8987e^{-5} \cdot T + 14.89615e^{-8} \cdot T^2. \quad (1.9)$$

Temkin's kinetic expression is very interesting: the rate of forward reaction is strongly retarded by hydrogen, which is one of the reaction products. According to the Temkin-Pyzhev mechanism, Eqn. 1.8 considers that the associative desorption of nitrogen is the rate-limiting step, and that if the influence of the inverse reaction can be neglected the reaction rate is expressed as a power law. Di Carlo et al. (2014), Prasad et al. (2009b), Zheng W. et al. (2007) investigated a Ru-based catalyst like the one used in this work, obtaining a good fitting of the Temkin-Pyzhev mechanism with their experimental data.

At high temperature and low hydrogen pressure, instead, Tamaru model described by Eqn. 1.10 gives a reasonable representation of the experimental data. In chemical engineering Eqn. 1.10 is usually interpreted with the Haugen-Watson theory, in enzyme kinetics with the Michaelis-Menten theory, and in physical chemistry with the Langmuir-Hinshelwood theory. In all these cases, it is assumed that the reactant is being chemisorbed by the catalyst and that the reaction rate is proportional to the amount of reactant adsorbed on it. However, Tamaru (1988) derives this expression investigating tungsten, molybdenum, iron, and platinum at higher temperature by a dynamic balance mechanism between the supply and desorption of chemisorbed nitrogen. In this way, he switched from a black-box approach based on conjectures to a dynamic approach, through the examination of the behaviour of nitrogen chemisorbed directly under the reaction conditions.

$$-r_{NH3} = \frac{k_{Tam} \cdot P_{NH3}}{(1 + K_{Tam} \cdot P_{NH3})}, \quad (1.10)$$

wherek_{Tam} is the kinetic constant and K_{Tam} (Pa^{-1}) is the adsorption constant.
The rate of reaction is a function only of P_{NH3}, namely it become zero order as regard P_{H2}.
The temperature at which the switch from Temkin-Pyzhev kinetic to Tamaru kinetic regime happens is described by Tamaru (1988) as a function of the desorption rates of ammonia and nitrogen from the catalyst surface and the partial pressure of hydrogen. Both the previous reaction rates are strongly dependent on the type of catalyst that is used: for example, dealing with tungsten the switch starts at around 1200 K, while with iron Tamaru kinetic is observed between 600 K and 1250 K at very low ammonia partial pressure(Lucentini et al., 2021).
The reason for which the transition temperature is dependent on the desorption rates is related to the kinetic limiting factor: when ammonia adsorbs dissociatively to the surface of the catalyst it can either re-hydrogenated back to ammonia, or the nitrogen atoms combine and desorb as nitrogen, thus successfully decomposing ammonia (Tsai et al., 1985).
According to Temkin-Pyzhev mechanism, the nitrogen chemisorbed from ammonia mostly goes back to ammonia before it desorbs to form nitrogen molecules. However, at high temperatures, Tamaru kinetic prevails, namely the re-hydrogenation of ammonia is slower and the desorption of nitrogen is faster.
In such a manner, ammonia decomposition on metals generally proceeds between the two limiting cases. This reaction kinetic behaviour is supported by different impact of hydrogen inhibition and change of activation energy with temperature observed during experimental tests (Tamaru, 1988).

1.4.3 Catalyst choice

A key role for the development of hydrogen production from ammonia is taken by the catalyst: it has to be designed to lower the reaction temperature and so reducing the energy cost, as well as improve the process safety. Although elevating the temperature can speed up the generation of hydrogen, it will dramatically increase energy consumption so the most attractive approach is to lower the activation energy by a rational catalyst design.
The catalyst should satisfy the following requirements: high activity at temperature below 600°C, long term stability or good recyclability and finally it should be as cheap as possible.
Supported metal-based system are the mostly adopted in ammonia decomposition and they are generally composed of active metal (single metal, bi-metal or their compounds), support (carbon-based or metal oxides) and sometimes promoter (Sun et al., 2022).
Historically the research has started assuming the principle of micro reversibility in heterogeneous catalyst, and so the first tested metals were the same used in Haber-Bosh process for the synthesis of ammonia, namely ruthenium and iron. Afterwards, other possible active metals have been studied like Cu, Ni, Ir, Mo, Pt, Pd, Pt. Nowadays, ammonia decomposition

has a niche application on metallurgical industry to create a protective and reducing atmosphere composed indeed of H_2 and N_2; the process relies on Ni supported on alumina catalyst, since it is required for these processes of heat treatment to be cheap and have sufficiently high activity (Schüth et al., 2012).

Despite all the different idea about kinetics and reaction mechanisms found in literature due to the catalyst-specific system taken in consideration, a complete agreement is present for which is the most active phase in ammonia decomposition: ruthenium (Lamb et al., 2019b). Indeed, Ru-based catalysts are the focus of much research and likely closest to be commercialized. However, Ru is a noble metal, rare in nature and consequently a quite expensive element. To have an idea about the scarce presence of this metal, its production is now estimated to be 30 tonnes/years (Fang et al., 2022). Moreover, the market price of this metal has been quite volatile in the past 10 years, until reaching $18500 USD/kg in 2021. In addition to the price, within the framework of environmental sustainability, it should be taken in consideration also the possible impact of the catalyst used, such as the energy demand of its extraction and refining.

Although more than 95% of Ru may be recovered from the catalyst, nowadays the feasibility of large scale application is still under investigation and a lot of effort is spent on investigating alternatives and optimizing catalyst's formulation (Schüth, et al. 2012). In the last case, it is involved the modification of the primary component, as well as the choice of support and of the promoter to increase activity, namely the number of active sites.

As regard support materials, it seems that the most active are electronically conductive and with basic surface groups. An optimum candidate are the carbon nanotubes (CNTs), which have already showed the highest performance, although due to the purity required and correlated cost it seems not a viable way toward the commercialization opportunities. There is more interest in developing high surface area and cheaper supports, like templated SiO_2, porous Al_2O_3 and mesoporous carbon (Lamb et al., 2019b). Indeed, another interest point is the stability: the catalyst may be active "enough", while being stable for a long period to reduce the maintenance costs in a future commercial vision of ammonia decomposition.

1.5 Hydrogen separation and purification

Hydrogen produced from ammonia decomposition needs further separation and purification to meet the standards of practical applications described in §1.4. To date, there are mainly four available methods: absorption, cryogenic distillation, membrane separation and pressure-swing-adsorption (Sun et al., 2022).

Absorption is a well-established technology for gas-phase removal of small concentration of ammonia, where the gas can be reacted by passing through liquids or solid-packed beds. Ammonia is easily dissolved in water, and the solubility can be further improved by adding acid. For example, phosphoric acid (H_3PO_4) has been adopted with a capacity up to 57% wt. As for solid materials, the alkali-chloride salts like $MgCl_2$ e $CaCl_2$ can react with ammonia to

form a metal-NH_3-chloride compounds. Silica in various forms (beads, gels, molecular sieves) can also adsorb ammonia depending on acidity, water content and surface area. A major advantage of these absorbents is that they can be regenerated through elevating the temperature, meanwhile ammonia is retrieved. On the other side, absorption cannot remove N_2 or unreacted contaminants, which limits its application for vehicle use (Lamb et al., 2019a).
Cryogenic distillation is not a valid alternative even for large-scale applications, since it doesn't fulfil the hydrogen purity levels and moreover it requires complex equipment and high costs not compatible with the vision of a sustainable economy.
Membrane separation technology is recently emerging as an energy efficient approach to generate ultrapure hydrogen. Further advantages related to this technology, explained in detail in §1.7, are the flexibility in operation, the compactness, the low operating cost, and the easy integration with established industrial process.
Pressure swing adsorption (PSA) has become a mature technique for the efficient separation and deep purification of the gas mixture under investigation, demonstrating to be capable of filtering out impurities even at ppm level hence to generate H_2 at concentration higher than 99.999%. PSA can be used both for industrial scales and small portable systems with quite a flexibility on the material choice (activated carbon, zeolites, silica compounds). The PSA process is based on the capacity of these materials to adsorb more NH_3 impurities at high pressure respect to the lower one. The main associated problem is that being a batch process, multiple units are necessary to ensure a continuous supply. For the distributed and on-demand H_2 production from stored NH_3 the cost of multiple units together with the energy input associated to the pressure cycles are likely to classify PSA as economically unfeasible (Sun et al., 2022).

1.6 Membrane separation technology

Membranes are basically barriers that selectivity allow the flow of one or more components of an inlet feed mixture. The stream containing the components that permeate through the membrane is called permeate, and the stream containing the retained components is called retentate. Membranes for hydrogen separation should have the following characteristics:

- high selectivity towards hydrogen.
- high flux.
- low cost.
- high mechanical and chemical stability.

1.6.1 Membrane materials

Currently there are three categories of membrane suitable for hydrogen separation: polymeric-based, metallic-based, and carbon-based membrane.
Polymeric membrane exploits different solution and diffusion rates of gas molecules thought a

rubbery or glassy polymeric layer to separate hydrogen. The diffusion through the layer depends on partial pressure, molecule size and interaction with the membrane. These membranes are limited by a trade-off between the selectivity and the permeability. Moreover, other drawbacks that exclude their application in ammonia-to-hydrogen field is the operability temperature range, specific for each polymer but in any case, lower than 400°C, and the susceptibility to certain chemicals (Lamb et al., 2019a).

Carbon molecular sieve membranes (CMSM) are under investigation for promising results and reduced costs of manufacturing. CMSM is produced through the carbonization of polymeric precursor at high temperatures and under controlled atmosphere. This type of membrane possesses high corrosion resistance, high thermal stability, excellent permeability and selectivity when compared with polymeric membrane. In this case the mechanism of separation operates on a size-exclusion principle, which means that is the dimension of the molecules the critical parameter. However, for this reason, the membrane may be not able to satisfy the hydrogen purity requirements: even if N_2 is easily separated since larger as a molecule, H_2 and NH_3 have similar atomic diameters (289 pm vs 260 pm) hence the selectivity will never be so high between these two species (Bernardo et al., 2020).

Dense metallic membranes are the commonly used in ammonia-to-hydrogen field, and more precisely palladium membranes are also commercialized to produce ultrapure hydrogen (purity up to 99.99%) (Adhikari and Fernando, 2006). The big advantage that they can offer respect the previous membrane types is the selectivity: when using dense metallic membranes, often, only one stage of separation is required.

1.6.2 Overview on Pd-based membranes

Palladium (Pd) is considered the most suitable metal for H_2 purification via membrane technology as showed in the last decades (Bernardo et al., 2020).

Pd is the preferred metal for a series of characteristics such as high H_2 permeability and solubility (pure metal can contain 600 times its volume of H_2 at room temperature without losing the mechanical structure), outstanding resistance to hydrogen embrittlement, and the capacity to auto-catalyse the dissociation of molecule in monoatomic hydrogen at the surface of the membrane permitting a rapid diffusion through the dense layer (Pal et al., 2020). Furthermore, Pd-membranes are able to achieve a high selective hydrogen permeation until to reach virtually infinite selectivity (Bernardo et al., 2020).

The barrier to the use of Pd-based membranes are the high cost and the volatility of its price: USD 1265.5$ per ounce at the end of 2018, USD 1942.2$ per ounce at the end of 2019, and USD 2203.5$ per ounce in January 2020 (Wang et al., 2022). The research had tried to develop membranes with metals of group V (Ta, V, Ni), which has shown 10 times higher permeability respect Pd. However, to exploit the membrane separation these metals need a catalytic layer, since they do not have the same capacity to dissociate hydrogen molecule, and moreover they

are susceptible to oxidation. The latter point precludes their utilization alone, and further implementation in alloys with Pd are subject to degradation around 400°C due to interdiffusion between the two metals with corresponding decline of permeation (Pal et al., 2020).

The main challenge related to Pd-based membranes for H_2 separation is that the metal undergoes a lattice phase transformation (α→β) from a low H/Pd atomic ratio to a high H/Pd atomic ratio when the temperature is below its critical point (298°C). This results in around a 10% volume expansion, which induces internal stress in the lattice structure leading to cracks, defects, or pinholes formation in the selective film (Bernardo et al., 2020).

Another issue with the use of Pd-based membranes is related to the chemical stability: they are highly susceptible to poisoning by CO, H_2O, and sulphur compounds, which reduce the permeability to hydrogen since these molecules block the surface-active site (Bernardo et al., 2020).

With the purpose of improving thermal and chemical stability, Pd is often alloyed with other metals such as Cu, Ag, Y, Ni, Au, Ce and Ta or Ru. Alloying was found to reduce the critical temperature for the phase transition as well as to improved H_2 permeation. For example, an increase in hydrogen flux of 1.7 times is reported by $Pd_{77}Ag_{23}$ (alloy compositions are expressed by the metal symbol followed by weight percentage as a subscript) due to the presence of the other metal that enlarge the atomic distance and facilitate atomic hydrogen diffusion (Ji et al., 2018).

An upper limit exists in the utilization of these membranes at high temperatures. As general statement, it has been observed that thin Pd-based supported membranes suffer from loss in hydrogen selectivity during long-term operation at temperature above 500°C, independently of the support used (Gallucci et al., 2017). Independently from the causes that vary support by support, the upper limit is inside the range of ammonia decomposition temperature.

Pd-based membranes may be classified into unsupported and supported ones. Unsupported membrane is generally a thick self-standing film (> 30 μm) able to achieve a minimal mechanical stability (Gallucci et al., 2017). The main drawback of this category is the large bulk diffusion resistance due to the thickness dense selective layer. Further, as Pd is very expensive, the costs of the separation sharply increase by increasing the membrane thickness.

For these reasons, industrially available membranes are supported, namely a thin metal film (<5 μm) is deposited into a porous support. Since it is the porous substrate to ensure the mechanical strength of the membrane, the supported Pd-based membranes can reduce the thickness of the metal layer, which not only improves the hydrogen permeability but also reduces the amount of precious metal, effectively reducing the cost.

An enormous increment in the palladium world supply demand would be necessary to produce metallic membranes for large scale application in hydrogen purification. Aiming to increase the cost-effectiveness as well as the permeation flux, some research has been focused on production of ultra-thin membranes, where the selective layer is around 1 μm or less (Bernardo et al., 2020).

The selection of the support is of paramount importance in the preparation of a thin and defect-free membrane: high surface roughness and presence of large pores inhibit the deposition of thin palladium films. Three types of materials are emerged as suitable support: porous ceramics, metals and Vycor glass. Asymmetric porous ceramics such as Al_2O_3, TiO_2, ZrO_2 are widely used due to their excellent stability and low cost. Among them, alumina has the advantages of chemical inertness, high-temperature resistance, excellent stability, narrow and controllable pore size, so it is commonly used as support material. Some disadvantages of the ceramic matrix are fragility and the difficulties in sealing and connecting with other metallic components of the process. Moreover, when temperature changes too fast, the membrane is at risk of breaking due to the large difference in thermal expansion coefficient between ceramic and palladium. The metal substrate represented by porous stainless steel (PSS) has been candidate to effectively overcome the above shortcomings. It has good weldability to ensure sealing and it has a similar thermal expansion coefficient respect Pd. However, the surface of commercial PSS is generally characterized by large and uneven pores, which leads to a thicker Pd coating to compensate for the roughness of the substrate (Wang et al., 2022).

A new research strategy regard the so-called double-skin membranes: they are characterized by an additional protective layer situated on the external surface of the selective layer. It is usually made of porous zeolite or ceramic material and the goal is based on the simple principle that the impurities with a large kinetic diameter are prevented from coming in direct contact with the Pd-alloy membrane. The result is a great improvement in operability, since not only the protective layer increases the chemical stability, but it also helps to limiting the detrimental effects of possible defects present on the selective layer due to production issue or abrasion with catalyst particles when the membrane is implemented inside a reactor (Bernardo et al., 2020).

Membrane geometries may be planar, tubular (that includes tubes, capillaries, and hollow fibbers), plate and frame and spiral wound. Currently the most used geometries for gas separation are planar and tubular. The planar membranes are often used in earlier laboratory research and development studies; instead for medium and industrial scale the tubular membranes are the most preferred option because of their higher surface area to volume ratio in comparison to planar membranes (Gallucci et al., 2013).

1.6.3 Hydrogen permeation mechanism

It is well known that hydrogen separation in Pd-based membranes follows the solution-diffusion model (Gallucci et al., 2013). The steps involved in hydrogen transport from a high to low pressure gas region are reported in Figure 1.2 and they can be summarized in: gas molecule diffusion to the membrane surface, reversible dissociative adsorption on the surface, dissolution of the atomic hydrogen into the bulk metal, association of hydrogen atoms on the metal surface and desorption of molecular hydrogen from the surface, diffusion of gas molecule away from the membrane.

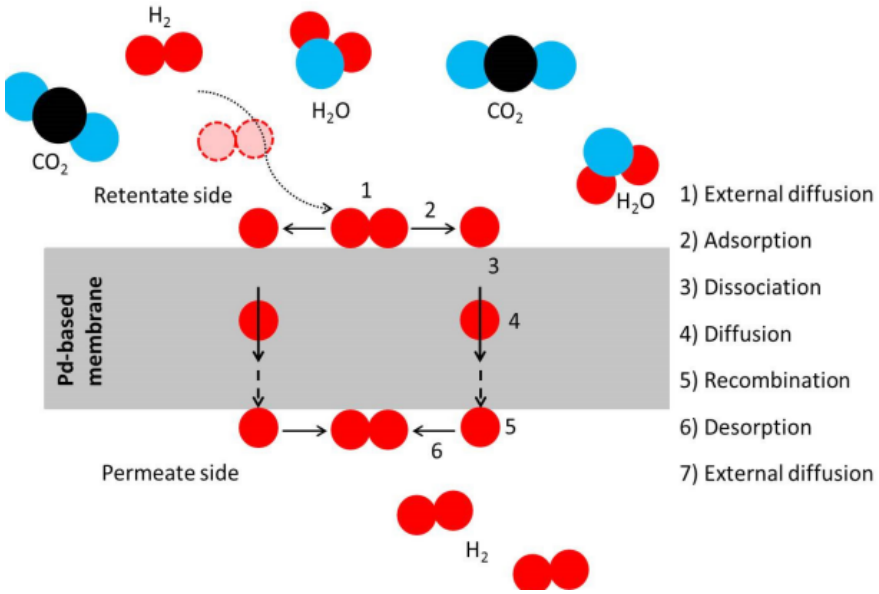

Figure 1.2. *Solution-diffusion mechanism of hydrogen permeation through a dense metal membrane* (Urquijo et al., 2017) .

The hydrogen flux through the membrane J_{H2}, expressed as moles of gas per unit time per unit of membrane area, can be generally described by the following equation:

$$J_{H2} = Pe_{H2} \cdot \left(\sqrt{P_{H2}^{ret}} - \sqrt{P_{H2}^{perm}} \right), \tag{1.11}$$

where Pe_{H2} is the hydrogen permeance (mol/m^2/s/Pa^n), P_{H2}^{ret} and P_{H2}^{perm} are respectively the partial pressures (Pa) in the retentate and permeate sides.

The pressure exponent n generally ranges between 0.5 to 1 depending on which is the limiting step in the hydrogen permeation (Yun and Ted Oyama, 2011). According to Sievert's law, when the rate controlling step is the hydrogen bulk diffusion through the palladium layer the value of the exponent is 0.5, because the diffusion rate is proportional to the concentration of hydrogen atoms in front of the selective layer and the last one is proportional to the square root of the partial pressure. When one of the following steps between hydrogen transfer to or from the membrane surface, dissociative adsorption or associative desorption become the slowest in the permeation process, the expected value of n should be of 1, since these processes depend linearly on partial pressure. Practically, the exponent value is obtained by fitting the

experimental data, and values between 0.5-0.8 for thin palladium membrane have been reported. The presence of defects and pinholes are possible causes of deviation from theory since they contribute to hydrogen permeation, and not only, through a different mechanism, the so-called Knudsen diffusion.

As can be seen from Eqn 1.11 the flux is inversely proportional to the membrane thickness: more area is required for achieving the same hydrogen flux for thicker membranes.

Permeability, the ratio between permeance and membrane thickness, is a fundamental property of the material. Furthermore, permeability can be expressed as the product of the diffusion coefficient and the solubility constant. As the diffusion of hydrogen is an activated process, the relationship between permeability (or permeance) and temperature follows an Arrhenius behaviour (Melendez et al., 2017):

$$Pe_{H2} = K_{Pe} \cdot exp\left(\frac{-E_{att,Pe}}{R_g \cdot T}\right), \tag{1.12}$$

where K_{Pe} is the pre-exponential factor (mol/m/s/Pa^n), $E_{att,Pe}$ is the permeance activation energy (J/mol), R_g is the universal gas constant (J/mol/K).

The membrane performance can be compared in term of permeability and selectivity. The latter represents the ability of the membrane to separate different gas species and it is evaluated through the ideal selectivity, or separation factor, defined as the ratio of the permeabilities of the species under investigation.

1.7 Packed Bed Membrane Reactor

A membrane reactor is a system combining reaction and separation of one or more products, with the separation operation performed precisely by a selective membrane.

The membrane reactor leads to improvement regarding both the reaction thermodynamic and kinetic if compared with the usual configurations. Indeed, removing the products from the reaction environment has as consequences both the equilibrium shift toward right by Le Châtelier principle, and the enhance of kinetic due to the increasing of reactant concentration (Basile, 2013). In the first case, the transport of products in the permeate side enables the reaction to proceed towards high values of conversion, overcoming those obtained in traditional reactors working under the same operative conditions, or alternatively to achieve the same conversion values but working under milder operating conditions.

Moreover, the integration of reaction and product separation into a single unit is a process-intensification strategy, which is expected to lower the system capital and operative costs.

Different types of membrane reactor for hydrogen production have been proposed in literature: packed bed membrane reactor (PBMR), fluidized bed membrane reactor (FBMR) and micro-membrane reactor.

In PBMR the catalyst is confined in a fixed bed and it is in contact with a selective membrane.

The most used packed bed configuration is the tubular one, where the catalyst may be packed either in the membrane tube (Figure 1.3a) or in the shell side (Figure 1.3b), while the permeation stream is collected in the opposite side of the membrane (Gallucci et al., 2013). Membrane reactor configuration as in the latter case has been reported to be less efficient in exploiting the catalyst activity since the heat exchange between the reaction zone and the external furnace is more complicated (Chiuta et al., 2013).

Often, a sweep gas can be used in the permeate side to keep the partial pressure of the permeating species as low as possible, and therefore increasing the driving force of separation and minimizing the membrane area required. This practice can be applied if hydrogen is generated for other synthesis, like the ammonia one in which nitrogen can be used to sweep the permeation side. If a sweep gas is used in the permeation side, then a packed bed membrane reactor can be used in both co-current and counter current modes depending on the flow directions. However, in ammonia-to-hydrogen technology the sweep gas is not desirable because the goal is obtaining purified H_2 not mixed with another gasses.

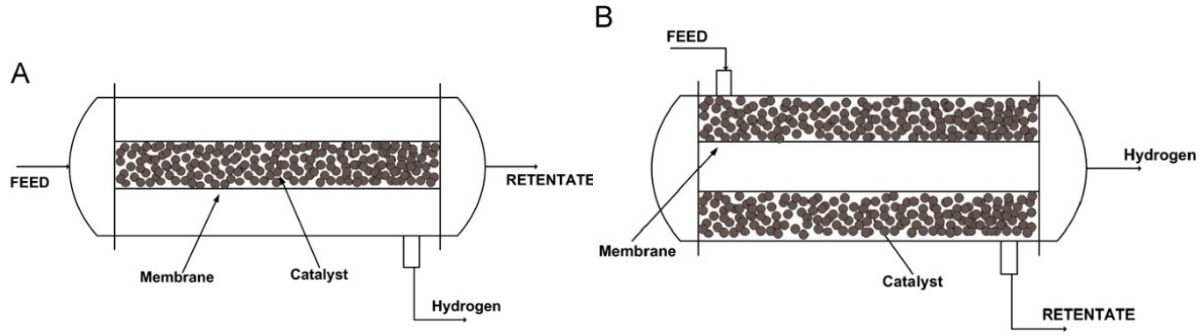

Figure 1.3. *Membrane reactors with catalyst in the tube (a) and in the shell (b) side* (Gallucci et al., 2013) .

The PBMR is the most popular configuration for palladium membrane reactor due to its simplicity and the catalyst particle immobility. The latter feature is fundamental to avoid damage and erosion of the membrane selective layer.

However, during the years, the use of PBMR has showed its disadvantages.

Concentration polarization is the first issue, which is more related to the membrane's properties than to the reactor. Due to the development of high permeable membranes, the external mass transfer of gas species toward the membrane surface may play a role in the entire process of permeation. Indeed, the presence of the other species in proximity of the membrane layer creates an obstacle to the transport of the interesting species, decreasing the actual driving force. For a correct design, it is necessary to evaluate the concentration polarization since it is usefulness decreasing the membrane thickness (higher fabrication costs and less stability) for increasing the permeating flux if the greatest part of the transport resistance is concentrated out of the membrane (Caravella et al., 2009) .

A second important limitation of packed bed reactor in general, and so also of PBMR, are the

presence of unavoidable pressure drops. To decrease the extent of this phenomena, larger particle size should be used, however in this way the extent of intra-particle mass transfer limitations increases and the final conversion decreases. In a PBMR the decreasing of the product's partial pressure on retentate side also reduce the driving force of permeation. The result is still an increase in membrane area required for a given conversion or product recovery (Gallucci et al., 2013).

Finally, as general consideration, the heat management and temperature control are quite difficult in a PBMR and so avoiding the formation of a temperature profile is quite difficult. Since in ammonia-to-hydrogen technology the reaction is endothermic, the possible losing of temperature's control inside the reaction system will be detrimental since it will lead to a decrease of both kinetic and membrane permeability as described in §1.7.3 (Gallucci et al., 2013).

1.8 Motivations and objectives of this Thesis

Different publications within the project *Arenha* (Cechetto et al., 2021, 2022) have demonstrated the feasibility of ammonia decomposition in lab-scale packed bed membrane reactor. However, during these experiments the ammonia conversion has been recorded to reach almost 100% and to be not strongly influenced by the inlet flowrate of reactant, as should be due to the relation between residence time and conversion. From these observations the idea of a catalyst excess is born, and the following work has been developed to prove it.

The kinetic study is the essential point to design a packed bed reactor: indeed, no reliable kinetic laws have been developed until now for the catalyst Ru/γ-Al_2O_3 (2 wt%) used in the membrane reactor. Attention has been made to design the kinetic study in a micro packed-bed reactor to guarantee the plug flow, the isothermal condition and the reaction under kinetic regime. However, also experimental test with the solid in form of pellet has required to assess the impact of mass transfer limitations.

Then the membrane *Arhena-5*, the one assigned to be investigated, has been characterized and tested under reaction condition (equal to the one of previous studies) to verify the same behaviour cited at the beginning. Since the set-up inlet flowrate of ammonia is limited at $1l_N$/min, the only possibility to assess the catalyst excess has through different catalyst concentrations inside the packed-bed reactor. Indeed, to fully exploit the membrane, all its surface should be covered by solid pellets; if not, the system has not more performing reaction and separation at the same time, condition that guarantees the improvement on final conversion. The dilution of catalyst in packed-bed reactor involving an endothermic reaction is also a possible solution to guarantee an easier heat management and hence avoid cold spots, detrimental both for reaction, membrane permeability and mechanical stability.

Chapter 2

Kinetic study: materials and methods

In this chapter the method used to carry out the kinetic study is described in detail. Specifically, guidelines are given for the reactor and experiment design, followed by a laboratory tuning to reach the best working conditions. Catalyst and inert description are provided to characterize the subjects of the kinetic study on ammonia decomposition and to permit a comparison with previous investigations present in literature. The chapter ends with the explanation of the model applied for the fitting of the most appropriate kinetic law starting from the raw laboratory data. The goal of Chapter 2 is thus to provide a guide for everyone who would like to repeat the same work.

2.1 Diffusion and reaction in porous catalyst

In general, a reaction rate is function of temperature and concentration, whose values are those evaluated in the catalytic region, where the reaction occurs. When dealing with porous catalyst the reaction takes place only on the active sites situated for the majority inside the pores.
Hence in a heterogeneous reaction system, first mass transfer of reactants takes place from the bulk of the fluid phase to the external surface of the catalyst particle (inter-phase or external mass transfer), then the same reactants diffuse from the catalyst surface into and through the pores within the solid (intra-particle or internal mass transfer), and finally on the active sites reaction takes place. A schematic representation of these steps in series is showed in Figure 2.1.

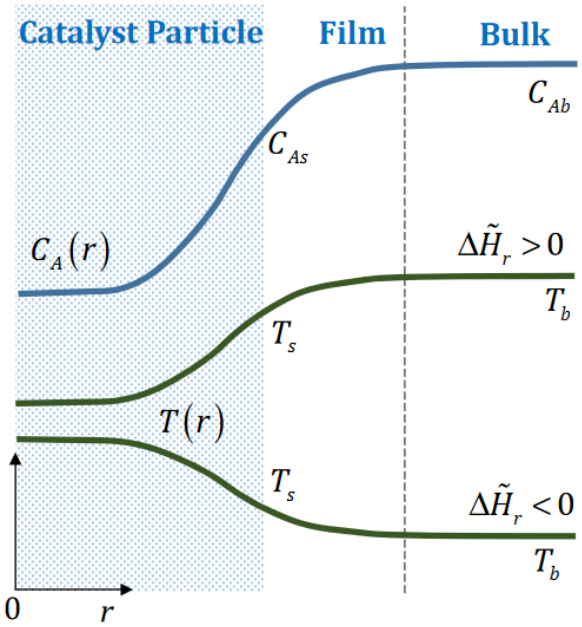

Figure 2.1. *Mass transfer and reaction steps for a porous solid catalyst: concentration and temperature profiles in the different regions.*

In general, the concentration of a reactant is always decreasing from the bulk towards the catalyst's pore. As for temperature, if the reaction is exothermic, the bulk temperature is lower than the catalyst one, whereas the opposite situation is found in case of endothermic reaction. The inherent problem with porous catalyst is that we can only measure properties in the bulk of the fluid phase, but not their profile developed along the particle radius. Therefore, the purpose of heterogeneous catalysis is to link bulk and catalyst's pore quantities through an appropriate transport model in order to express the kinetic expression in terms of concentrations and temperature of the bulk.
However, it is also possible that one of these steps in heterogeneous catalysis is the dominant one, namely it determines the speed of the entire process, while the others two can be consider negligible. An example, suitable during the development of kinetic studies, is the case where the process is guided by the reaction step, and if it occurs the system works under the so-called kinetic regime which assume negligible the resistance given by the chemical species transport. The same concept can be applied to the cases when external or internal mass transfer are the dominant step.

2.2 Reactor design criteria

Ammonia decomposition takes place in a heterogeneous system, with catalyst in solid phase and reactants/products in gas phase. Hence, the fixed bed laboratory scale reactor is the selected one to measure intrinsic kinetic rates.
As suggested by Perego and Peratello (1999), some conditions must be satisfied to correctly carry out a kinetic study:

- ideal flow pattern for continuous operation ensures an easy data treatment because of the simple mathematical description.
- isothermal condition, namely no temperature gradients inside the reactor, to catch the correct temperature's dependence of the kinetic parameters.
- working under kinetic regime, limiting as much as possible the influence given by intraparticle, inter-phase and macro-reactor concentration gradients.

Simple practical rules, theoretical criteria and experimental diagnostic tests have been taken in consideration to satisfy the points above mentioned when dealing with a fixed-bed reactor system. However, with complex reaction mixtures the most reliable conclusions are usually reached from careful experimentation (Satterfield, 1996).

2.2.1 Flow pattern

As motivated in §2.5, the plug flow is the flow pattern targeted inside the fixed bed reactor, which is defined as the condition of well-mixed radially and zero-mixed axially.
Two rules of thumbs are suggested for gas-solid systems to ensure this flow pattern: the reactor diameter (D_R) must be at least 30-10 times bigger than the catalyst diameter (d_p), while the

length of catalyst bed (L) should be at least 50 times bigger respect the particle diameter.
The first rule targets the minimization of the flow maldistribution through packed bed caused by the influence of the reactor wall to the flow pattern: since in proximity of the wall the void fraction of a packed bed is higher than in the centre, the linear velocity next to the wall will be greater because of the lower resistance (*Perry's Chemical Engineers' Handbook*, 2008). The second criteria, instead, is taken usually as guideline to realize an industrial packed bed reactor (Fogler, 2004). Focusing on laboratory reactor, the previous rule of thumb is sufficient if particle Reynolds number (Re_p) is 10 or above. However, since in laboratory scale Re_p <0.1 is common, a procedure based on dimensionless numbers may be required to determine the correct ratio L/d_p, as suggested by Dautzenberg (1989):

$$\frac{L}{d_p} > 92 \cdot {Re_p}^{-0.23} \cdot N_{tot} \cdot ln\left(\frac{1}{1-X}\right), \tag{2.1}$$

where N_{tot} (mol/s) is the total molar flowrate and X the reactant conversion.
The flow of fluids through a packed bed generally results in a decreasing of pressure, which affects the partial pressure of chemical species involved in the reaction. Checking pressure drops throughout the reactor is hence fundamental to understand if the isobaric condition can be reasonable assumed or instead momentum balance (i.e. Ergun equation) must be added on the reactor model. In the last case, more complexity is involved and generally it is advisable, when possible, to select an appropriate catalyst diameter in the fixed bed reactor to avoid it: the higher the catalyst particle size, the lower the pressure drop associated. A rule of thumb to neglect the existence of a pressure profile is that the pressure drop should be lower than approximately 20% of the total operating pressure in the reactor (Pérez-Ramírez et al., 2000).

2.2.2 Isothermal condition

It is extremely important to obtain kinetic parameters under isothermal conditions since very small changes in temperature can affect reaction rates significantly.
When dealing with gas-solid reactions temperature gradients at different levels are present: macro-gradients at the reactor level both in the axial and radial direction, inter-phase gradients at the boundary between the catalyst and the gas phase, intra-particle gradients within the catalyst particles. The severity of these temperature gradients decreases as the scale where they are present is decreasing (Dautzenberg, 1989).
The experimental methods for reducing temperature gradients at reactor scale, namely counteract the heat removal from the reaction in our case, are the dilution of both feed and catalyst and the decreasing of reactor diameter (Perego & Peratello, 1999). Different from axial gradient that is inevitable due to the conversion and so can just be minimized, the radial one is detrimental for the reliability of the data collection and the plug flow hypothesis.
The feed dilution with inert gas is a strategy that allows to maintain relative high inlet flowrate without causing a heat effect along the axial direction too difficult to manage, since the

concentration of the reactant is controlled, and the low effective thermal conductivity of ammonia is balanced by the appropriate inert one.

The catalyst dilution inside the fixed bed is made with a solid inert characterized by high conductivity, like quartz or silica carbide, and to avoid non homogeneity the use of same particle size is recommended to facilitate the solid mixing. The final goal is to reduce the local hot or cold spots and improve the temperature distribution along the catalytic bed. Berger et al. (2002) have discovered a possible negative deviation of the conversion caused by bed dilution, since it does not yield a homogeneous activity decrease, but it gives rise to a discrete local activity in an inert surrounding. For practical applications, they suggest to avoid the combination of high dilution with high conversion, which is also prevented in a kinetic study.

The decrease of reactor diameter to facilitate the heat transfer with a large heat exchange area, has as a consequence also the decreasing of the particle diameter to fulfil the previous rules of thumbs about the flow pattern and to avoid the uneven distribution of the solid phase inside the catalytic layer.

In regard to the inter-phase gradients, they are more difficult to overcome than the macro-gradients and the reason for this is the relatively low thermal conductivity between the reaction fluid layer surrounding the catalyst particle and relatively higher one of the solid catalysts. The extent of this gradient can be reduced by properly reducing the particle diameter and by increasing the flowrate, namely acting on the hydrodynamic of the gas-solid boundary layer.

Inside the catalyst domain, conduction is the governing mechanism for heat transfer. Since the effective thermal conductivity for solids respect gasses is larger and the size are quite smaller (μ-meter as order of magnitude), the intraparticle temperature gradients are inconsequential.

Dautzenberg (1989) collects a list of mathematical formulations to evaluate the extent to which catalyst activity measurements are disturbed by temperature macro-gradients, interphase and intraparticle effects. However, these criteria are not useful to establish isothermal condition from a priori evaluation since they require the knowledge of reaction rate and activation energy, impossible to known in the design step of a kinetic study. For this reason, the strategy implemented relies on temperature monitoring in the reaction bed as explained later in §2.3.2.

Looking at the mathematical criteria, nevertheless it is possible to have some guidelines about which reactor features can be manipulated to achieve a better thermal control during reaction tests:

- working at relative low conversion.
- using small particle size, always monitoring the pressure drop.
- decreasing the bed porosity.
- selecting catalyst support with high thermal conductivity.
- adding feed diluent with high thermal conductivity (e.g. H_2 and He above 250°C).
- apply relative high flowrates.

2.2.3 Mass transfer limitations

As regards the diagnose of mass transfer limitations, it is essential to ensure that the operative conditions of the experiments make the kinetic the slowest step of the process, namely the controlling one. Recalling indeed the concepts present in §2.1, the objective is to be able to describe the system using the properties of the bulk phase, in particular concentrations since the reactor work isothermally. In this way, it is possible to avoid misinterpretations of the experimental data when, through a model of the system, fitting parameters are looked for.

A common method to determine whether a system is affected by mass transfer limitations consists in applying theoretical criteria: to check if internal mass transfer is playing a role the Weisz-Prater criterion is used, instead the external mass transfer importance is assessed by the Mears criterion (Fogler, 2004).

The Weisz-Prater criterion compares the actual observed reaction rate to the internal porous diffusion rate, through C_{WP} coefficient defined as:

$$C_{WP} = \frac{-r_{NH3}^{exp} \cdot {\rho_{cat}}^{app} \cdot r_p^2}{D_{NH3,eff} \cdot C_{NH3}(r_p)}, \tag{2.2}$$

where $-r_{NH3}^{exp}$ is the observed reaction rate (mol/kg$_{cat}$/s), ${\rho_{cat}}^{app}$ is the catalyst bulk density (kg/m^3), r_p the particle radius (m), D_{eff} is the effective diffusivity inside the catalyst particle (m^2/s), and $C_{NH3}(r_p)$ the molar concentration at the catalyst surface (mol/m^3). If $C_{WP} << 1$, then the reaction rate is much slower than the diffusion rate and no internal mass transfer limitation is present. It must be underlined that the criterion is strictly valid with first-order reaction rate and spherical porous particle, namely applying it an approximation is done to have a rough estimation of the situation.

The Mears criterium, instead, compares the observed reaction rate to the external diffusion rate from the bulk gas to the catalyst surface and it is defined as:

$$C_M = \frac{-r_{NH3}^{exp} \cdot {\rho_{cat}}^{app} \cdot (1 - \varepsilon_b) \cdot r_p \cdot n}{K_c \cdot C_{NH3,bulk}}, \tag{2.3}$$

where ε_b is the bed void fraction (dimensionless), K_c is the mass transfer coefficient at the boundary layer between the solid and the gas phase (m/s), $C_{NH3,bulk}$ is the molar concentration in the bulk (mol/m^3), and n is the reaction order. If $C_M < 0.15$ external mass transfer limitation can be neglected because it means that the external diffusion rate is sufficiently larger than the reaction rate. Like the Weisz-Prater criterion, a simplified first order form has been used for the Mears criterion due to the added complexity when using the proposed ammonia kinetics. This rough estimate is deemed sufficient to determine if there are external mass transfer limitations when the value for the criterion is sufficiently far away from 0.15.

However, experimental tests can be performed to evaluate whether a certain concentration gradient is relevant. The advantage of these tests is that they no require a priori assumptions or

estimates of property's numerical value, and they are general valid for each kind of kinetic.
The diagnostic test applied to check the presence of inter-phase limitations is based on the principle that the conversion at any gas hourly space velocity ($GHSV$) must be independent of the linear velocity through the bed. $GHSV$ ($l_N/min/g_{cat}$) is defined as the volumetric flowrate of reactant fed per mass of catalyst and so it is inversely proportional to the residence time. The test aim to verify the independence of the reaction extent from the fluid velocity. This variable, indeed, influences the extent of the external boundary layer between solid particle and gas fluid: higher velocity decreases the thickness of the layer through which chemical species have to diffuse until the external mass transfer no longer limits the reaction rate. The experimental test consists on carry out different trials varying both the amount of catalyst and the feed volumetric flowrate but with the constraint that their ratio is kept constant. The expected result is described in Figure 2.2 (a): the conversion of reactant will change until inter-phase mass transfer limitation is present, more probably in the low range flowrates.
In the particle domain, concentration gradients are usually more important than temperature gradients for the reason explained previously. A useful diagnostic test consists of determining the isothermal conversion for catalyst particle of different size maintaining constant all the operating variables. The theoretical basis of the experiment is that under kinetic regime the conversion should not be affected by the catalyst dimension, whereas if internal diffusion is present the conversion tends to be proportional to the dimension of the granule. To be accurate, however, it must be added that this test is valid only as long as it is assured beforehand that the external mass transfer, which also depends on d_p, is negligible.
In principle, it is expected a behaviour like in Figure 2.2 (b), where there is a critical particle diameter for which another decrease of size is no more influencing the conversion reached.

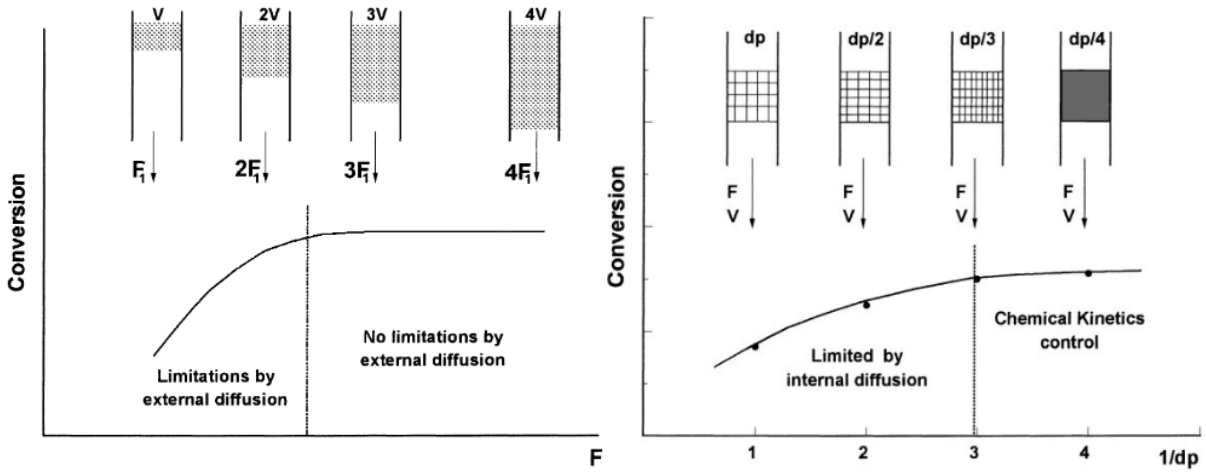

Figure 2.2. *The experimental methodologies and the expected trends are illustrated on the left* (a) *for inter-phase mass transfer check and on the right* (b) *for intra-particle check (Perego & Peratello, 1999).*

2.3 Set-up configuration

The central core of the experimental set-up used in the first part of this work consists of a tubular ceramic reactor, which has an inner diameter of 8.5 mm and a total length of 52 cm. Inside the reactor tube, different layers of materials are present to fulfil all the criteria suggested in §2.2. For the design of the fixed bed, some suggestions are taken from the kinetic study realized by Poto et al. (2022).

2.3.1 Fixed-bed reactor build-up

More in details, the reactor, illustrated in Figure 2.3 (a) and Figure 2.3 (b), is composed by the following layers listed from the top to the bottom:

- 10 mm of quartz wool to dampen the contact between gas and solid bed and avoiding spreading of powder (ensure complete isolation).
- about 1.500 g of SiC (height ≃15 mm) with particle diameter in the range of 425-325 μm, which stand as pre-packed bed to facilitate the heating up of the gasses, before the catalyst layer, at the desired temperature.
- the catalytic layer made of variable amount of catalyst $Ru/\gamma\text{-}Al_2O_3$ and inert SiC with the same particle size, but different quantity and dimension depending on the type of experiment performed.
- about 0.450 g of SiC (height ≃5 mm) with the same particle size of the catalytic layer as precautional protection from possible losing of catalyst solid powder (prevent penetration of active layer into the wool).
- 15 mm of quartz wool layer as intermediate and protection from losses of powder around the set-up.
- metallic perforated disc weld with a thinned tube based at the end of the reactor to support the entire layers of solid.

Different particle sizes between layers are a technical choice to avoid that the gas flow is going to mix different powders. Considering that the gas flow is from the top to the bottom of the reactor, to avoid the fluidization of the bed, the solid particle dimension is going to decrease in the same direction.

The reproducibility and the uniform distribution of the packing is an essential requirement along the experimental tests to avoid channelling and segregation. A systematic procedure has been applied with suggestions taken by Al-Dahhan et al. (1995) and the pressure drops are measured to quantify its reproducibility.

Briefly, the construction of the bed includes the following steps: crushing and sieving of solids in the correct size's range, preliminary weighting of the quantity necessary with analytical balance (accuracy ±0.001g), positioning of the perforated disk, filling the reactor with quartz wool and solids with the help of a spatula and a glass funnel. After each insertion, first the

reactor is vibrated to ensure formation of flat layer and no particles stick on the walls, then a metallic bar is used to compact and measure the relative height.

Figure 0.3. *On the left (a) the simulation of the fixed bed construction for kinetic study in a quartz tube of the same diameter of the actual reactor used; on the right (b) the reaction section of the set-up.*

2.3.2 Control and monitor system

The reactor is placed inside an electric oven with three heating areas (one at the top, one in the middle and one on the bottom), each one is fed with power to reach the relative temperature set-point. To obtain the maximum performance from the oven, hence temperature homogeneity, the position of the particle solids inside the reactor is designed in a way that the catalyst layer is precise in the middle of the oven.

As regard the temperature control, since the goal is to establish isothermal condition, two K-thermocouples are located respectively in the middle of the catalyst bed and just behind the perforated disk. The thermocouple inside the catalyst bed is inserted from the top part of the reactor tube, and to reduce the influence on the layer separation and flow pattern the smallest filament diameter has been chosen (less than 1 mm). The other thermocouple is inserted from the bottom of the reactor in a way that the filament is never in contact with the reactor wall or the metallic disk. The problem encountered with temperature control is that the three set points (one for each oven heating zone) refer to the temperatures measured by thermocouples placed in the boundary between the internal oven wall and external reactor wall. It is hence necessary, in order to achieve the experimental set points inside the reactor, a manual adjustment of the controlled temperatures along the time. This practically means take always in consideration the heat resistances due to the external gas layer, the reactor wall thickness, and the convection inside.

The outlet pressure of the reactor is set by means of a back-pressure regulator, instead for the inlet pressure a simple indicator is present on the line. So, while the outlet pressure can be controlled, the inlet one is just read. In particular, the inlet pressure tends to oscillate due to the action of the back-pressure regulator. Moreover, with different trials it is spotted that the inlet pressure is always smaller than the outlet one. Since this cannot be realistic because the direction of the fluid always follows the pressure gradient, a home-made calibration is performed with the empty reactor tube: the criteria used has been to establish a linear correlation between inlet and outlet pressure considering the pressure drop negligible.

As regards the gasses fed to the set-up, four species are available: N_2 (99.9990% vol), He (99.997% vol) from the central lines and H_2 (99.9990% vol), NH_3 (99.98% vol) from the cylinders contained in a proper cabinet. Three thermal mass-flow meters and controllers provided by *Bronkhorst* are available to feed the reacting system. More in details: one is exclusive for dealing with NH_3, one for H_2 and the last one presented, instead, three different calibration curves installed for a high versatility in controlling both H_2, N_2 and He stream. Excluding the one for NH_3, the other present a working flow range from 0.4 to 10 l_n/min, in which an accuracy of +/- 0.5% read data + 0.1% full scale is ensured. The specific mass-flow controller for NH_3 presents the same accuracy, but the working range is limited between 0.02 and 1 l_n/min.

Due to the corrosion properties of NH_3 and its high solubility in water, no other flowmeters are available to measure with accuracy the content of a gas mixture containing that species. For this reason, in the kinetic study, an alternative way is applied to overcome this problem as described in §2.5. The outlet gas mixture from the reactor is directed to the analysis section, where a T-junction permits the inline sampling to supply the micro gas chromatograph *CP-4900 Varian* (μ-GC). The reproducibility of the measurements is affected on the pressure at the sampling point that must be kept constant. For taking a correct gas sample, an overpressure should be present at the correspondence of the T junction to provide the driving force to push the gas inside the capillary tube. The set-up is hence equipped with a barometer installed on the main line in correspondence of the junction and, after it, a manual valve to regulate the overpressure (set to 0.3 bar).

Finally the gas mixture passes through three bottles filled with water to reduce the NH_3 content and make possible the disposal of the gasses in the exhaust.

2.3.3 Micro gas chromatography

The μ-GC allows to analyse the molar composition of the gas mixture. The instrument is equipped with three different channels: the first one analyses H_2 and He, the second one N_2 and the third NH_3. Two capillary columns in series are present (Varian CP-4900 Micro-GC User Manual): *PPQ* pre-column (10 m length) followed by analytical column *Molsieve 5Å* (20 m length). H_2, N_2 and He are eluted more quickly than the NH_3 on the first column and so they

are separated inside the second one. The backflush option has been configured to vent and it is used to avoid NH_3 reach the analytical column and kept it clean. Three thermal conductivity detectors (TCD) are necessary to analyse the four species since H_2 and He have similar thermal conductivity (0.182 vs 0.151 W/m/K) and are monitored by the same one. The instrument method is configurated to permit the elution of narrow and distinguishable peaks in the chromatograph: attention is cared to reach the separation of H_2 and He peaks. In Table 2.1 the main settings tuned to reach the goal in this work are presented.

Table 2.1. *Parameters setting values in the μ-GC instrument method customized for this study.*

Settings	Channel 1	Channel 2	Channel 3
Injection temperature [°C]	100	100	100
Injection time [s]	30	30	30
Column temperature [°C]	45	70	110
Column pressure [kPa]	100	150	150
Carrier gas	Argon	Helium	Helium
TCD autozero [μV]	-20.6	-40.7	-35.8
Run time [s]	80	80	80

After the method tuning, a calibration curve for each chemical species has been performed. The procedure used aims to establish a linear correlation between the molar composition of a species in the mixture and the corresponding area under the peak. Different gas mixture compositions are created through the mass-flow meters/controllers and injected inside the instrument by-passing the reactor section. For each point in the calibration, the mean of three sampling runs is taken as reference value. The procedure is carried out in the correct way since the coefficient of regression R^2 is always higher than 0.99. An exception for N_2 has been made and, depending on the range of concentration, two different calibration equations are applied to convert the peak area into molar fraction.

2.4 Catalyst and inert

The commercial catalyst (CAS: 7440-18-8) is provided by *Alfa Aesar* and it is made of Ruthenium impregnated on γ-alumina pellets (7440-18-8 - Ruthenium, 2% on 3.18mm (0.125in) Alumina Pellets - 44575 - Alfa Aesar). The specific lot (S04F086) contains 2% by mass of Ru with a total metallic impurity of less than 100 ppm, as found in the certificate of analysis. The pellet is characterized by an average diameter of 3.18 mm and approximately 5 mm of length. No additional information is present since the product is used to research and development only, except an indication on the superficial area (S_g) of 200 m^2/g. The price of our provider is 359 € for 100 g of product.

As regards the inert, Silicon carbide (SiC) in powder form (particle range 425-325 μm) has been chosen. This solid is a product available in the market (CAS 409-21-2) and it is provided by

Thermo Scientific. Due to interesting properties like high thermal conductivity, mechanical strength, and surface inertness, silicon carbide is considered one of the ideal inert to use in catalysis (Kulkarni et al., 2022).

To perform the kinetic study both the solids have been crushed and sieved in order to reach the size of μ-meter. In particular, molecular sieves of 75, 150, 250, 355 μm has been used to investigate the impact of different particle size range on NH_3 conversion. However, since the range 250-150 μm has been the one giving better results during the kinetic study, solid physical properties have been investigated just in that range.

Dealing with porous solids in PBR has required to estimate in order: the skeletal density, the catalyst porosity, the bulk solid density, and the packed bed density.

The skeletal density is defined as the ratio between solid mass and the sum of solid plus the blind pore volumes within the material. It can be measured through an He pycnometer, an instrument which working principle is the Boyle's law: using the volume-pressure relationship it compares two chambers of known dimension, one containing the powders and the other empty, to determine the actual volume of the solid. The resulted skeletal densities are reported in Table 2.2 as the mean of 10 runs followed by standard deviation obtained through the instrument *Ultrapyc 1200e*.

The specific surface area, the pore volume and the pore diameter have been determined via the BET and BJH elaboration of N_2 adsorption-desorption isotherms at -196°C, obtained using a *Micromeritics ASAP 2020* gas adsorption device. Before the analysis the samples have been degassed 4 hours at 400°C. The measurement reports are attached in appendix, while the results collected inside the Table 2.2. The physisorption analysis revealed an isotherm of type IV with hysteresis (even if the last part is a bit critical), typical of a mesoporous material (i.e. pores in the range of 2-50 nm) for each solid.

Starting from the definition of pore volume (V_{pore}), the particle porosity (ε_{cat}) has been estimated as reported in Eqn. 2.4. With this information it is possible to calculate the bulk density of the catalyst (ρ_{cat}^{app}) defined in Eqn. 2.5.

$$\varepsilon_{cat} = \frac{V_{pore}}{V_{solid}} = \frac{V_{pore}}{\frac{1}{\rho_{CAT}} + V_{pore}}, \tag{2.4}$$

$$\rho_{cat}^{app} = \rho_{cat} \cdot (1 - \varepsilon_{cat}). \tag{2.5}$$

As expected, the catalyst in form of pellet has higher skeletal density than the one in form of powder because of the larger porosity. Crashing slightly decreases the pore diameter, but the pore volume results almost univariate between the two maybe because both are mesoporous materials and the dimension of the pore is not affected by crashing. However, the estimated catalyst porosity is slightly larger for the pellet, as should be, resulting in a higher bulk density.

Table 2.2. *Physical properties measured of the different solids involved in the study.*

Physical Property		**Ru/γ-Al_2O_3**	**Ru/γ-Al_2O_3**	**SiC**
Particle diameter $\boldsymbol{d_p}$	[μm]	pellets	250-150	250-150
Skeletal density $\boldsymbol{\rho_{cat}}$	[g/cm^3_{cat}]	3.0709 ± 0.0548	2.7237±0.0009	2.8801±0.0009
BET surface area $\boldsymbol{S_g}$	[m^2/g]	227.4483	246.7485	0.3338
Pore volume $\boldsymbol{V_{pore}}$	[cm^3_{pore} /g]	0.622944	0.644201	0.000703
Pore diameter $\boldsymbol{P.D.}$	[nm]	10.14157	8.8242	10.9109
Catalyst porosity $\boldsymbol{\varepsilon_{cat}}$	[cm^3_{pore}/cm^3_{solid}]	0.656709	0.6368	0.0020
Catalyst bulk density $\boldsymbol{\rho_{cat}^{app}}$	[g/cm^3_{solid}]	1.0542	0.9892	2.8743
Bed porosity $\boldsymbol{\varepsilon_{bed}}$	[cm^3_{pore}/$cm^3_{reactor}$]	0.33	0.40	0.40

Two important information are retrieved, instead, comparing catalyst and the inert powders: they have similar skeletal density, however due to the discrepancy in particle porosity, the bulk density is almost three times larger for the inert. The analysis suggests that the polytype of SiC used is the α (non-porous), which results stable at temperatures as high as 1700°C and it has hexagonal crystal structure(Kulkarni et al., 2022).

The packed bed porosity has been estimated experimentally for the pellet and the data obtained is in line with what expected from cylindrical pellets (Fogler, 2004). For the inherent difficulty to deal with fine powders, instead, the packed bed porosity has been assumed as 0.4, namely the hypothesis applied is to deal with spherical particle.

The possibility that the catalyst deactivated along the time has been investigated previously by Cechetto et al. (2021): the stability of the pellet has been verified for more than 800 h of reaction experiment.

An important discover in this work, as later described, is that the catalyst absorbs elevated quantity of water, namely it is hygroscopic. Before any use, Ru/γ-Al_2O_3 must be dried for at least 2 hours at 150°C to avoid water condensation on the set-up.

2.5 Reactor operating method

Two are the choices still to define, which are also linked one to each other: the type of reactor operating method and the experimental conditions to investigate.

The starting point is the fixed-bed reactor; however, it can work in a differential or integral way depending on the degree of conversion targeted. A reactor is defined as differential when the reaction rate can be assumed constant at each point throughout the catalytic mass. This implies the conversion to remain small enough, usually the reference value is 5% (Perego & Peratello, 1999). Under differential condition the perfect mixing hypothesis is applied, and the reactor can be model as a CSTR. The differential design is practically realized with an accurate dose of the small amount of catalyst used. It constitutes the preferred choice since embedded a series of advantages:

- it is the simple gradientless reactor due to the thin catalytic bed, which permits to assume both temperature, pressure, and concentration as constant.
- as regard the outlet concentration is approximately equal to the inlet one.
- the heat required from the reaction will be small and isothermal condition easy to achieve.
- relatively easy to construct and at a low cost.

From a previous kinetic study on ammonia decomposition (Gutiérrez Martinéz, 2022), however, it has been highlighted the main limit of the differential method: by its nature it gives a small incremental conversion, which can be difficult to measure for a multicomponent mixture and furthermore lead to misleading conclusions. The change in mixture composition between the inlet and outlet stream of the reactor, indeed, should be significantly larger than the experimental error linked with the instrument measurement. Moreover, two additional cons of the differential reactor support the choice of an integrate operative method: the high probability of catalyst by-passing, fatal in term of accurate residence time estimation (Perego and Peratello, 1999), and the assessment of plug flow conditions since the amount of catalyst to deal with is remarkably increased.
The previous statements motivate the choice of an integral reactor approach in this work.
The main consequences are the possibility to extend the range of ammonia conversion reachable and, as regard the modelling, the PFR equation is applied which means to have concentration profiles along the reactor domain. These points influence both the reactor construction as described in §2.3.1, and the operative conditions as reported in the next paragraph.

2.6 Design of experimental conditions

The operative conditions are an important point of the experiment design: the kinetic formulations obtained will be valid inside the variable range investigated, since an extrapolation outside them is always subjected to uncertainty.
A total of 39 experimental runs have been chosen, in which specific combinations between the factors have been selected, as reported in appendix. Temperature and pressure ranges are chosen to simulate the conditions in which ammonia decomposition in PBMR has been investigated in the past (Collins & Way, 1994). Even if reaction tests at higher pressure (until 10 bar) have been reported in literature, the maximum pressure has been limited to 4.5 bar first by the set-up configuration and then by the reactor stability: working at 5 bar (maximum pressure allowed) destabilizes the system as showed by the difficulty to keep a constant overpressure in the reactor outlet main line, essential to perform reliable GC measurements. As regard temperature, the upper limit of 500°C is chosen to guarantee the mechanical stability of the membrane in PBMR. Then also the gas hourly space velocity and the inlet reactant molar composition have been varied to study their influence on the reaction performance. The first is investigated by changing

the total inlet flowrate (runs 16-21). The latter one, instead, leads to different initial NH_3 concentration (runs 22-27) and to co-feeding with the reactant respectively also H_2 (runs 28-33) and N_2 (runs 34-39) to simulate the possible behaviours in PBR or PBMR, where different concentration profile can develop. Moreover, H_2 presence is essential to investigate the possible inhibition that occurs following Temkin's kinetic.

Feed compositions and flowrates are tuned through a trial-error procedure in laboratory and the resulted ranges are limited by the constraints described in §2.2. It has to be noticed the feed dilution always applies by addition of He, which is used to achieve suitable residence time in the reactor, namely suitable NH_3 conversion (between 5% and 50%).

All the possible factor combinations have been considered between temperature (5 levels) and pressure (3 levels) to have a clear information of their effect. Meanwhile, for the other factors investigated (GHSV, NH_3, H_2 and N_2 initial compositions), three levels for each have been considered keeping temperature and pressure constant in three different combinations: high temperature coupled with high pressure, medium temperature coupled with medium pressure and low temperature coupled with low pressure. The resulting number of experiments represents a trade-off between the time/cost consuming and the necessity to investigate all the factors combinations. From this point of view, it has to be specified that the choice of temperature and pressure combinations associated to the other factors investigated, has been motivated by two reasons:

- high temperature and high pressure are the conditions to obtain the optimal performances as regard ammonia decomposition in packed bed membrane reactor.
- since the opposite combinations promote the thermodynamic of the system, in this way the final conversion has been limited especially at high temperature avoiding encountering troubles in manage the drop in temperature profile inside the reactor.

A recap of the factors investigated and the levels of each of them is present on Table 2.3.

Table 2.3. *Experimental conditions approached in the kinetic study.*

Factor investigated	Levels
Temperature	400°C -425°C -475°C -500°C
Pressure	1bar -3bar -4.5 bar
Total inlet flowrate	$0.75 l_N$/min -$1 l_N$/min -$1.25 l_N$/min
Ammonia inlet molar fraction	0.1 -0.2 -0.4
Hydrogen inlet molar fraction	0 -0.1 -0.2
Nitrogen inlet molar fraction	0 -0.1 -0.2

2.7 Data treatment and fitting model

The data retrieved by experiments and necessary for the modelling are temperature T (°C), pressure in the inlet P_{in} and outlet P_{out} (Pa), inlet mass flowrates Q_i^{in} (l_N/min) of each component, and molar composition Y_i^{out} of the exit stream from the reactor.

Ammonia conversion is determined by taking advantages of the inert role of He in the system: the same amount in the inlet has to be retrieve in the outlet, since it does not take part at any reaction. Knowing Q_{He}^{in} and Y_{He}^{out} results straightforward to determine first the total mole flowrate at the outlet N_{tot}^{out} (mol/min), later the outlet flowrate of each component N_i^{out}, and finally X_{NH3}^{exp} as described in Eqn. 2.6.

$$N_{He}^{in} = Q_{He}^{in} \cdot \hat{\rho}_{He} \cdot MW_{He} = N_{He}^{out} = N_{tot}^{out} \cdot Y_{He}^{out}, \tag{2.6}$$

where the He density $\hat{\rho}_{He}$ (kg/m^3) at standard conditions (0°C and 1 bar) and He molecular weight MW_{He} (g/mol) are necessary for the conversion from mass to moles.

On the other hand, the numerical conversion for each run is determined via the integral analysis method, thus solving the ODEs describing the mole balance equations in a fixed bed reactor:

$$\frac{dN_i}{dW_{cat}} = \nu_i \cdot R, \qquad i = \mathrm{NH_3},\ \mathrm{H_2},\ \mathrm{N_2},\ \mathrm{He} \tag{2.7}$$

where W_{cat} (g) is the mass of catalyst, ν_i is the stoichiometry coefficient (0 for He as inert) and R is the reaction rate (mol/min/g_{cat}) defined as Temkin or Tamaru kinetic. The domain of integration is expressed as mass of catalyst and not as volume because it is the general rule in literature, and moreover results simpler to deal with. Indeed, retrieve the catalyst volume is quite uncomfortable since the catalytic bed is made by both catalyst and inert with different densities.

The mole balances in Eqn. 2.7 have been applied under the following hypothesis:

- steady state regime.
- isothermal operation.
- negligible pressure drops along the catalytic bed.
- absence of mass transfer limitations both internal and external.

All the hypotheses are confirmed experimentally: the reaction performance is evaluated at steady state (i.e. when no changes in the outlet composition were recorder over three consecutive runs of GC sampling); the temperature difference between inlet and outlet positions is always monitored to be at maximum equal to 1°C; the pressure drop along the reactor is always less than 5% of the inlet pressure when working under pressure, instead at atmospheric conditions it reaches a maximum of 10% of inlet pressure; the kinetic regime is assessed through the experimental tests described in §2.2.3 and permit to assume constant composition profile along the boundary layer and the pore diameter, namely to deal with bulk compositions.

The parameter looked to verify the goodness of the experiment at each condition is the sum of

the molar composition at the exit of reactor: more close it is to 100%, more accuracy on the GC measurements and also on the mass balance closure since the way it is used to calculate the experimental conversion.

Between the 39 experiments, 5 are randomly chosen not to be part of the fitting procedure but to be used as validation of the kinetic model parameters founds. Since the division of the points is suspected to influence the value assumed by the fitting parameters, the modus operandi is to repeat the fitting operation different times to evaluate the degree in which sampling the experiment runs is going to influence the results. This procedure is required since all the experimental conditions is selected to investigate a precise factor influence on the kinetic, and not redundant runs are present.

Depending on the experimental results, the most appropriate kinetic has been chosen from the one described in §1.7.2. The next step has been the fitting procedure, namely the determination of the three kinetic parameters: k_0, E_{att}, β for Temkin's kinetic and k_0, E_{att}, K_{Tam} for Tamaru's kinetic. The modelling has been carried out entirely in *Matlab R2021b* using *GlobalSearch* as algorithm, an optimization routine to find the global minimum of an objective function. *Global search* runs *fmincon*, a local solver to find out the minimum of a constrained nonlinear multivariable objective function, starting multiple points to sample different basins of attraction within the upper and lower bounds provided (MathWorks).

The objective function (OBJ), reported in Eqn. 2.8 is defined in this work as the sum of squared residuals (SSR) between numerical (X_{NH3}^{num}) and experimental (X_{NH3}^{exp}) conversion.

$$SSR = \sum_i^N \left(X_{NH3,i}^{num} - X_{NH3,i}^{exp}\right)^2, \tag{2.8}$$

where N is the number of tests in the kinetic study considered.

The same OBJ is chosen in similar kinetic studies by Chiuta et al. (2016) and Zançat (2020).

The optimal kinetic parameters have been obtained when the model converged at OBJ's values equal to the function tolerance fixed at 1e-15.

The selected algorithm requires an initial guess for the fitting parameters, which has been taken from literature. For example, in Temkin's kinetic: E_{att} is generally found to varies between 65 and 140 kJ/mol (Prasad et al., 2009b); from the definition of Temkin, β can assume only value between 0 and 1; as regard k_0, the starting value is 3.75e13 mol $Pa^{0.5}/m^3/s$ retrieved in a similar Ru-based kinetic study of Chiuta et al. (2016). However where data are subjected to uncertainty, the optimization routine has larger intervals to looking for a minimum.

Chapter 3

Kinetic study: results and discussion

In chapter 3 the results of the kinetic study are presented. The first part of the chapter focuses on catalyst and reactor design, which have been the preliminary steps to assess if the catalyst activity is stable and if the system fulfils the principles of a correct kinetic study. Then the comparison between experimental and numerical trends highlights the evidence that helps to choose the appropriate kinetic law. The chapter ends with a statistical analysis and a comparison of the fitting parameters with data present in literature.

3.1 Catalyst pre-treatment

During the experimental campaign, it has been discovered that the replication of the same experimental run after some tests leads to an improving in catalyst performance noticed by a systematically increment of NH_3 conversion. From that observation, it has been understood the need for a catalyst activation, better classified as catalyst reduction in this case. Indeed, when dealing with a commercial catalyst, there is a high probability that the active sites of Ru^0 have to be regenerated from the metallic oxide (Itoh et al., 2014; Prasad et al., 2009a; Zheng et al., 2007). The treatment adopted is a flushing of the reactor with a stream of 1 l_n/min of 50% H_2 (N_2 balanced) for 45 minutes at 400°C and 1 bar. Figure 3.1 shows the effectiveness of the treatment used: there is not overlapping of the error bars between points collected at the same operative conditions.

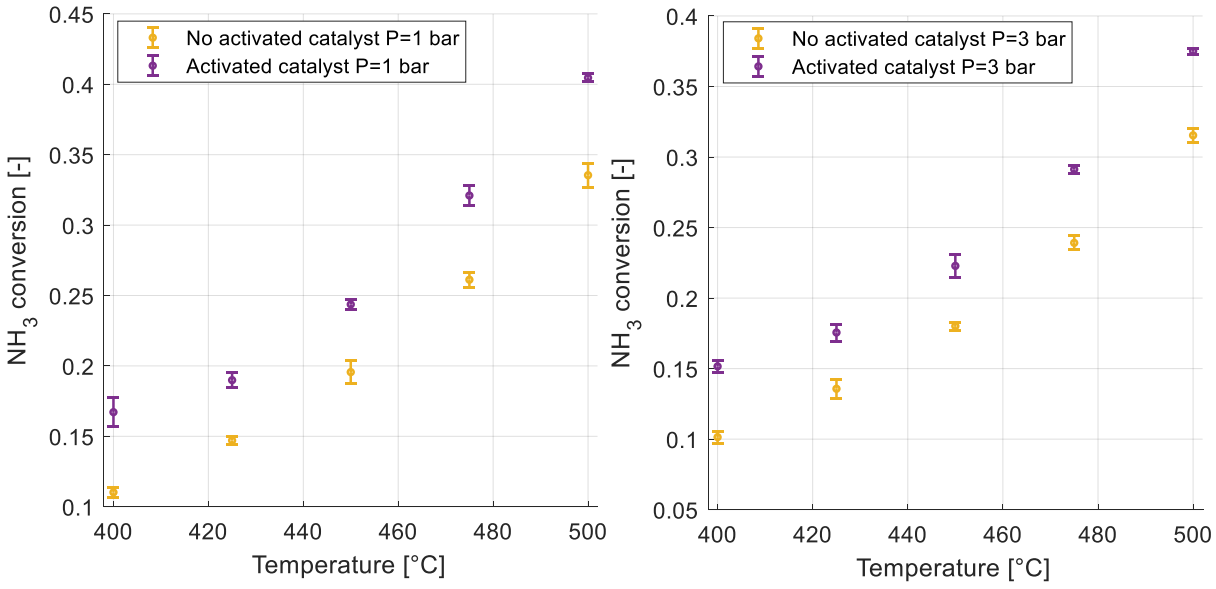

Figure 3.3.1. *Improvement on ammonia conversion with Ru/γ-Al_2O_3 before and after the catalyst activation as function of temperature and parametric on pressure: on the left* (a) *at 1 bar and on the right* (b) *at 3 bar.*

More precise the conversion increment is between 3.9% to 6.9%, and when the temperature increases a positive trend is spotted for both pressures under investigation, except for data at 400°C.

The hypothesis that part of the active metal is not reduced to a zero-valent state and additional reduction may occur during ammonia decomposition is not the only possibility that can account for explain the increment in catalyst activity. Excluding the presence of promoter or inhibitor in the catalyst formulation (i.e. Cl), since NH_3 decomposition on Ru has been demonstrated to be structured sensitive, the morphology modification of the surface active sites under reaction condition could alter activity (Bradford et al., 1997).

3.2 Catalyst dimension choice

The way to proceed in reactor design in this work gives the priority on diagnose and minimize the mass transfer limitations, and just after to fulfil the conditions regarding the flow pattern and isothermal condition. Moreover, laboratory tests have been considered more reliable than the correlations to assess the kinetic regime in the system.

Starting from internal mass transfer limitations, three catalyst particle size ranges have been evaluated under different conditions of temperature (from 400 to 500°C) and pressure (1 and 3 bar). The main results are reported in Table 3.1, where a clear distinction is presented between activated and inactivated catalyst. Despite this non uniformity due to the discover of the need for a catalyst treatment during the experimental campaign, the data are considered still meaningful. Indeed, reducing the size from 350-250 μm to 250-150 μm, an improving in conversion is showed up under the same operative conditions. In addition, higher is the reaction temperature more pronounced is the difference in agree to the theory: the reaction should be diffusion-limited at high temperatures, instead kinetic should be the rate determining step at lower temperatures (Fogler, 2004).

A further decreasing of catalyst size to 150-75 μm particle diameter range has an unexpected result: the conversion is going down systematically at each run. Moreover, the pressure drops are increased: a minimum of 30% of pressure is lost respect the inlet one for tests at 1 bar, while working at 3 bar makes the pressure lost decreasing to 15% of the inlet value. The impact on NH_3 conversion may be due to a higher pressure which slows down the reaction rate if the ammonia decomposition can be described by Temkin kinetic. Indeed, a pressure profile develops along the reactor: since flow direction follows the pressure gradient, at lower particle dimension the pressure is always higher compared to the other range inside the reactor, except for the outlet coordinate. If the previous hypothesis on kinetic mechanism is verified, it may be stated that the pressure drop influences more the conversion than the internal mass transfer limitation does, since they have opposite effects on it. The large pressure drop increment can be reasonable, remembering that a part from the catalyst layer there is an inert layer of the same particle dimension just after it (as described in §2.3.1), where further pression can be lost.

Table 3.1. *Experimental results to assess the impact of internal mass transfer limitations on the kinetic study.*

		NH_3 conversion [-]			
		inactivated catalyst		activated catalyst	
T	P	particle diameter range		particle diameter range	
[°C]	[bar]	355-250 μm	250-150 μm	250-150 μm	150-75 μm
400	1	10.17 ± 0.67%	11.02 ± 0.35%	16.71 ± 1.03%	14.45 ± 0.60 %
425	1	12.17 ± 0.62%	14.71 ± 0.83%	18.99 ± 0.54%	17.80 ± 0.95%
450	1	17.88 ± 0.66%	19.56 ± 0.86%	24.36 ± 0.37 %	22.57 ± 0.40 %
475	1	23.35 ± 0.43%	26.12 ± 0.66%	32.10 ± 0.68%	28.87 ± 0.55%
500	1	30.42 ± 0.33%	33.54 ± 0.49%	40.46 ± 0.30%	36.66 ± 0.42%
400	3	9.44 ± 0.48%	10.14 ± 0.27%	15.16 ± 0.44%	13.48 ± 0.58%
425	3	11.44 ± 0.31%	13.57 ± 0.53%	17.56 ± 0.60%	16.50 ± 0.50%
450	3	16.37 ± 0.25%	18.01 ± 0.43%	22.28 ± 0.79 %	20.83 ± 0.73%
475	3	21.92 ± 0.53%	23.91 ± 0.29%	29.13 ± 0.27%	25.90 ± 0.30%
500	3	28.92 ± 0.47%	31.54 ± 0.50%	37.50 ± 0.21%	34.20 ± 0.28 %

The range of particle diameter 250-150 μm is the chosen to carry out the kinetic study, namely it is considered acceptable that the internal diffusion is not the slowest step in the process. With this choice the right trade-off is found between internal mass transfer limitations and pressure drop.

The Weisz-Prater criterion is applied to confirm the statement above. The approximation of the diffusivity in the transient regime between molecular diffusion ($D_{i,m}$) and Knudsen diffusion ($D_{i,k}$) is reported in Eqn. 3.1, where both catalyst porosity (ε_{cat}) and tortuosity (τ_{cat}) are involved:

$$D_i^{eff} = \frac{\varepsilon_{cat}}{\tau_{cat}} \cdot \left(\frac{1}{D_{i,m}} + \frac{1}{D_{i,k}} \right). \tag{3.1}$$

The molecular diffusivity has been estimated through Eqn 3.2, which rely on the binary diffusion coefficient ($D_{i,j}$) calculated using the empirical correlation proposed by Fuller (Eqn. 3.3) (Bird et al., 2002):

$$D_{i,m} = \frac{1 - Y_i}{\sum_{j \neq i}^{N} Y_i / D_{i,j}}, \tag{3.2}$$

$$D_{i,j} = \frac{1.013 e^{-2} \cdot T^{1.75}}{P \cdot \left(\sqrt[3]{V_i} + \sqrt[3]{V_j} \right)} \cdot \sqrt{\frac{1}{MW_i} + \frac{1}{MW_j}}, \tag{3.3}$$

where V_i is the molecular diffusion volume of NH_3 and He, respectively 14.9 and 2.88 $\dot{A}^3$. The worst-case scenario is chosen to understand if internal mass transfer limitations could play a role: C_{WP} is calculated for the lowest temperature (400°C) and highest pressure (4.5 bar) for the mixture He-NH_3 ($Y_{NH3}^{in} = 0.2$).

As regard the Knudsen diffusion, instead, the following formula has been applied (Bird et al., 2002):

$$D_{i,k} = \frac{d_p}{3} \cdot \sqrt{\frac{8 \cdot R_g \cdot T}{\pi \cdot MW_i}}. \tag{3.4}$$

Moreover, the concentration near the surface has been replaced by the bulk one in the Weisz-Prater correlation, and this may negatively affect the evaluation since this approximation increases the denominator value. In any case, $C_{WP} = 1.57e^{-3}$ has been calculated (<<1), which is another proof to confirm our experimental assessment. Similar value of C_{WP} is obtained under comparable condition by Prasad et al. (2009).

For the external mass transfer limitation, the comparison in the Figure 3.2 (a) and 3.2 (b) is made between the 'Single packed bed' and the 'Double packed bed' configurations: the first one refers to a standard catalytic bed described in §2.3.1, instead in the later one the amount in mass of catalyst and inert is doubled during the building up of the catalytic layer (400 mg of Ru/γ-Al_2O_3 and 1600 mg of SiC). The operative conditions are the one described in runs 1-15, except for the inlet flowrates, which are doubled in the case of 'Double packed bed' to keep constant the gas hourly space velocity in the comparison.

Both at 1 and 3 bar the 'Single packed bed' configuration has demonstrate a significant higher NH_3 conversion since in any point the error bars are not overlapping each other. From the theory about external mass transfers, the opposite behaviour is expected: higher gas velocity should facilitate the mass transfers and improve the reaction performance. Once again, the comparison is distorted by different pressure profiles along the reactor. When dealing with 'Double packed bed' configuration the catalyst/inert layer is longer and the velocity is doubled: this combination

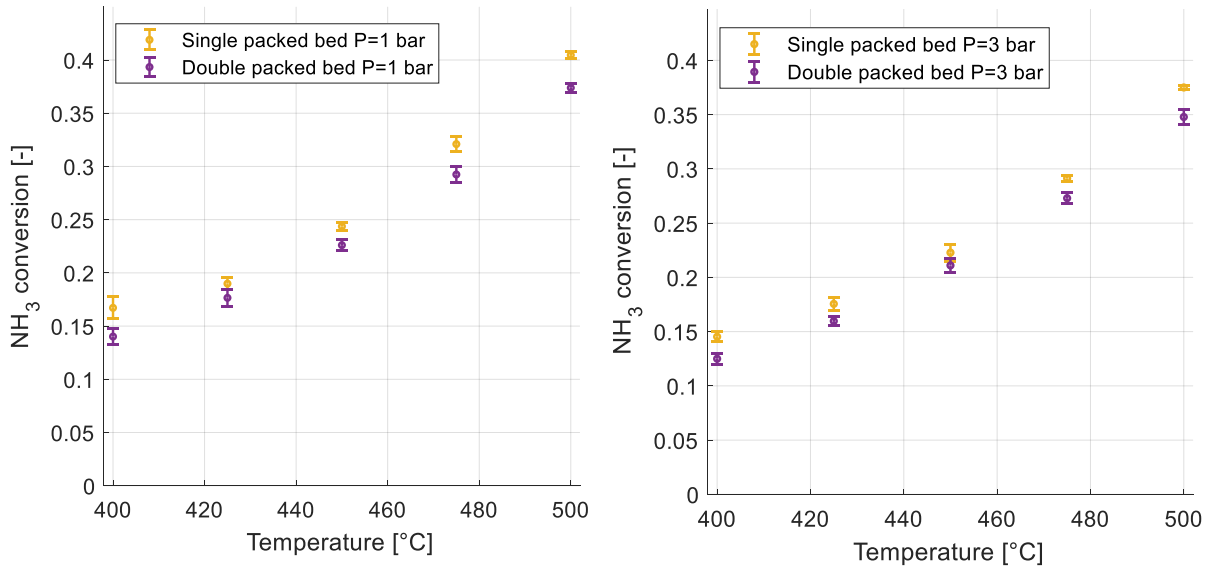

Figure 3.2. *Experimental results to assess external mass transfer limitations before the kinetic study: on the left* (a) *the ammonia conversion is collected at 1 bar, and on the right* (b) *at 3 bar for the same temperature range.*

of factors is the cause of not negligible pressure drops, especially at 1 bar where the conversion is higher and hence the velocity increases more due to the reaction which occurs with an increment in number of moles.

Indeed, focusing on data at 3 bar where the pressure decrement is always lower than 6% respect the inlet one, the NH_3 conversions are never differing more than 2% between the two configurations as showed in Figure 3.2 (b). Therefore, even if external mass transfer limitations may be present, their impact can be reasonably neglected because the effect of relatively small pressure drops is still more relevant.

The Mears criterion is applied as further proof of our statement. The operative conditions used to calculate the properties are the same of Weirs criteria. The particle Reynolds number, defined in Eqn. 3.5, is used to find the more appropriate correlation for the mass transfer coefficient:

$$Re_p = \frac{u_s \cdot d_p \cdot \hat{\rho}}{\mu}, \tag{3.5}$$

where u_s is the superficial velocity (m/s), μ the gas mixture viscosity (Pa·s) calculated through Wilke model. Since the low Re_p (equal to 0.8045), the Eqn. 3.7 used the Biot number, defined in Eqn 3.6, to estimate the mass transfer coefficient (k_c) in the boundary layer gas solid.

Eqn. 3.7 is valid for 0.1 <Re_p< 10 (Zançat, 2020):

$$Bi_i = \frac{r_p \cdot k_c}{D_i^{eff}}, \tag{3.6}$$

$$Bi_i = \frac{0.015 \cdot Re_p \cdot D_{i,m}}{2 \cdot D_i^{eff}}. \tag{3.7}$$

Finally, it results C_M = 1.83e^{-3} smaller than 0.15, the limited value to discriminate the presence of external limitations. The order of magnitude of the estimations is congruent (Bi_{NH3}equal to 5.84e-2, k_c equal to 6.82e-2 m/s), and those confirms that no big impact is expected from the mass transfer limitations between gas and solid phase.

The catalyst particle size which ensures to work under the kinetic regime, namely 150 <d_p< 250 μm, also satisfies the rules of thumbs regarding the flow pattern, since: L/d_p= 65 is larger than the minimum one required (equal to 50) when the Re_p>0.1, and D_R/d_p= 42.5 (>30).

Zheng et al. (2007) have performed a similar kinetic study on ammonia decomposition using particle size of 100 μm.

3.3 Experiments versus model predictions

In this section, the catalyst performance is discussed as a function of the reaction conditions explored both experimentally and via the model predictions. Experimental conversion (points) and simulation results (solid lines) are combined in the same figures to show both the experimental trends and the fit's quality.

As anticipatory result, the model applied Temkin's kinetic as the results of experimentally observations discussed in §3.3.1 and §3.3.5.

3.3.1 Temperature and pressure effect

Figure 3.3 displays the trends of ammonia conversion for temperatures between 400 and 500°C and parametric in total pressure (1-3-4.5 bar): the first variable positively affects the reaction due to the kinetic (i.e. Arrhenius type) and, on the contrary, the latter one decreases NH_3 conversion. The second observation must be underline since just with Temkin's kinetic the pressure negatively affects the reaction rate. This constitutes the first proof that Temkin's kinetic is the more appropriate model to describe this specific reaction.

Focusing on the experimental points, it can be noticed how the pressure effect change drastically with temperature: before 450°C there are not big differences between the three operative pressures; moreover, there is not a clear difference between conversions at 3 and 4.5 bar until 475°C since the experimental error bars overlap each other. At 500°C, instead, the pressure influence is clear and markable.

The model commits the larger errors in the reaction's fit at 400°C, instead all the other points have relative errors always lower than 10% as reported in Figure 3.9. Indeed, it is possible to notice in the experiments how the temperature is influencing the conversion more after 450°C, as already obtained by Chiuta et al. (2016), and the model presents difficulties to follow these trends at 400°C.

In general, the model is underestimated the experiments in all the conditions.

3.3.2 GHSV effect

The model describes accurately the experimental reaction performance in term of NH_3 conversion as a function of the gas hourly space velocity in different operative conditions, as showed in Figure 3.4. As expected from a kinetically controlled system, the conversion decreases with the increasing of inlet reactant flowrate, being the contact time of the gas with the catalyst bed shorter. From experiments the data more sensible to this variable are at 500°C and 4.5 bar, where the conversions are overall higher. Instead, increasing the inlet flowrate decreases the impact on reaction rate at relative low temperatures: from 0.75 to 1.25 l_N/min the ammonia conversion decreases respectively from 25.6% to 19.9% at 450°C and from 17.6% to 13.8% at 400°C. This behaviour can be explained by looking at the stoichiometry: when the reaction occurs, the total moles increase. Hence, since at 500°C the conversion is higher despite the high pressure, the larger molar flowrates highlight better the GHSV effect.

The results agree with previous literature studies (Antunes et al., 2022; Chiuta et al., 2016).

Again, the model always underestimates the experimental conversions, and the relative error overcomes the 10% bound just in run 17 (namely at 400°C, 1 bar, 300 $l_N/h/g_{cat}$) hence a good agreement is present overall.

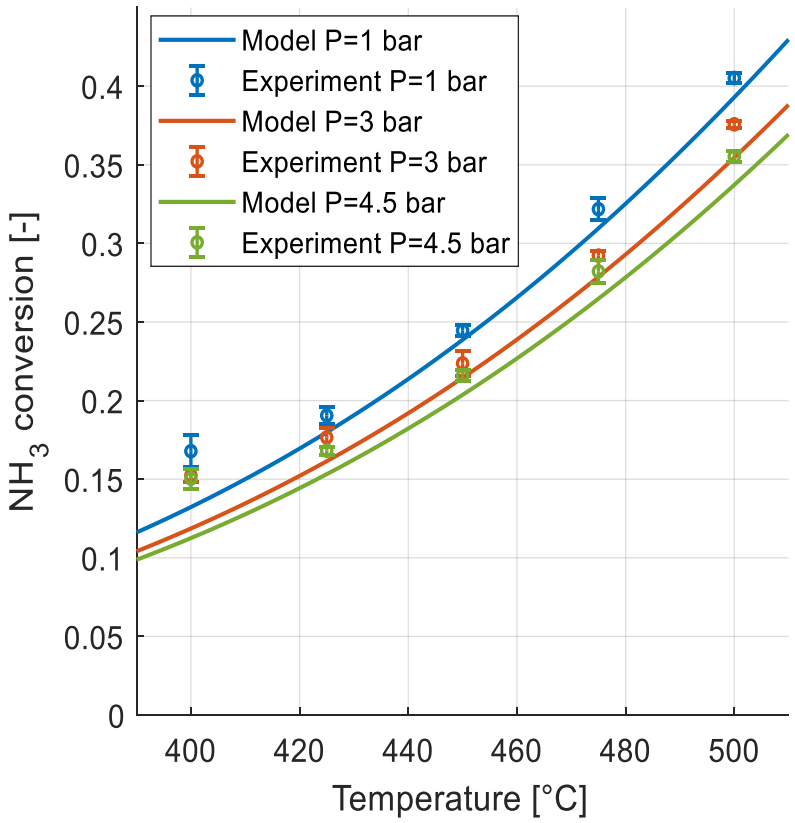

Figure 0.3. *Experimental and numerical ammonia conversion at different temperatures and parametric on pressures for an inlet stream composed by 0.8 l_N/min of He and 0.2 l_N/min of NH_3 (runs 1-15).*

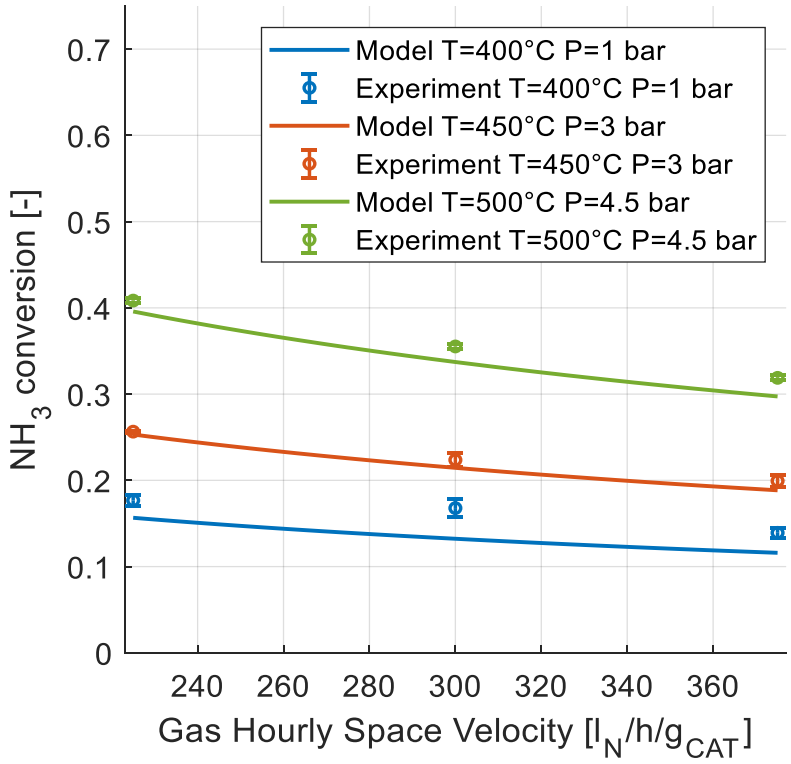

Figure 0.4. *Experimental and numerical ammonia conversion as function of GHSV at different temperature and pressure conditions obtained varying the inlet total flowrate between 0.75-1-1.25 l_N/min and keeping constant the ammonia inlet molar composition (runs 16-21).*

3.3.3 Inlet ammonia concentration effect

As regard the NH_3 initial concentration, Figure 3.5 can lead to misleading conclusion: indeed, the conversion decreases with the increasing of initial reactant concentration at each temperature/pressure conditions investigated. However, independently on the kinetic law applied, it is expected that the increment in reactant concentration leads to higher reaction rate. This is true indeed, if the reaction rate is observed: the Figure 3.6 shows the expected trend in the logarithmic scale of the absolute value of NH_3 reaction rate at 400°C and 1 bar, taken as example. Although the reaction rate increases, the decreasing trend in Figure 3.5 is obtained since the ammonia inlet flowrate increases more quickly than the reaction rate. The same factor has been investigated by Zheng et al. (2007) for Ru/Al_2O_3 1.9 wt.% and the trends experimentally obtained are identical.

Moreover, it can be again noticed from experiments how the improvements on ammonia conversion are different in the three temperatures for the same ammonia inlet concentration: despite high pressures are unfavourable, the temperature effect is larger, especially at 500°C.

From the fitting a discrepancy appears between experiments and model, since the later one overestimates the trend for Y_{NH3}^{in}=0.1 for both conditions of 400°C-1 bar and 450°C-3 bar.

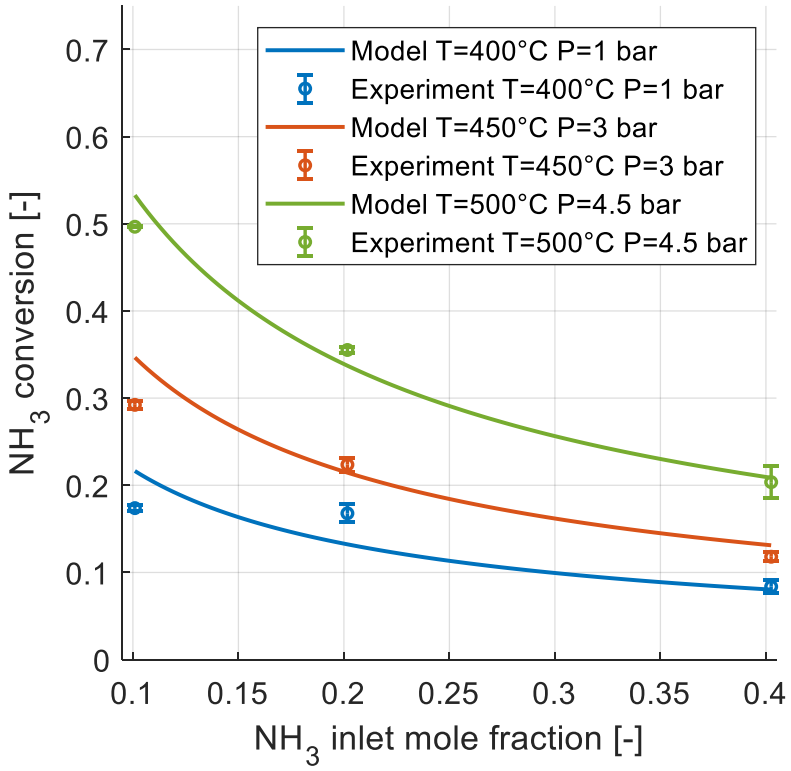

Figure 0.5. *Experimental and numerical ammonia conversion as function of ammonia inlet molar fraction parametric at different condition of temperature and pressure (runs 22-27).*

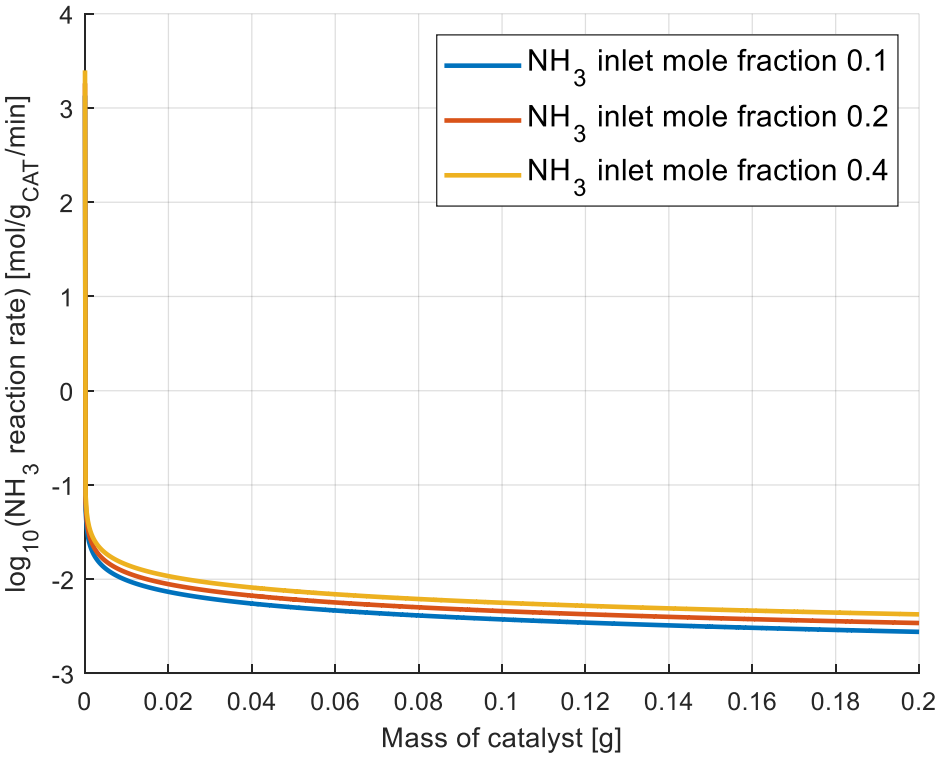

Figure 3.6. *The ammonia reaction rate are plotted along the mass domain at 1 bar and 400°C for different ammonia inlet molar fractions.*

3.3.4 Inlet hydrogen concentration effect

The more interesting investigation is on the effect of introducing H_2 in the inlet together with a fixed amount of reactant. In this case, since H_2 is a product, the conversion is a meaningful index of reaction performance. Both the model and the experiment demonstrate the inhibition given by the presence of H_2 in the reaction environment: with 10% and 20% of H_2 inlet molar concentration the conversion is respectively around 65% and 40% the one without H_2.

These observations constitute the final proof that the ammonia decomposition with the catalyst on exam follows the Temkin's kinetic, indeed Tamaru's kinetic does not take in consideration the influence of P_{H2}.

In literature the behaviour is confirmed by numerous studies, both for Ru-based catalyst (Antunes et al., 2022; Itoh et al., 2014; Prasad et al., 2009a) and for other active sites like Ni-La (J. Zhang et al., 2005), Pt (Tamaru, 1988) and Cs (Srifa et al., 2017). However, the inhibition effect of hydrogen should be gradually disappeared increasing the temperature as obtained by Antunes et al. (2022), which has reported no inhibition at 355°C and 1.5 Pa for a similar Ru-based catalyst. In contrast with the previous statement, in our case the hydrogen effect is approximately constant at different conditions of temperature and pressure. The model fit is poor as highlighted both by trends in Figure 3.7 and by relative errors in Figure 3.9, where all the experimental conversions with H_2 injection are underestimated and they have a relative error higher than 10%.

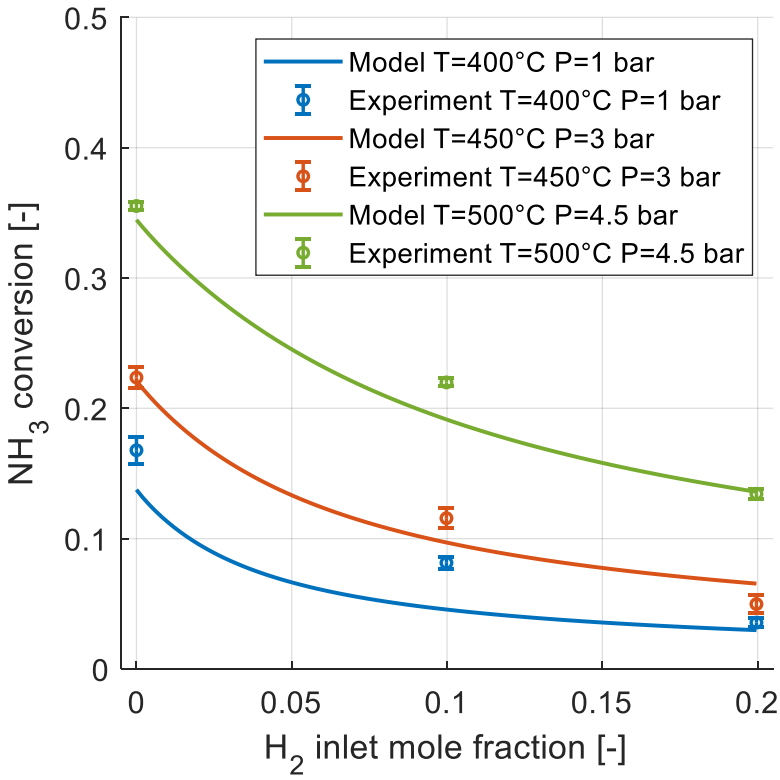

Figure 0.7. *Experimental and numerical ammonia conversion as function of hydrogen inlet molar fraction parametric at different condition of temperature and pressure (runs 28-33).*

3.3.5 Inlet nitrogen concentration effect

In Figure 3.8 it can be seen as during experiments introducing N_2, together with the reactant at the inlet, influences the ammonia conversion. If, indeed, the ammonia conversion is compared in the case of absence and of higher concentration of nitrogen starting from conditions of high temperature and pressure and going down, it shows a decrease respectively from 34.44% to 28.7%, from 22.3% to 17.1% and from 16.7% to 8.8%. The nitrogen seems to have a slight negative effect on reaction rate just in presence of larger inlet composition as showed from the experimental points.

On the other hand, the model does not take in consideration the effect of this factor: despite P_{N2} is present in Temkin's kinetic, it appears on the synthesis term of the formulation, which has no effect since at the temperature range investigated the equilibrium constant, present at the denominator and squared, assumes a value so high to make negligible the contribution of the entire term.

The previous studies present in literature (Antunes et al., 2022; Itoh et al., 2014; Prasad et al., 2009a; Zheng et al., 2007) are in agree with the neutral effect of nitrogen.

Since the trend found is not completely clear, a further investigation is the worth way to proceed, namely repeating the experiments to verify the real role of nitrogen on ammonia decomposition.

Moreover, when N_2 has been injected in reactor inlet, the mass balances do not close at value near 100% as in all the other runs; specifically, the sum of the outlet mole fractions is around

96% and 94% respectively with 10% and 20% initial N_2 mole fraction independently on the conditions of temperature and pressure.

For sure the physics of the system changes when also N_2 is introduced. For example, the kinetic diameter of NH_3 and He is quite different from the one of N_2 (364 vs 260 pm), and it may be possible that this creates an obstruction at the level of active sites.

Nevertheless, the optimization routine has been able to find a good fit: just when the higher N_2 inlet flowrate is fed the relative error overcomes the 10% bound.

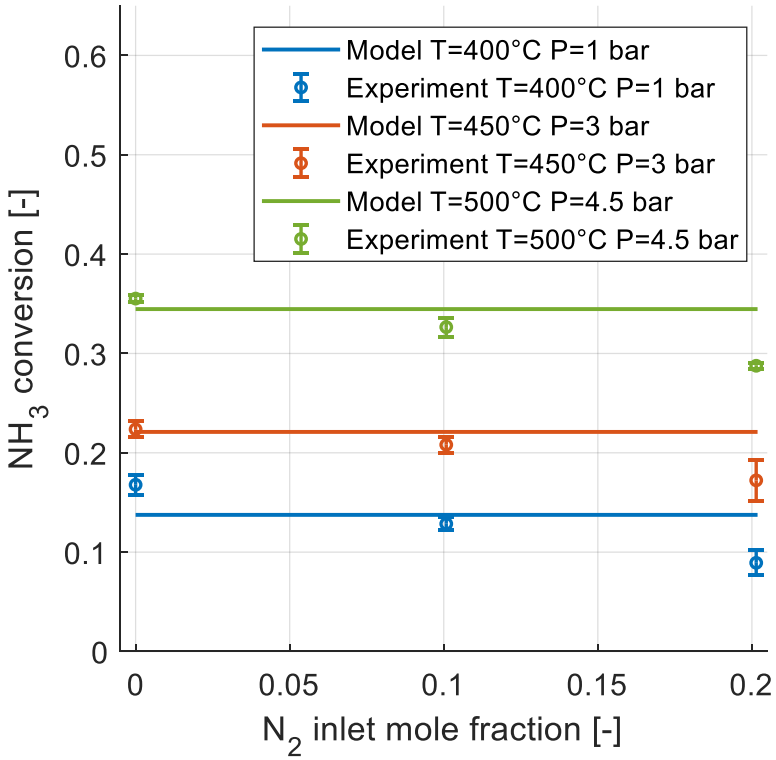

Figure 0.8. *Experimental and numerical ammonia conversion as function of nitrogen inlet molar fraction parametric at different condition of temperature and pressure (runs 34-39).*

3.4 Assesment of the fitting procedure

The Temkin's kinetic parameters obtained from the fit and used on the previous figures are the mean of five optimization routines, each one has datasets for calibration and validation randomly constituted by different runs. This procedure, as mentioned in §2.7, has been required due to the missing of redundant runs that are not essential in capture the factor's effect. The approach adopted guarantees results as parsimonious as possible.

The standard deviations of kinetic parameters reported in Table 3.2 highlight how k_0 is quite sensitive to the chosen validation dataset, meanwhile both β and E_{att} do not present a large variation between the different optimizations. Moreover, focusing on the last three optimizations in Table 3.2, the parameter's values are quite independent from the validation dataset chosen. Although this spotted variability, the model prevision capacity, evaluated

through the coefficient of regression, is similar in all the optimizations.
The exact values estimated from this work to apply at Temkin's kinetic law are:

- k_0 = 23305.41 ± 6170.38 mol·Pa$^{\beta}$/min/g_{CAT}.
- E_{att} = 80.7324 ± 1.7573 kJ/mol.
- β = 0.2206 ± 0.0008.

Table 3.2. *Estimated kinetic parameters of Temkin's law with different calibration dataset.*

	Val. dataset run number	k_0 [mol·Pa$^{\beta}$/min/g_{CAT}]	E_{att} [kJ/mol]	β [-]	**R^2 CAL** [%]	**R^2 VAL** [%]
OPT_1	4-7-11-22-38	18082.28	79.3077	0.2217	94.91	86.92
OPT_2	5-14-18-21-37	15210.86	78.3755	0.2202	94.88	86.83
OPT_3	1-7-17-23-26	27625.11	81.9903	0.2200	94.84	87.52
OPT_4	5-18-20-26-39	28222.52	81.9921	0.2200	94.73	87.06
OPT_5	6-14-17-19-27	27386.29	81.9965	0.2210	94.83	87.68

The reactivity of Ru catalyst for ammonia decomposition is strongly influenced by various factors, such as the preparation condition, the support or the metal dispersion. It is therefore suggested for a fair comparison between catalysts to fix as much physical characteristics as possible.
It is reasonable though, indeed, that the reactivity increases with the percentage of active metal loading on the catalyst, as showed by Zheng et al. (2007). However, in the same work Zheng et al. (2007) have demonstrated as increasing Ru loading on support increases the metal particle size and enlarges the particle size distribution causing a sharp loss in effective utilization of noble metal.
It is reasonable thought according to Di Carlo et al. (2014) that the activation energy and the exponential constant could depend only on the active metal, which is ruthenium in this case, while the pre-exponential factor depends on the catalyst loading on the support. Due to this last observation and the difficulty to find in literature comparable values on the pre-exponential factor, only a comparison respects the other two parameters has been done in Table 3.3.
The activation energy is the lowest between the ones cited, which is a result to highlight since it defines a good catalyst activity. In any case this value of activation energy is found to be in the range of 79-122 kJ/mol, which is the one individualized in previous studies (Zançat, 2020). As regards the exponent of Temkin's law, our model agrees with the value reported in literature, which are all pretty close to 0.2.

Table 3.3. *Comparison of the kinetic parameters obtained in this work with the one retrieved in literature.*

Catalyst and Ru loading	T [°C]	P_{NH3} [bar]	E_{att} [kJ/mol]	β [-]	Reference
Ru/γ-Al_2O_3 (1.9 wt. %)	380-460	0.01-0.05	95	0.179	(Zheng W. et al., 2007)
Ru/γ-Al_2O_3 (2.9 wt. %)	380-460	0.15-0.5	92	0.197	(Zheng W. et al., 2007)
Ru/γ-Al_2O_3 (4 wt. %)	350-450	0.6-0.75	117	0.27	(Prasad et al., 2009b)
Ru/Al_2O_3 (8.5 wt. %)	450-600	1	117	0.5	(Chiuta et al., 2016)
Ru/γ Al_2O_3 (2 wt. %)	400-500	0.1-1.8	80.73	0.221	This study

As regard the goodness of the experimental data fit, evaluating the R^2 coefficient on all the data a value of 94.15% is obtained, which indicate a good capacity of the model to catch reality.
The relative error has been evaluated comparing the experimental and numerical conversion, as defined in Eqn. 3.8 and collected in Figure 3.9.

$$e_{rel} = \frac{\left|X_{NH3}^{exp} - X_{NH3}^{model}\right|}{X_{NH3}^{exp}} \tag{3.8}$$

Even if the experimental trends of ammonia conversion versus the investigated variables are followed by the model, one third of the relative errors are larger than 10%. In particular, the model struggles more to describe the data taken at 400°C and with co-feed of hydrogen in the inlet.
The parity plot in Figure 3.10 shows the correlation between the experimental and calculated value of ammonia conversion for all 39 runs. The points are positioned all pretty close to the bisector indicating a good overall fit result. Moreover the linear trendline that correlates the points differs slightly from the bisector since the equation is: $y = 0.9869 \cdot x$ with R^2 equals 0.9893. Together all these results comfort the goodness of our kinetic study.

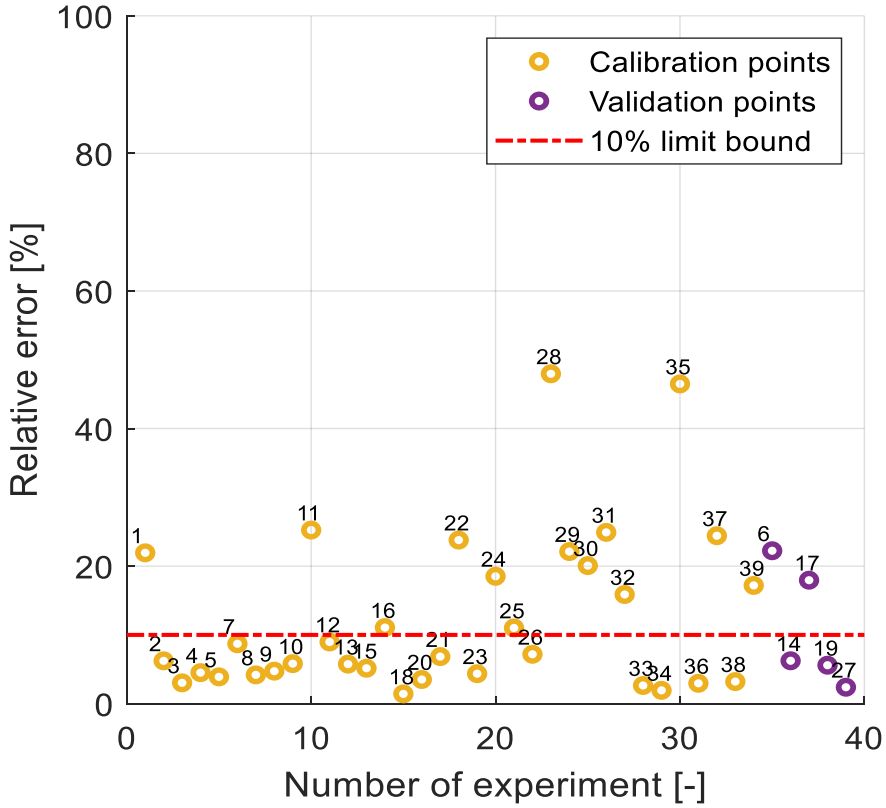

Figure 3.9. *Relative error of each experimental run in the kinetic study.*

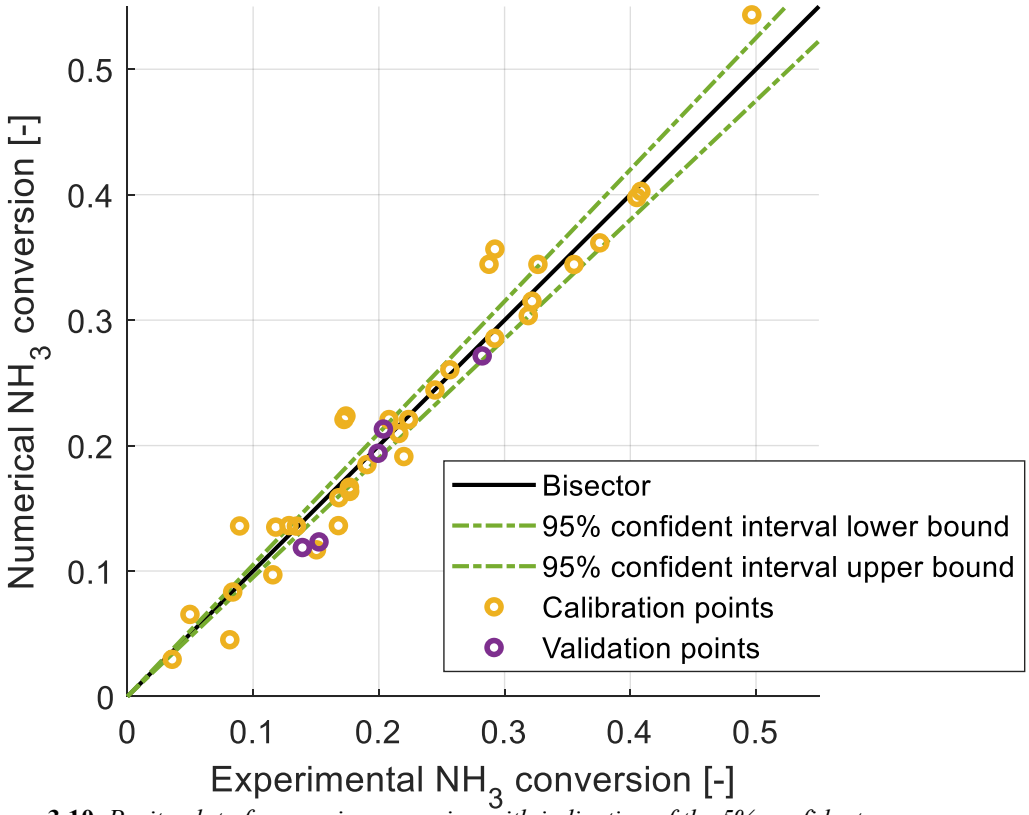

Figure 3.10. *Parity plot of ammonia conversion with indication of the 5% confident error.*

Chapter 4

PBMR: materials and methods

In this work ammonia decomposition has been experimentally performed in a PBR and in a PBMR at laboratory scale. In this chapter a description of the equipment used is provided with a special focus on the Pd-based membrane investigated. It is explained how to deal with the membrane and the procedure followed to characterize its permeation. The reasons under the investigation of ammonia decomposition in PBR and PBMR with different amounts of catalyst are discussed together with the approach followed to perform and elaborate the data of the reaction tests. The results of the experimental tests are then discussed in chapter 5.

4.1 Experimental set-up configuration

The principal features of the set-up illustrated in §2.3 are kept constant in the experiment involving the PBR and PBMR. The major change regards the reaction section: now a cylindrical reactor is set, made of stainless steel SS310, with an inner diameter of 4.5 cm and an active length of 28 cm (versus a total volume of around 0.7 liters). The mixture of gas is pre-heated in a tube that follow with a spiral the external reactor wall before entering from the bottom, as illustrated in Figure 4.1 (a). At the freeboard of the catalyst bed, the reactor has a conical shape which allows to reduce the gas velocity and therefore minimize the risk of catalyst particle escaping.

To switch from PBR to PBMR the membrane is located inside the reactor with a metallic junction on the upper part, which connects the open end of the membrane itself with the permeate tube exiting from the reactor head, as shows in Figure 4.1 (b). There is about 3 cm of catalyst bed between the reactor bottom and the lower part of the membrane to avoid the direct contact of the membrane with pure ammonia fed.

The temperature control is ensured by three K-thermocouples located at different heights in the packed bed, plus one K-thermocouple positioned inside the membrane (permeate side). The pressure is controlled as described in §2.3.

The stream of retentate in PBMR, as well as the outlet in the PBR, is analysed by the μ-GC as described in §1.3. The permeate stream, instead, undergoes alternately a composition analysis through a Fourier-transform infrared spectrometer (FTIR) and a volumetric flowrate monitoring by a high precision film-flowmeter. The FTIR is provided by *Shimadzu* and mounts a 10 m gas cell from *Specac*, and a mercury-cadmium-telluride detector, which is used to quantify only the traces of NH_3 with a detection lower limit of 0.03 ppm. The film flowmeters are provided by *Horiba* and depending on the range of flow analyse, the most suitable one is chosen.

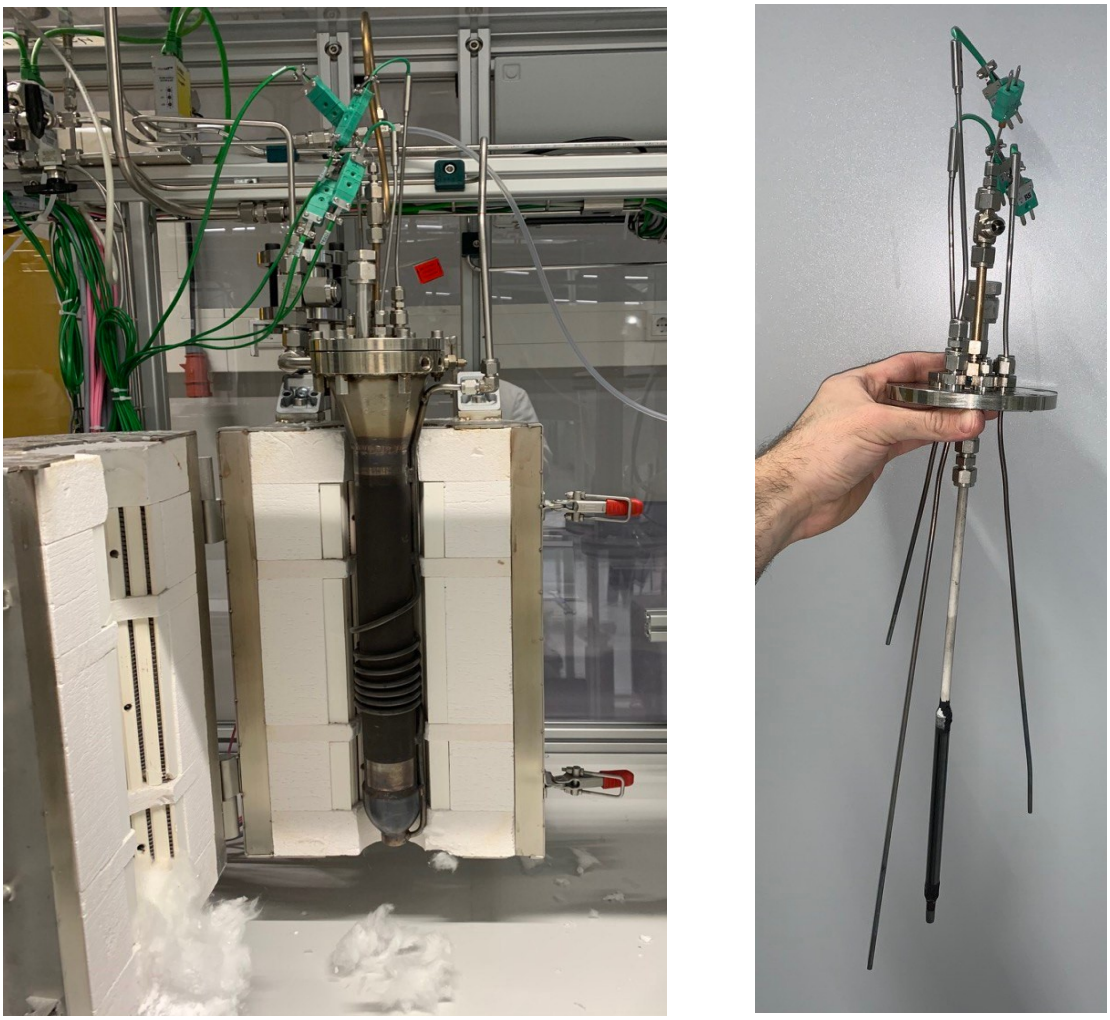

Figure 4.0. *Zoom on the reaction section: on the left (a) the cylindrical reactor located inside the oven; on the right (b) the head of the reactor with the connection for the membrane (not the one used in this work) and the three thermocouples at different heights.*

4.2 Membrane *Arenha-5*

The membrane used in this work (*Arenha-5*) is a double-skin Pd-based membrane provided by *Tecnalia*. In Figure 4.2 it is possible to notice the black shades of the selective layer, which has an active length of 19.4 cm and an external average diameter of 14.3 mm.

4.2.1 Preparation technique

The preparation technique follows the description of Arratibel et al. (2016), which involves the steps described in Figure 4.2.

Making a brief recap, the ceramic tube support is made of α-Al_2O_3 with diameter around 10.0 -10.3 mm and wall thickness of 1-1.5 mm. The support is characterized by an asymmetrical multilayer, namely the porosity decreases from inside to outside with a top surface pore dimension of 100 nm. The ceramic support, above described, is joined with a dense alumina tube to provide proper handling of the membrane (6 mm outside diameter and 1 mm thickness) through a glass junction. Two nano-porous layers are deposited on the external surface: the

selective and the protective one. The manufacture procedure starts with the deposition of a first layer of yttria-stabilized-zirconia (YSZ) and γ-Al_2O_3 (50-50 wt%) through dip-coating and a subsequent activation with nano-palladium nuclei (seeds). The support is again coated with another ceramic layer identical to previous one that form the protective external layer (usual thickness of 1 μm). For last, the tube, with palladium seeds, has been immersed into a plating bath for co-deposition of the Pd-Ag layer.

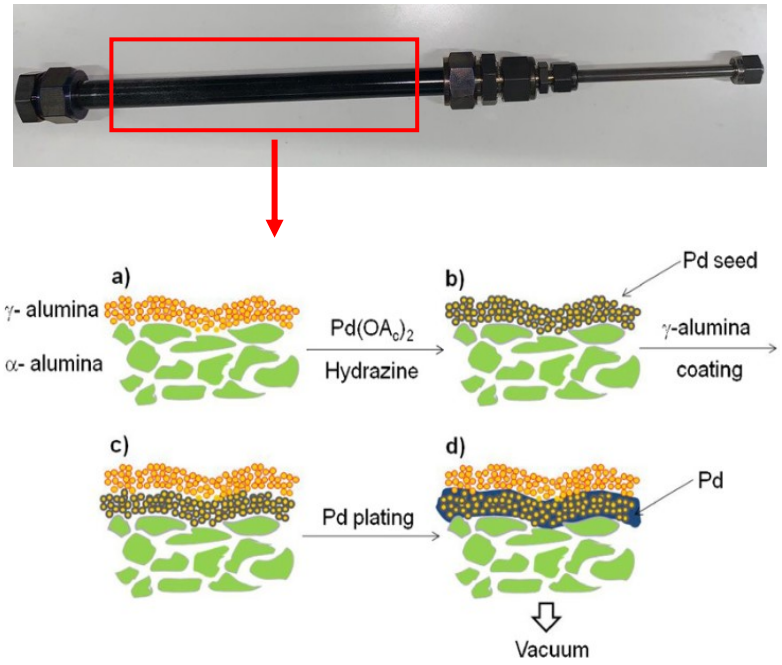

Figure 4.2. *Picture of the membrane under investigation Arhena-5 with a scheme of preparation technique.*

The exact phyco-chemical characteristics of the bi-layer metallic film are unknown: as regard the composition it is estimated usually by measuring the Pd and Ag concentrations of the plating bath before and after the deposition of the layer, while the exact thickness of the different layers can be known just by examining the cross-section of the membrane by scanning electron microscope (SEM). Since *Tecnalia* has not specified the selective layer composition and the membrane has not been cut yet for SEM, the only indication is that the selective layer thickness should be around 1-4 μm.

One end of the membrane is connected to a metallic tube for junction with the exit of the reactor, instead the other end is close with a metallic tap using graphite ferules (Arratibel et al., 2018), since there is no advantage in using a swept gas.

4.2.2 Characterization of the permeation properties

The permeation's characteristics have been evaluated in the range of temperature between 400°C and 500°C, where the ammonia decomposition has proven to be feasible (Collins & Way, 1994; Z. Zhang et al., 2019). Isothermal conditions in both retentate and permeate side have been applied to avoid strain of the membrane and to produce uniform permeation rates as

suggested by Hughes (2001). The pressure, instead, has been always kept at atmospheric condition on the permeate side, instead, on the retentate the investigated range has varied during the different experiments between 1.5 and 5 bar.

Before heating up the system, a leakage test has been performed: the membrane is immersed in a cylinder containing pure ethanol and He is pumped through the junction in the permeate side. A pressure of 1 bar is established, then the inlet gas stream is close meanwhile the same pressure has been monitored. The absence of raising bubbles in the cylinder together with a stable value of pressure ensure the absence of defects not visible with naked eye. After the membrane has been fixed inside the reactor (without catalyst), the system is gradually heating up (0.04°C/min) in the more uniform way to avoid membrane damage. All the temperature increases and decreases are performed under N_2 flow. Once reached 450°C the membrane has been activated, namely the active sites of Pd on the selective layer are woke up. The procedure consists of feeding the system with just H_2 at fixed condition of driving force and monitoring the temporal evolution of the permeate flowrate until it reaches a plateau value, meaning that the performance of the membrane is stable.

Just after the above-mentioned treatments, the single gas tests with both H_2 and N_2 has been made, while for NH_3 the criticality regards its corrosivity make it impossible to measure the flow with the available equipment. To perform these tests the base concept is that the membrane has a maximum of permeate flux reachable for a given driving force applied (Barreiro et al., 2015). Hence the inlet gas flowrate has set by trial-and-error procedure, namely it has been increasing until no increasing on permeation flowrate has been monitored during 15 min. The hydrogen flow is measured by a film-flowmeter, while for N_2 since very low permeation was expected, a *Bronknorst* thermal mass flowmeter has been used capable of reaching quite low range (maximum capacity of 0.7 ml_N/min).

The H_2 flow is described by Sievert's law as explained in §1.7.3, while N_2 should not permeate the membrane ideally, but the presence of small pores/defects makes it possible. Knudsen diffusion is assumed to describe these phenomena (Melendez et al., 2017) due to the hypothesis that it occurs when the pore radius is very small, as should be in a dense selective layer of Pd-base membrane. The permeation takes place following this mechanism if the pore radius is smaller than the mean free path of the gas (in the range of 50- 200 nm for common gas at atmospheric pressure). In this situation, gas molecules have more collisions with the pore walls than with other molecules, and that makes them adsorb momentarily and then release in a random direction (Baker, 2012). Inside a gas mixture in which different species move at different velocities, a separation is possible.

The gas flow due to Knudsen diffusion in a membrane made of cylindrical right capillaries is given by the following equation (Baker, 2012):

$$J = \frac{4 \cdot r_{pore} \cdot \varepsilon_m \cdot (P^{ret} - P^{perm})}{3 \cdot R \cdot T \cdot l_{pore}} \cdot \left(\frac{2 \cdot R \cdot T}{\pi \cdot MW}\right)^{1/2} \quad (4.1)$$

where r_{pore}, l_{pore} and ε_m are physical characteristics of the membrane, respectively pore radius, length, and porosity, instead MW is the permeating species molecular weight. The Knudsen flux results to be inversely proportional to the square root of temperature and direct proportional to the difference in pressure between retentate and permeate. These relationships should be proof by experiments to justify the correctness of the assumption made a priori.
The goal is to obtain the H_2 and N_2 permeance and ideal perm-selectivity to compare the membrane with the other developments within the *Arenha* project (Ammonia Dehydrogenation | ARENHA). Moreover, for as regard H_2 permeation, the values of the parameters n, $E_{att,Pe}$, $k_{0,Pe}$ (illustrated in §1.7.3) permit the eventual modelling of the membrane performance.

4.3 Design of the reaction test

Recalling the project goal, the focus is on understanding if, adopting the membrane *Arenha-5*, an overload of catalyst is present in the PBMR configuration adopted in the previous studies on this topic (Cechetto et al., 2021b, 2022) and on trying to quantify this excess. Indeed, with previous membranes tested in the PBMR, ammonia conversion reaches values around 99% independently on the ammonia feed flowrate provided. The way of proceeding adopted is an experimental evaluation step-by-step.

First the performance of the catalyst (Ru/γ-Al_2O_3 2 wt%) are evaluated in a simple PBR to compare the experimental results with the model based on the kinetic law retrieved previously. In this way it is possible to understand how far the reality is from an ideal case of kinetic regime described by the same equations implemented in §2.3, where the only change regard the extent of the mass domain. The amount of catalyst chosen is 125 g, exactly half the one adopted in the past evaluations.
Based on the result obtained in PBR, different reaction tests are performed in the PBMR varying the gas hourly space velocity and monitoring the key indexes performances: ammonia conversion (X_{NH3}), hydrogen recovery in the permeate (Rec), and the ammonia impurities on the permeate flow (Y_{NH3}^{perm}). The recovery refers to the total amount of pure H_2 separated through the membrane compared to the one fed into the reactor in the form of ammonia as described in Eqn. 4.2.

$$Rec = \frac{N_{H2}^{perm}}{3/2 \cdot N_{NH3}^{in}} \quad (4.2)$$

For an optimal operation, it is desirable both to maximize X_{NH3} and Rec of all the H_2 chemically storage into ammonia, while looking for the minimum traces of reactant in the permeate to obtain a stream directly suitable for feeding the PEMFC.

The experimental set-up has as upper limit 1 l_N/min of NH_3 as possible feed, hence the only way to decrease the gas hourly space velocity is to decrease the amount of catalyst.
The catalyst bed in the PBMR should be able to cover almost completely the surface of the membrane to guarantee the overlapping of the region where there are both reaction and separation simultaneously to take advantage of the benefits derived by the configuration adopted.
For these reasons, the different packed beds are built up keeping constant the solid pellet mass and diluting the catalyst with the use of an inert γ-Al_2O_3, the same species that constitutes the catalyst support. The assumption in which the dilution relies on is that the bulk densities of the two solids are similar like the geometrical shape of the pellet.
Hence, starting on the statement that 250 g of catalyst is the amount necessary to build-up the concept of PBMR, the different catalyst beds evaluated are made respectively by total catalyst (250 g), by half (125 g) and by a quarter (62.5 g) of catalyst where the complementary mass is provided by inert addition. The two solids are randomly distributed inside the catalyst bed as shown in Figure 4.3 (a) and 4.3 (b).

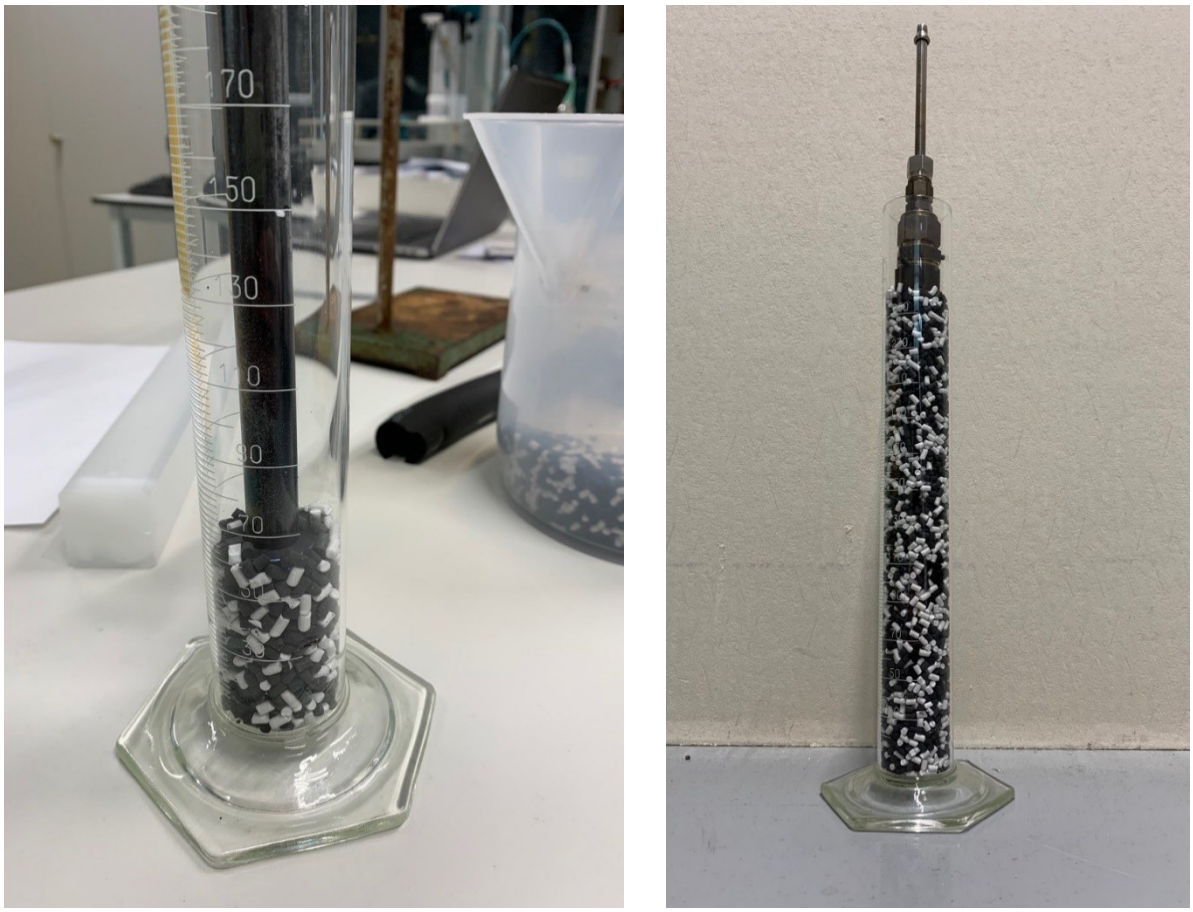

Figure 4.3. *The pictures aim to show the catalyst dilution inside the PBMR simulating the situation in a transparent cylinder of diameter comparable to the reactor one. On the left (a) the base of the reactor where just pellets are present; on the right (b) the entire PBMR where the catalyst and inert cover entirely the membrane area.*

Finally, the influence of temperature and pressure on the index's performance are monitored to understand if the catalyst dilution changes the impact in which these variables affect the PBMR. A recap of the variables manipulated in the experiment with PBR and PBMR are reported in Table 4.1.

Table 4.1. *Overview of the experimental conditions investigated in this work. *Same conditions for permeate and retentate in PBMR.*

Experimental condition	Range investigated
Temperature*	400°C -425°C -450°C -475°C -500°C
Pressure PBR	1 bar -3 bar
Pressure retentate side in PBMR	3 bar -4 bar -5 bar
Pressure permeate side in PBMR	1 bar
Ammonia inlet flowrate	0.5 l_N/min -0.7 l_N/min -0.9 l_N/min
Amount of catalyst	250 g -125g -62.5g

4.4 Elaboration of the experimental data

In order to calculate the ammonia conversion achieved with PBR Eqn 4.4 has been used. It derives by the resolution of system (4.3), where the unknown variables are the outlet ammonia flowrate (N_{NH3}^{out}) and the conversion; indeed, the only data available from experiments is the outlet molar fraction of the ammonia (Y_{NH3}^{out}) retrieved by μ-GC.

$$\begin{cases} X_{NH3} = 1 - \dfrac{N_{NH3}^{out}}{N_{NH3}^{in}} \\ Y_{NH3}^{out} = \dfrac{N_{NH3}^{out}}{N_{NH3}^{in} \cdot (1 + X_{NH3})} \end{cases} \tag{4.3}$$

$$X_{NH3} = 1 - \frac{2 \cdot Y_{NH3}^{out}}{1 + Y_{NH3}^{out}}. \tag{4.4}$$

On the other hand, about the PBMR, the experimental data collected for each test are the following, with at least three repetitions to ensure the achievement of steady state condition and the experimental error evaluation :

- inlet mass flowrate of reactant F_{NH3}^{in} (l_N/min).
- retentate outlet molar composition Y_i^{ret} obtained by μ-GC.
- permeate volumetric flowrate Q^{perm} (ml/min) with correspondent temperature and pressure.
- ammonia composition in the permeate Y_{NH3}^{perm} (ppm) obtained by FTIR.

The procedure followed to retrieve the parameter indexes (X_{NH3}, Rec, Y_{NH3}^{perm}) is based on two assumptions: 1) in the permeate side just hydrogen is present, 2) the ideal gas law is applied.

Both are not strong assumptions since the impurities are quantified in traces and the permeate conditions are high temperatures and atmospheric pressure.

From the permeate volumetric flow through the ideal gas law and the H_2 molecular weight, the mass outlet flowrate in that side of the membrane is retrieved. Based on the mass conservation principle, the retentate mass flowrate is calculated subtracting at the inlet mass flowrate the permeate one. Then from the retentate molar composition, the molecular weight of the mixture is calculated. The retentate mass flowrate is divided for its calculated molecular weight to obtain finally the molar flowrate. At this point through the retentate composition, it is straightforward to estimate both conversion and recovery.

A countercheck is made to verify the validity of the procedure described above: the permeate and retentate hydrogen mole flowrates are summed up and divided for H_2 stoichiometric coefficient (1.5) in order to obtain the theoretical amount of N_2. This value is compared with the calculated one present in the retentate, and the relative error is estimated to monitoring the accuracy of the experimental test.

Chapter 5

PBMR: results and discussion

In this chapter the results obtained experimentally as described in chapter 4 are presented by looking first separately to the membrane unit and the PBR, then at the global picture of the PBMR.

The membrane *Arenha-5* permeance characteristics are compared with the characteristics of other membranes developed within the project *Arenha*, whereas the PBR evaluations help to understand the impact of phenomena like mass transfer limitations and catalyst dilution on the final ammonia conversion. Finally, the results of ammonia decomposition in PBMR are presented and the influence of temperature, pression and especially catalyst dilution are discussed.

5.1 Membrane characterization

First permeation tests with N_2 are performed to investigate the integrity of the membrane, to describe the mechanism of permeation through the defects/pores of the external layer and to quantify how much of the total H_2 flows through the membrane with a mechanism different from the solution-diffusion model.

The test's result reported in Figure 5.1 confirms that Knudsen mechanism can be assumed to

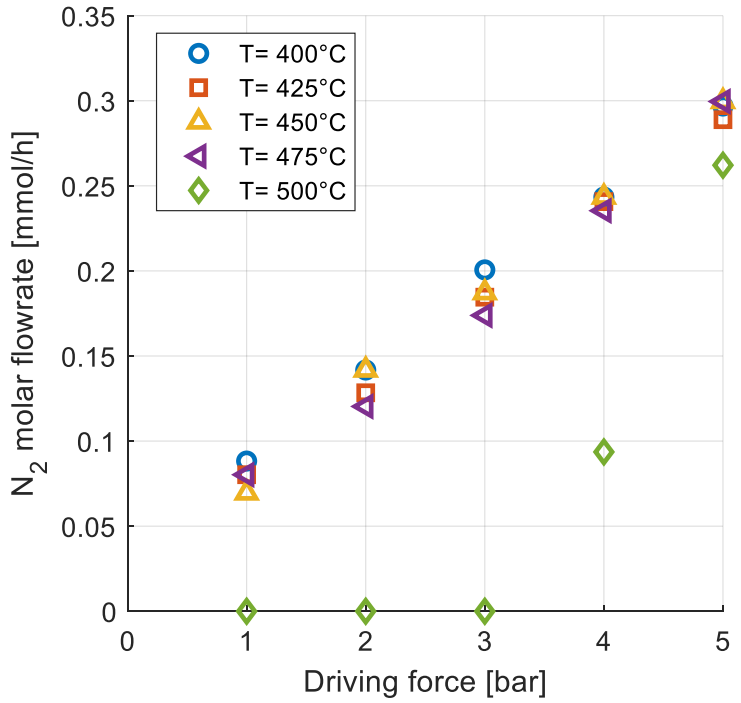

Figure 5.1. *Trend of nitrogen flowrate as function of pressure difference between retentate and permeate side parametric in temperature for the membrane Arenha-5.*

describe the N_2 permeation: the flux is, indeed, function of the pressure difference across the pore in a linear way, instead the temperature makes it decrease. The latter point is evident when operating the membrane at 500°C: the resulting flow is under the limit of relevance for the instrument until a driving force of 4 bar. However, since for the overall data the flow rate value fluctuates in the lower range of measure for the mass flowmeter, the points overlapped frequently in Figure 5.1. Indeed, during the experiments the more stable value is taken as reference.

The relevance of H_2 permeation through Knudsen diffusion is established by correcting the measured N_2 flowrate by $\sqrt{MW_{N2}/MW_{H2}}$, namely multiply for a factor of 3.74 (Arratibel et al., 2016). Then, the calculated H_2 molar flow for each temperature and pressure has been compared with the one measured during single gas test, and the first results at least 5 orders of magnitude smaller than the latter one. Again, after the leakage test response, this provides another proof that defects/pores are not expected to be present at the time in which the tests have been performed.

The trend of the difference of square root of the H_2 partial pressures in retentate and permeate versus the molar flux follows quite well the Sievert's law, which is demonstrated by the R^2 coefficients reported in Table 5.1 referring to the Figure 5.2.

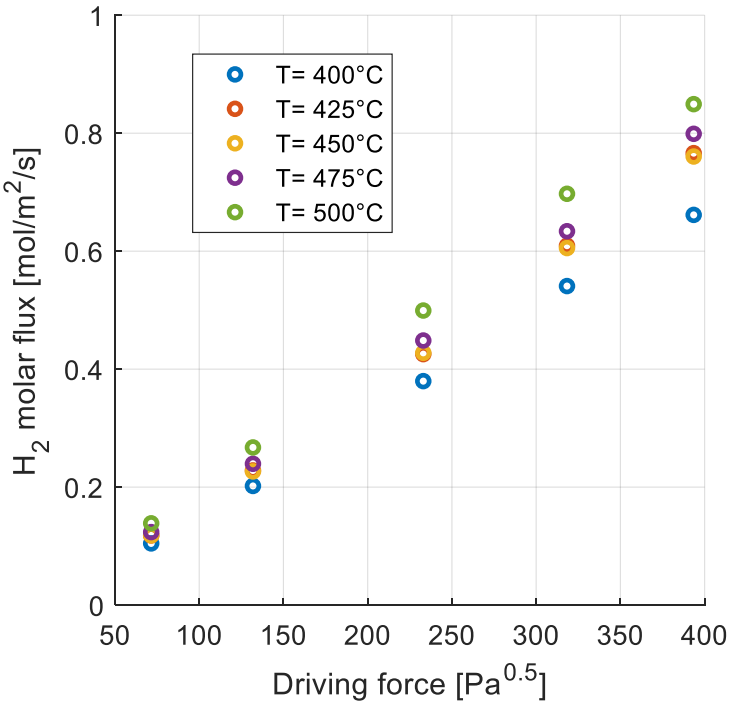

Figure 5.2. *Experimental result of hydrogen single gas permeation test: trend of hydrogen permeating flux versus the Sievert's driving force.*

The implication is that probably the limiting step of permeation is the diffusion of atomic hydrogen through the selective layer. It is evident from Figure 5.2 that for the same driving force applied, increasing temperature also the hydrogen flux permeating the membrane increases.

Table 5.5.1. *The coefficient of correlation (R^2) for different exponents n applied at the H_2 partial pressure in Sievert's law to describe the experimental data.*

T [°C]	Exponent driving force by Sievert's law	R^2 fitting	Exponent driving force by optimization	R^2 fitting
400	0.5	0.9992	0.68	0.9997
425	0.5	0.9988	0.71	0.9999
450	0.5	0.9989	0.69	0.9999
475	0.5	0.9990	0.70	0.9999
500	0.5	0.9996	0.60	0.9998

By linearizing the equation and plotting the logarithm of the hydrogen permeance versus the reciprocal of temperature, a linear relationship is obtained from the Arrhenius law reported in Eqn. 5.1, where the slope is directly related to the activation energy $\left(E_{att,Pe}\right)$ and the intercept to the pre-exponential factor ($k_{0,Pe}$):

$$ln(Pe_{H2}) = \frac{-E_{att,Pe}}{R \cdot T} + \ln\left(k_{0,Pe}\right). \tag{5.1}$$

In Table 5.2 the resulted values obtained for each different retentate pressure are reported. It can be noticed how both $E_{att,Pe}$ and $k_{0,Pe}$ present a variability unexpected when different driving forces are applied.

Table 5.2. *Estimating values of activation energy and pre-exponential factor that describe Arenha-5 permeance through Arrhenius law at different pressures applied.*

P_{ret} [bar]	$E_{att,Pe}$ [kJ/mol]	$k_{0,Pe}$ [mol/m^2/s/Pa$^{0.5}$]
1.5	11.52	1.13e-2
2	11.51	1.18e-2
3	11.24	1.20e-2
4	10.48	1.10e-2
5	10.72	1.14e-2
mean	11.10	1.15e-2

This can be explained by looking at the Figure 5.3, where H_2 permeance is not independent from pressure as expected.

Although hydrogen flux versus the difference of the square root of the hydrogen partial pressure shows a good fitting, the n exponent has been re-estimated by optimizing the experimental data using the method of least squares. The results on Table 5.1 highlight an increase in n values, indicating the influence of something else on the permeation flux (as could be surface processes or transport resistance through the support), and moreover also a dependence on temperature as already reported by Melendez et al. (2017).

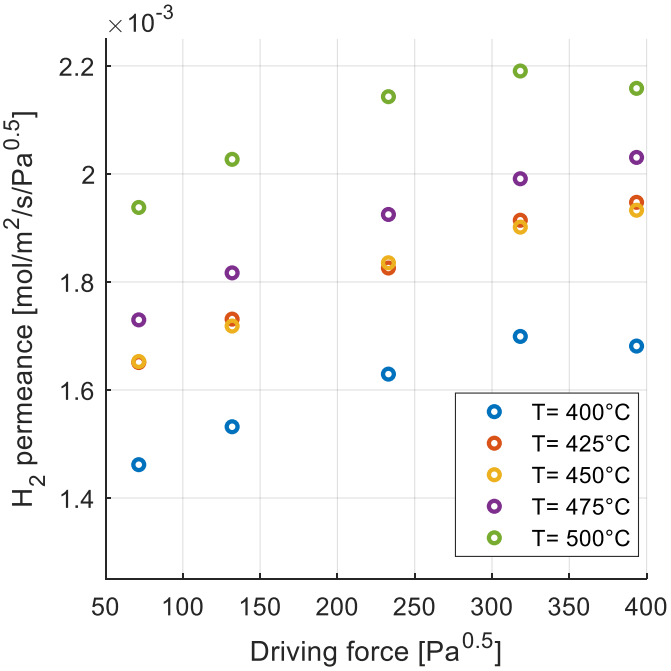

Figure 5.3. *Estimation of hydrogen permeance adopting Sievert's law at different temperatures from experimental data.*

This procedure has as final goal to explain the reason why the H_2 permeance is not independent from pressure. However, as regard the membrane characterization, the Sievert's driving force is taken as reference to compare the result obtained with literature: the mean value retrieved for $E_{att,Pe}$ is in line with the results reported by Liguori et al. (2014), which are in the range between 5.7 kJ/mol and 18 kJ/mol.

In this context, the membrane ideal perm-selectivity defined as the ratio between the H_2 and N_2 flux has been taken as objective function, since the mechanisms of permeation are different and hence the ratio between permeances is not correct. Indeed, the pressure driving force that led the two permeation mechanisms is different.

A comparison with data obtained from previous Pd-based membrane within the project *Arenha* has been reported in Table 5.3. *Arenha-5* seems to be the more promising between the previous membranes: its H_2 permeance is comparable to the one guarantee by the thinner *Arenha-1*, and at the same time it shows the lowest N_2 permeance. The combination of the two features guarantees the best performance in term of ideal perm-selectivity.

Table 5.3. *Comparison between Pd-base membranes developed within the project Arenha at temperature of 450°C and pressure of 2 bar in the retentate.*

Membrane code	Thickness selective layer [μm]	H_2 permeance [mol/m^2/s/Pa$^{0.5}$]	N_2 permeance [mol/m^2/s/Pa$^{0.5}$]	Ideal perm-selectivity H_2/N_2
Arenha-1	≃1	2.22e-6	4.26e-10	5.21e3
Arenha-3	≃6-8	1.15e-6	1.66e-10	6.90e4
Arenha-5	N/A	2.18e-6	2.18e-11	1.03e5

5.2 Reaction tests in PBR

After the characterization of the membrane, the PBR performance is experimentally studied. The approach followed aims at evaluating separately the two units of reaction and separation which constitute the PBMR. In this way it is possible to isolate the issues related to the fixed bed reactor (mass transfer limitations and catalyst dilution) without checking for them in a more complex unit.

5.2.1 Assessment of mass transfers limitations

The performance of packed bed reactor, in terms of ammonia conversion, establishes the catalyst activity in form of pellet, and it is used to compare the experimental results with the ones obtaining applying the Temkin's law previously derived in the kinetic presented in §2.7. The amount of catalyst weighted initially is 125 g, that becomes 115 g after the experiment due to the loss of hygroscopic water. The quantity has been chosen after checking that it is enough to reach theoretically a reasonable high conversion. The only variable changed during experiment is temperature, while the outlet pressure is kept at 1 bar and the reactor is fed with 0.9 l_N/min of pure ammonia. The results are summarized in Table 5.4, where the thermodynamic conversion is also inserted. The pressure drops are negligible in these experiments.

Table 5.4. *Ammonia conversion at different temperatures, atmospheric pressure and 0.9 l_n/min of feed flowrate from experiments, calculated by kinetic model and by thermodynamic.*

Temperature	Ammonia conversion			
	Experiment	Std deviation	Kinetic model	Thermodynamic
400°C	50.12%	± 1.31%	98.91%	99.57%
425°C	71.70%	± 1.59%	99.23%	99.69%
450°C	90.23%	± 0.27%	99.44%	99.77%
475°C	95.65%	± 0.01%	99.58%	99.83%
500°C	96.11%	± 0.01%	99.68%	99.87%

Some observations can be retrieved:

- despite the thermodynamic is not more a constraint at temperature above 400°C and atmospheric pressure, the experimental conversion is quite far from the upper limit.
- the difference between the model and the experiment decreases as temperature increases.
- in any case, both experiment and model derived conversions are lower than the thermodynamic limit.
- 125 g of catalyst guarantee to reach conversion >90% starting from 450°C and working at 1 bar.

The first point is explained by the presence of mass transfers limitations, which result detrimental for the performances of this reactor configuration. There are no doubts about that, since dealing with large and porous particle pellets, and not more with small quantity of powders, both the external and the internal mass transfer resistances become relevant. Indeed, the mass transfer coefficient between bulk of the gas phase and catalyst surface decreases as the catalyst particle diameter increases and the fluid velocity decreases. If the conditions in which the kinetic study is applied are compared with this study, it is possible to observe that the catalyst size is increased of two orders of magnitude while the total flow is approximately the same. Instead, the internal mass transfer depends on the gas diffusion inside the porosity of the pellet since the active sites are present on the pore walls. Moreover, some doubts about the flow pattern inside the reactor should be clarify since the plug flow condition may be not verified. Indeed, a catalyst support plate is missing respect the standard packed bed reactor.
The second point seems to be in contrast with the behaviour expected theoretically: at lower temperature the kinetic should be the slowest step and, instead, at high temperature the mass transfer should govern the process. Therefore, it is expected a closer conversion between the model and the experiment at low temperature respect to high temperature. Indeed, the model implemented to describe the packed bed reactor is based on Eqn. 2.3, namely it has as assumption that the reactor works under kinetic regime. A possible answer at that issue can be found looking at the values of conversion predicted by the model: since they are always higher than 99%, the kinetic at 400°C doesn't represent a limiting step. Hence, the trend of difference between numerical and experimental conversion may be explained by the decrease of mass transfer limitations with increasing temperature. However, to confirm this statement a model should be implemented to describe the situation since the mass transfers are, in general, less affect by temperature than kinetic.
The third point highlights the consistency of the kinetic model derived previously, since the related conversion never crosses the thermodynamic upper limit as expected.
The last point, instead, gives an indication about the mass of catalyst to use in the PBMR experiments considering that the conversion is already high at 450°C and an improvement is expected by the co-presence of the membrane. Hence, as first trial, the catalyst mass used in the following study has been of 125 g.

5.2.2 Effect of catalyst dilution

The catalyst dilution in packed bed has been investigated since its effect is quite difficult to imagine. Usually, the catalyst dilution is applied to make the heat removal easier and to reduce the hot spots when dealing with exothermic reactions. However, also with endothermic reaction the heat manage should be improved, since the impact of cold spots in the initial part of the packed bed can be minimized if the catalyst is diluted. Namely, what is expected is an easier control of temperature to reach isothermal conditions.

The experimental results described in §5.2.1 have been compared with tests carried out in the same operative conditions but adding 125 g of inert γ-Al_2O_3 with the 125 g catalyst.
The data reported in Table 5.5 show that there is a systematic small improvement in terms of conversion where the packed bed of catalyst is diluted with inert material.
However, the effect on conversion is quite limited and in a future modelling the assumption to neglect the catalyst dilution may be not so strong; if it has to be taken in consideration it will go to influence the energy balance. Indeed, this result is probably due to the thermal effect of inert that damps the temperature oscillations, hence it increases the probability to effectively have an isothermal condition inside the reactor, which favours the kinetic.

Table 5.5. *Experimental comparison of ammonia conversion in PBR at atmospheric pressure and 0.9 l_N/min of feed flowrate in case of 125 g of Ru/ γ-Al_2O_3 and 250 g of half Ru/γ-Al_2O_3 and half γ-Al_2O_3.*

Temperature	Catalyst		Catalyst (50 wt%) + inert		Comparison
	X_{NH3}	Exp. error	X_{NH3}	Exp. error	
400°C	50.12%	± 1.31%	51.87%	± 1.52%	+1.74%
450°C	90.23%	± 0.27%	93.34%	± 0.29%	+3.11%
475°C	95.65%	± 0.01%	96.13%	± 0.08%	+0.49%
500°C	96.11%	± 0.01%	96.33%	± 0.04%	+0.21%

5.3 Improvement adopting PBMR

Working with PBMR has different advantages as already explained in §1.8, and in Table 5.6 it is possible to quantify them. The experimental conversions are compared in the case of packed bed made-up of 125 g of catalyst diluted with 125 g of inert with and without the implementation of the membrane.

Table 5.6. *Experimental comparison of ammonia decomposition: PBR versus PBMR. Both packed beds have a catalyst concentration of 50 wt%.*

T	P	Q_{NH3}	Ammonia conversion ± Experimental error [%]			
[°C]	[bar]	[l_n/min]	PBR		PBMR	
450	3	0.5	90.2%	± 2.2%	97.69%	± 0.47%
450	3	0.7	88.6%	± 0.8%	95.34%	± 0.36%
450	3	0.9	80.7%	± 2.2%	91.36%	± 0.21%
450	5	0.9	73.1%	± 1.8%	96.11%	± 0.37%

In the PBMR the conversion is closer to the thermodynamic limit (around 99%) respect the PBR, even if in the conditions reported the shift effect is not present. Indeed, it has to be underline that the thermodynamic gives just the maximum endpoint that can be reached by reaction, but the kinetic is governing for a finite value of GHSV.
The improvement must be linked to the membrane action of depleting selectivity hydrogen from the environment of reaction, which has a marked inhibited effect as shown in the kinetic

study. This statement is clearly justified by the different trend of conversion versus pressure for the two configurations.

5.4 Reaction tests in PBMR

In paragraph §5.2 it has been demonstrated that the system under study is strongly affected by mass transfer limitations, while the dilution of the catalyst has instead a marginal effect. For sure these phenomena can be found again when dealing with a PBMR. Moreover, related to the use of high permeable Pd-membrane, concentration polarization may be another aspect to take in consideration as reported in §1.8.
For these reasons, it has been preferred an experimental approach to the problem of finding the best conditions of catalyst quantity, temperature, and pressure to maximize the performance of ammonia decomposition in PBMR, with the numerical simulation of the system leaves as future prospective.

5.4.1 Analysis of catalyst mass

Following the procedure described in §4.3, three different cases of PBMR have been studied: in the first configuration just Ru/γ-Al_2O_3 constitute the catalyst bed with an amount of 250 g, then two different configurations are obtained diluting the catalyst with γ-Al_2O_3 (inert). The dilution 50 wt% refers to a catalytic bed made of half catalyst and half inert (125 g each); the dilution 25 wt% refers to a catalytic bed made of 62.5 g of catalyst and 187.5 g of inert.
The results regarding ammonia conversion are reported in Table 5.7.

Table 5.7. *Experimental analysis on ammonia conversion in PBMR with different compositions of the packed bed and at different operative conditions.*

Operative conditions			**Ammonia conversion ± Experimental error [%]**					
T	**P^{ret}**	**Q_{NH3}**			**Diluted catalyst with inert**			
[°C]	[bar]	[l_N/min]	**100 wt% catalyst**		**50 wt% catalyst**		**25 wt% catalyst**	
475	4	0.9	98.23%	± 1.56%	98.12%	± 0.09%	98.14%	± 0.13%
475	4	0.7	98.05%	± 0.79%	98.28%	± 0.07%	98.07%	± 0.38%
475	4	0.5	97.81%	± 0.13%	98.24%	± 0.11%	98.36%	± 0.25%
450	4	0.9	97.75%	± 0.29%	95.24%	± 0.19%	87.52%	± 1.91%
450	4	0.7	97.64%	± 0.79%	96.69%	± 0.25%	92.12%	± 0.57%
450	4	0.5	97.70%	± 0.41%	98.10%	± 0.10%	98.00%	± 0.87%
400	4	0.9	65.76%	± 3.12%	42.80%	± 0.30%	32.42%	± 3.44%
400	4	0.7	70.27%	± 1.94%	43.66%	± 9.52%	37.89%	± 4.37%
400	4	0.5	81.46%	± 0.56%	53.47%	± 0.89%	44.28%	± 0.84%

Starting with 100 wt% catalyst configuration, it can be noted that at 475°C varying the inlet flow of ammonia has not influence on the achieved conversion. The same is observed also at 450°C, and more interested, there is no significative difference respect the conversion at higher temperature. This can lead immediately to the conclusion that the temperature as the flowrate

have not influence in these cases. The probable cause is an overload of catalyst, since in any of the case described until now the conversion is high (around 98%). Indeed, theoretically, a decrease of the residence time should lead to a decrease in conversion, as well as a decrease in temperature should lead to the same conclusion since the kinetic is slowed down at low temperature. Moreover, also the permeability of the membrane is function of temperature as reported in §1.7. These trends are identical to the one reported by Cechetto et al. (2021, 2022), as expected thanks to the optimal membrane permeation. At 400°C, instead, an overall decreasing in conversion is present together with the expected negative effect increasing the reactant flowrate.

In the second column of ammonia conversion on Table 5.7, the results of 50 wt% catalyst packed bed configuration are reported. At 475°C still there is no difference varying the inlet flowrate, and moreover the conversions are the same as the previous configuration, even better in the case of 0.5 l_N/min probably due to a higher isothermal condition inside the reactor. At 450°C the expected trend with the increase of feed flowrate is noted; however, the conversions are not so distant from the configuration with just catalyst in the packed bed, but rather there are similar results for both 0.7 l_N/min and 0.5 l_N/min. At 400°C a drastic decrease on performance is present both compared the same configurations at higher temperatures and the different configurations at the same operative conditions. Furthermore, less improvement in conversion is noticed by decreasing the feed flowrate with respect to the identical condition in the first configuration case.

A further dilution experiment (25 wt% catalyst), third column of ammonia conversion on Table 5.7, provides a further proof of our initial idea of catalyst overload: again, at higher temperature there is not an appreciable difference with respect to previous two catalyst beds. Instead, at 450° a difference is present since probably the catalyst is not more in excess to compensate its decrease activity with temperature, even if still with 0.5 l_N/min of ammonia the conversion reaches the maximum reported in this work of about 98%. At 400°C the smallest conversion obtained in this work is recorded.

To explain the experimental evidence the comparison between 100 wt% and 25 wt% catalytic bed concentrations should be taken in consideration. In both cases at the beginning of the reactor the highest reaction rate is expected since the concentration of ammonia is higher. Linked to this, also cold spots may be present which make decrease both the kinetic and the membrane permeation. The excess of catalyst, however, permits to reach at the same way optimal performance. As an alternative, if catalyst is diluted, the peak of temperature decreasing can be imagined to be smoother, namely low temperature membrane zone at the beginning of the reactor are less probable. Moreover, the fact that the inert and the catalyst surrounded the membrane alternatively, makes also possible the separation to take place easier, since at high pressure in the retentate at the beginning it may occur that locally the membrane capacity to permeate the hydrogen is not balanced with the reaction rate.

To characterize the performance in the three packed bed configurations, also the hydrogen recovery, reported in Table 5.8, is a useful index to quantify the system productivity.

At highest temperature (475°C), the hydrogen recovery shows similar values between the three configurations for the same GHSV. This behaviour is very important in our study: indeed, even if the final conversion is the same for high temperature, it does not follow automatically that also the recovery will be equal. For the hydrogen produced to permeate, it is required the contact with the membrane: this is not guaranteed if the reaction occurs until the end of the reactor. The conclusion after this statement is that the final conversion is reached before the end of the PBMR, and so the catalyst can be further decreased inside the reactor at 475°C, thus the optimum condition is not still reached.

Moreover, always at 475°C, the fact that the recovery is almost the same for different flowrates and packed bed means that the membrane is not the limiting step of the process: increasing the flowrate and keeping constant the conversion, means higher quantity of hydrogen developed that in any case is able to permeate since the capacity of the membrane is not reached.

Decreasing the temperature both the kinetic and the membrane permeability goes down, leading to lower recovery theoretically.

At 450°C, the trend of recovery reflects the one of conversion: indeed, where there is no change in conversion (Q_{NH3} =0.5 l_N/min) the recovery performs at the same way between the three configurations and also in similar way respect higher temperature. Instead, where the conversion is decreasing also the recovery is decreasing: this trend is expected since lower ammonia conversion means lower hydrogen partial pressure on the retentate side, hence lower driving for the recovery.

At 400°C there is a steep decrease in recovery, that becomes even lower 10% in the case of 25 wt% diluted catalyst and 0.9 l_N/min of ammonia feed.

Table 5.8. *Experimental analysis on hydrogen recovery in PBMR with different compositions of the packed bed at different operative conditions.*

Operative conditions			**Hydrogen recovery ± Experimental error [%]**					
					Diluted catalyst with inert			
T	**P^{ret}**	**Q_{NH3}**						
[°C]	[bar]	[l_N/min]	**100 wt% catalyst**		**50 wt% catalyst**		**25 wt% catalyst**	
475	4	0.9	90.77%	± 0.06%	88.67%	± 0.06%	90.09%	± 0.38%
475	4	0.7	91.78%	± 0.04%	92.84%	± 0.04%	92.75%	± 1.85%
475	4	0.5	92.51%	± 0.09%	93.21%	± 0.02%	93.81%	± 0.50%
450	4	0.9	88.84%	± 0.13%	81.38%	± 0.06%	72.48%	± 0.20%
450	4	0.7	91.79%	± 0.08%	87.81%	± 0.19%	84.38%	± 0.82%
450	4	0.5	92.16%	± 0.20%	91.42%	± 0.19%	92.06%	± 0.22%
400	4	0.9	39.62%	± 0.04%	16.04%	± 0.02%	8.14%	± 0.08%
400	4	0.7	49.09%	± 0.16%	17.42%	± 0.12%	13.71%	± 0.04%
400	4	0.5	65.27%	± 0.15%	32.72%	± 1.01%	23.35%	± 0.05%

As final index, the quality of the permeate is monitored in Table 5.9, referring to the ammonia as impurity present. Ideally the ammonia should not permeate through the selective layer. However, the presence of defects in the external layer, as well in the connections, permits to find traces of that species in the permeate. The mechanism of permeation should follow the Knudsen's law as demonstrated in in §5.1, hence the permeate flow decreases with increasing of the temperature. Moreover, it is expected to find more ammonia where the conversion is lower, namely its driving force to permeate is higher.

The experiment data do not show the expected trends. Indeed, the impurities content presents a maximum at 450°C and not a systematic trend varying the inlet flowrate. Since the reactant enters from the bottom part of the reactor, where there is also the dead-end of the membrane, the composition of the permeate should depends on the amount of catalyst that is positioned between the start of the packed bed and the membrane sealing: the higher the conversion achieved before reaching the membrane, the lower probability to find impurities on the permeate. This factor varies a lot when the dilution of catalyst in the packed bed is applied, and the configuration with 25 wt% of catalyst should be the worst situation, which results true only at 475°C in the experiments. The explanation to this misalignment is probably due to the timing in which the work has been developed: indeed, the built-up of the PBMR leads to unavoidable mechanical wear of the sealing as well as birth of defects due both to the abrasion with the pellets and the continuous heat up and cold down of the system. A possible verification (not done) could be the monitoring of the nitrogen permeation at each test to establish the presence or not of a decrease in the selectivity.

Table 5.9. *Experimental analysis on ammonia traces in permeate stream of PBMR with different compositions.*

Operative conditions			**Ammonia concentration in permeate side ± Experimental error [ppm]**					
T	**P^{ret}**	**Q_{NH3}**			**Diluted catalyst with inert**			
[°C]	[bar]	[l_N/min]	**100 wt% catalyst**		**50 wt% catalyst**		**25 wt% catalyst**	
475	4	0.9	63.9	± 8.2	78.3	± 2.8	89.6	± 1.0
475	4	0.7	52.8	± 0.4	68.0	± 3.9	92.9	± 1.3
475	4	0.5	37.7	± 2.7	60.5	± 4.6	98.0	± 2.3
450	4	0.9	122.4	± 0.4	120.2	± 2.2	92.8	± 1.5
450	4	0.7	121.1	± 0.8	123.3	± 0.1	92.3	± 1.4
450	4	0.5	118.7	± 1.7	122.3	± 1.3	86.6	± 0.9
400	4	0.9	105.4	± 0.9	95.3	± 1.7	54.5	± 1.8
400	4	0.7	106.1	± 1.2	94.2	± 0.1	63.3	± 1.0
400	4	0.5	107.4	± 1.3	99.0	± 2.4	62.4	± 2.4

5.4.2 Effect of temperature and pressure

The next step is the tuning of temperature and pressure to reach the highest performances.

The temperature effect has been indirectly investigated previously: higher temperature leads to higher conversion and recovery since both the reaction rate and the membrane permeability

increase. However, it has been shown that also working at 450°C, instead of 475°C, with a reduction of the ammonia feed at 0.5 l_N/min can lead as well at the highest performance. A further analysis is needed to understand the more convenient way to proceed: at higher temperature with maximum quantity of hydrogen produced or at the lower temperature, namely less energy consumed, but with lower hydrogen production.

In regard to the pressure effect, data are reported in Table 5.10 for the configuration with 25 wt% catalyst concentration in the packed bed. Nevertheless, it must be stated in advance that the observations made are valid independently on the packed bed catalyst concentration, as experimentally verified.

The conversion seems to be slightly affected by pressure: an increase of the average value is present as pressure increases, independently on the operative temperature, but for most of the cases the improvements are not larger than the experimental error, so not significative.

A trade-off is theoretically present: high pressures are needed to exploit the advantages of the PBMR illustrated in §5.3, but on the other hand the reaction kinetic is inhibited by high pressure. These two effects seem to cancel each other.

As regard the recovery, instead there is a clear advantage to increase the total pressure on the retentate side: acting on the driving force is possible to increase the productivity of the system. The optimal solution should be working at the highest pressure.

For the impurities, reliable data are not available as in §5.4.1. Theoretically the increase in driving force is the same both for hydrogen and impurities, like ammonia and nitrogen, so high pressures may be detrimental for the permeate stream purity (Cechetto et al., 2022).

Still the membrane used in this study is quite far from allowing to obtain high quality hydrogen as required by PEMFCs (Y_{NH3}^{perm} ≤0.1 ppm): just looking at the order of magnitude, consider reliable for the experiments performed, the ammonia concentration should decrease of two/three orders of magnitude.

Table 5.10. *Experimental analysis on PBMR performances, in particular the case of 25% wt catalyst concentration in packed bed at different operative conditions.*

T [°C]	**P^{ret}** [bar]	**Q_{NH3}** [l_N/min]	**NH_3 conversion** [%]		**H_2 Recovery** [%]		**NH_3 concentration in permeate** [ppm]	
475	3	0.7	97.83%	± 0.51%	83.25%	± 0.13%	115.11	± 3.19
475	4	0.7	98.07%	± 0.38%	92.75%	± 1.85%	92.89	± 1.34
475	5	0.7	98.23%	± 0.76%	94.90%	± 0.98%	88.64	± 0.66
450	3	0.7	90.40%	± 1.70%	68.80%	± 0.59%	90.01	± 0.43
450	4	0.7	92.12%	± 0.57%	84.38%	± 0.82%	92.27	± 1.37
450	5	0.7	93.81%	± 0.48%	90.08%	± 0.15%	98.99	± 1.62
400	3	0.7	34.05%	± 0.72%	3.98%	± 0.09%	77.31	± 6.54
400	4	0.7	37.89%	± 4.37%	13.71%	± 0.04%	63.25	± 0.95
400	5	0.7	36.14%	± 0.64%	19.21%	± 0.06%	59.07	± 0.71

5.5 Progress in membrane development

As already discussed in §5.1, the membrane *Arenha-5* has shown performance at single gas permeation tests very promising comparing with the previous prototypes. In regard to the reaction test, the performances indexes of *Arenha-5* are compared with the ones of *Arenha-3* when dealing with the packed bed 100 wt% of catalyst in Table 5.11. Even if the previous study goal is different, namely, to look for the conditions of obtaining the required purity in the hydrogen stream exiting on the permeate, a reasonable discussion is necessary to carry out. Comparing, indeed, data at 500°C of *Arenha-3* versus data at 475°C of *Arenha-5* is possible to see a clear improvement in recovery with comparable conversion on the other side. This means that the membrane itself is responsible of a better performance as expected from the hydrogen permeation test: even if the lower temperature, that motivate the small difference in conversion, the hydrogen which permeates is higher, despite the permeance is also itself a clear function of temperature. To reach comparable hydrogen recovery, *Arenha-3* has to work at both higher temperature and pressure in the retentate. Instead, the permeate purity is worst for *Arenha-5* in any case. For sure this is influenced by the more time using of the membrane itself before this study, but anyway it is on the same order of magnitude. Definitely, the procedure to build and disassemble inevitably involved the abrasion of pellets with the membrane external layer and this is going to increase the N_2 permeance.

Table 0.11. *Comparison of the performances in reaction test for membranes developed inside Arenha project.*

Membrane Code	T [°C]	P^{ret} [bar]	Q_{NH3} [l_N/min]	X_{NH3} [%]	Rec [%]	Y_{NH3}^{perm} [ppm]
Arenha-3	500	4	0.5	99.8	84.84	<0.750
Arenha-3	500	6	0.5	99.8	91.57	3.650
Arenha-5	475	4	0.5	97.8	92.5	37.74

Conclusions

The Thesis's work has targeted the improvement of the Ru-based catalyst usage in ammonia decomposition carried out in a lab-scale packed bed membrane reactor. The decrease of its quantity constitutes an important step toward the economic feasibility of the hydrogen economy due to the high cost of the catalyst itself. Indeed, even if alternative metals have been tested, the high purity of hydrogen required together with the need of relative low temperature operations lead to prefer ruthenium, since it has been demonstrated to be the more active for ammonia decomposition reaction.

The kinetic study to characterize the ruthenium (2 wt%) on γ-Al_2O_3 catalyst has showed to follow Temkin's kinetic model, with the following fitting parameters obtained: k_0 = 23305.41 ± 6170.38 mol·Pa^{β}/min/g_{CAT}, E_{att} = 80.7324 ± 1.7573 kJ/mol, β = 0.2206 ± 0.0008. The reaction results to be not favoured by high pressure and, more important, hydrogen is a species which inhibits the kinetic. This last point reinforces the reasons which have guided towards the used of membrane reactors to improve the ammonia conversion. The nitrogen seems to have a slight negative effect on ammonia conversion in contrast with the previous studies reported in literature, hence a further investigation should be done. However, in this study the experimental runs involving nitrogen in the inlet are still part of the fitting procedure. Moreover, further experimental points can be added on the kinetic study to improve its accuracy, maybe changing the amount of catalyst involved and, of consequence, the inlet flowrate.

When, instead, dealing with simple packed bed reactor the negative effect of internal and external mass transfer limitations has been showed to be detrimental for the final conversion: a large difference has been noticed between the experiments and the numerical simulation of the reactor under the kinetic regime in term of ammonia conversion. Further, the addition of inert pellets of γ-Al_2O_3 in the catalytic bed has experimentally showed a slight increase on ammonia conversion and an easier temperature control of the system. For an endothermic reaction, like this dehydrogenation, the more probable explanation is a better isothermal condition ensures by the presence of inert, which facilitates the heat transfer and decreases the probability of cold hotspots.

The catalyst dilution within the membrane reactor has been performed keeping constant the mass of total solids to cover entirely the membrane surface. The experimental results highlight as decreasing the quantity of catalyst from 250 g to 62.5 g has not showed significant differences in ammonia conversion and hydrogen recovery at 475°C. Lowering the reaction temperature at 450°C, instead, has demonstrated to make the system sensible to inlet ammonia flowrate variations.

The best performance recorded in this study are ammonia conversion of 98.83% and hydrogen recovery of 94.90% obtained at 475°C and 5 bar, independent by the catalyst concentrations

and inlet reactant flowrates adopted during this work.

The idea of catalyst dilution with inert in a PBMR offers as further advantage to avoid the presence of local cold spots detrimental for kinetic, permeance and membrane stability.

As regard the membrane used (*Arenha-5*), it represents a step forward respect the previous prototypes due to the improvement on hydrogen recovery, meanwhile the ammonia traces on permeate side largely exceed the fuel cell limits of 0.1 ppm. However, the usage in repeated experiments may have influenced the mechanical integrity of the membrane and it may have created some small superficial defects not visible by naked eye. A continuous monitoring of the membrane's property to not permeate NH_3 should be done from the beginning.

In this work a lot of experimental data has been collected and a reliable kinetic law retrieved. These two things represent almost all the ingredients necessary to start a detailed modelling approach of the system. Starting from the packed bed reactor, it may be possible to describe the mass transfer limitations and to validate the model with experimental data. Further the membrane reactor may be modelled since the law describing the permeation has already retrieved from the single gas tests. The only missing information will be the one respect the impact of concentration polarization, which could be established experimentally with binary mixture tests without involving the catalyst. With a validated model it will be possible to obtain the optimum quantity of catalyst in each condition of the membrane reactor, since as observed in this study with a catalyst concentration of 25 wt% in the packed bed, an excess is still present.

Nomenclature

Bi_i	Biot number of component *i*	[-]
C_i	Molar concentration of component *i*	[mol/m^3]
C_M	Mears coefficient	[-]
C_{WP}	Weisz-Prater coefficient	[-]
$D_{i,j}$	Binary mixture molecular diffusion coefficient	[m^2/s]
$D_{i,m}$	Molecular diffusion coefficient of component *i* in bulk gas	[m^2/s]
$D_{i,k}$	Knudsen diffusion coefficient of component *i*	[m^2/s]
$D_{i,eff}$	Effective molecular diffusion coefficient in catalyst	[m^2/s]
d_p	Particle diameter	[m]
D_R	Reactor diameter	[m]
E_{att}	Activation energy	[J/mol]
$E_{att,Pe}$	Permeance activation energy	[J/mol]
e_{rel}	Relative error	[-]
F_i	Molar flowrate of component *i*	[mol/s]
$\Delta H^0_{\mathrm{f},298K}$	Standard enthalpy of formation at 298 K and 1 bar	[kJ/mol]
J_i	Molar flux rate of component *i*	[mol/s/m^2]
k_0	Pre-exponential Arrhenius constant for reaction	[mol/s/g$_{CAT}$]
$k_{0,Pe}$	Pre-exponential Arrhenius constant for permeance	[mol/s/m^2/Pa^n]
k_c	Mass transfer coefficient between solid particle and gas	[m/s]
K_{eq}	Reaction equilibrium constant	[Pa^{-1}]
k_{Tam}	Tamaru kinetic constant	[mol/s/ g$_{CAT}$]
K_{Tam}	Adsorption constant in Tamaru reaction	[Pa^{-1}]
L	Reactor length	[m]
MW_i	Molecular weight of component *i*	[g/mol]
n	Power factor for permeation flux	[-]
N_i	Mole flow of component *i*	[mol/s]
P	Total pressure	[Pa]
P_i	Partial pressure of component *i*	[Pa]
P_i^{perm}	Partial pressure of component *i* in permeate	[Pa]
P_i^{ret}	Partial pressure of component *i* in retentate	[Pa]
Q_i	Mass flowrate of component *i*	[l$_N$/min]
r_p	Particle radius	[m]
r_i	Reaction of production/consumption of component *i*	[mol/s/g$_{CAT}$]
R_g	Universal gas constant	[J/mol/K]
R	Reaction rate	[mol/s/g$_{CAT}$]

R^2	Regression coefficient	[-]
S_g	BET surface area of catalyst particle	[m^2/g]
T	Temperature	[K]
u_s	Interstitial velocity	[m/s]
V_i	Molecular diffusion volume of component *i*	[$\dot{A}^3$]
V_{pore}	Pore volume in catalyst particle	[cm^3/g]
X_i^{num}	Numerical conversion of component *i*	[-]
X_i^{exp}	Experimental conversion of component *i*	[-]
Y_i	Molar fraction of component *i*	[-]
W_{cat}	Mass of catalyst	[g]

Greek symbols

β	Kinetic parameter for Temkin's kinetic	[-]
ε_{bed}	Packed bed porosity	[-]
ε_{cat}	Catalyst porosity	[-]
μ	Gas viscosity	[Pa s]
ν_i	Stoichiometry coefficient of component *i*	[-]
$\hat{\rho}$	Mass density	[kg/m^3]
ρ_{cat}	Catalyst skeletal density	[kg/m^3]
${\rho_{cat}}^{app}$	Catalyst bulk density	[kg/m^3]
τ	Tortuosity of catalyst particle	[-]

Abbreviation

$GHSV$	Gas hour shift velocity	[$l_N/h/g_{cat}$]
OPT	Optimization routine	
PBR	Packed bed reactor	
$PBMR$	Packed bed membrane reactor	
SSR	Sum of square residuals	[-]

Bibliography

7440-18-8 - Ruthenium, 2% on 3.18mm (0.125in) alumina pellets - 44575 - Alfa Aesar. (n.d.). Retrieved October 8, 2022, from https://www.alfa.com/it/catalog/044575/

Adhikari, S., & Fernando, S. (2006). Hydrogen Membrane Separation Techniques. *Industrial and Engineering Chemistry Research*, *45*(3), 875–881. https://doi.org/10.1021/IE050644L

Al-Dahhan, M. H., Wu, Y., & Dudukovié, M. P. (1995). Reproducible Technique for Packing Laboratory-Scale Trickle-Bed Reactors with a Mixture of Catalyst and Fines. *Ind. Eng. Chem. Res*, *34*, 741–747. https://pubs.acs.org/sharingguidelines

Ammonia dehydrogenation | ARENHA. (n.d.). Retrieved October 26, 2022, from https://arenha.eu/content/ammonia-dehydrogenation

Antunes, R., Steiner, R., Marot, L., & Meyer, E. (2022). Decomposition studies of NH3 and ND3 in presence of H2 and D2 with Pt/Al2O3 and Ru/Al2O3 catalysts. *International Journal of Hydrogen Energy*, *47*(30), 14130–14140. https://doi.org/10.1016/J.IJHYDENE.2022.02.155

Arratibel, A., Astobieta, U., Pacheco Tanaka, D. A., van Sint Annaland, M., & Gallucci, F. (2016). N2, He and CO2 diffusion mechanism through nanoporous YSZ/γ-Al2O3 layers and their use in a pore-filled membrane for hydrogen membrane reactors. *International Journal of Hydrogen Energy*, *41*(20), 8732–8744. https://doi.org/10.1016/J.IJHYDENE.2015.11.152

Arratibel, A., Pacheco Tanaka, A., Laso, I., van Sint Annaland, M., & Gallucci, F. (2018). Development of Pd-based double-skinned membranes for hydrogen production in fluidized bed membrane reactors. *Journal of Membrane Science*, *550*, 536–544. https://doi.org/10.1016/J.MEMSCI.2017.10.064

Baker, R. W. (Richard W. (2012). *Membrane technology and applications*. John Wiley & Sons.

Barreiro, M. M., Maroño, M., & Sánchez, J. M. (2015). Hydrogen separation studies in a membrane reactor system: Influence of feed gas flow rate, temperature and concentration of the feed gases on hydrogen permeation. *Applied Thermal Engineering*, *74*, 186–193. https://doi.org/10.1016/j.applthermaleng.2013.12.035

BASILE A. (2013). *Inorganic membrane reactors for hydrogen production: an overview with particular emphasis on dense metallic membrane materials*.

Berger, R. J., Pérez-Ramírez, J., Kapteijn, F., & Moulijn, J. A. (2002). Catalyst performance testing: Bed dilution revisited. *Chemical Engineering Science*, *57*(22–23), 4921–4932. https://doi.org/10.1016/S0009-2509(02)00273-7

Bernardo, G., Araújo, T., da Silva Lopes, T., Sousa, J., & Mendes, A. (2020). Recent advances in membrane technologies for hydrogen purification. *International Journal of Hydrogen Energy*, *45*(12), 7313–7338. https://doi.org/10.1016/J.IJHYDENE.2019.06.162

Bird, Warren, & Lightfoot. (2002). *Transport Phenomena*.

Bradford, M. C. J., Fanning, P. E., & Vannice, M. A. (1997). Kinetics of NH3 Decomposition over Well Dispersed Ru. *Journal of Catalysis*, *172*(2), 479–484. https://doi.org/10.1006/JCAT.1997.1877

Byun, M., Lee, A., Cheon, S., Kim, H., & Lim, H. (2022). Preliminary feasibility study for hydrogen storage using several promising liquid organic hydrogen carriers: Technical, economic, and environmental perspectives. *Energy Conversion and Management*, *268*, 116001. https://doi.org/10.1016/J.ENCONMAN.2022.116001

Caravella, A., Barbieri, G., & Drioli, E. (2009). Concentration polarization analysis in self-supported Pd-based membranes. *Separation and Purification Technology*, *66*(3), 613–624. https://doi.org/10.1016/j.seppur.2009.01.008

Cechetto, V., di Felice, L., Gutierrez Martinez, R., Arratibel Plazaola, A., & Gallucci, F. (2022). Ultra-pure hydrogen production via ammonia decomposition in a catalytic membrane reactor. *International Journal of Hydrogen Energy*, *47*(49), 21220–21230. https://doi.org/10.1016/J.IJHYDENE.2022.04.240

Cechetto, V., di Felice, L., Medrano, J. A., Makhloufi, C., Zuniga, J., & Gallucci, F. (2021a). H2 production via ammonia decomposition in a catalytic membrane reactor. *Fuel Processing Technology*, *216*. https://doi.org/10.1016/j.fuproc.2021.106772

Cechetto, V., di Felice, L., Medrano, J. A., Makhloufi, C., Zuniga, J., & Gallucci, F. (2021b). H2 production via ammonia decomposition in a catalytic membrane reactor. *Fuel Processing Technology*, *216*. https://doi.org/10.1016/j.fuproc.2021.106772

Chiuta, S., Everson, R. C., Neomagus, H. W. J. P., & Bessarabov, D. G. (2016). Hydrogen production from ammonia decomposition over a commercial Ru/Al2O3 catalyst in a microchannel reactor: Experimental validation and CFD simulation. *International Journal of Hydrogen Energy*, *41*(6), 3774–3785. https://doi.org/10.1016/J.IJHYDENE.2015.12.130

Chiuta, S., Everson, R. C., Neomagus, H. W. J. P., van der Gryp, P., & Bessarabov, D. G. (2013). Reactor technology options for distributed hydrogen generation via ammonia decomposition: A review. *International Journal of Hydrogen Energy*, *38*(35), 14968–14991. https://doi.org/10.1016/J.IJHYDENE.2013.09.067

Collins, J. P., & Way, J. D. (1994). Catalytic decomposition of ammonia in a membrane reactor. *Journal of Membrane Science*, *96*(3), 259–274. https://doi.org/10.1016/0376-7388(94)00138-3

Column - Varian CP-4900 Micro-GC User Manual [Page 47] | ManualsLib. (n.d.). Retrieved October 7, 2022, from https://www.manualslib.com/manual/1236923/Varian-Cp-4900-Micro-Gc.html?page=47#manual

Dautzenberg, F. M. (1989). *Ten Guidelines for Catalyst Testing* (pp. 99–119). https://doi.org/10.1021/bk-1989-0411.ch011

di Carlo, A., Vecchione, L., & del Prete, Z. (2014). Ammonia decomposition over commercial Ru/Al2O3 catalyst: An experimental evaluation at different operative pressures and temperatures. *International Journal of Hydrogen Energy*, *39*(2), 808–814. https://doi.org/10.1016/J.IJHYDENE.2013.10.110

Fan, L., Tu, Z., & Chan, S. H. (2021). Recent development of hydrogen and fuel cell technologies: A review. *Energy Reports*, *7*, 8421–8446. https://doi.org/10.1016/J.EGYR.2021.08.003

Fang, H., Liu, D., Luo, Y., Zhou, Y., Liang, S., Wang, X., Lin, B., & Jiang, L. (2022). Challenges and Opportunities of Ru-Based Catalysts toward the Synthesis and Utilization of Ammonia. *ACS Catalysis*, *12*(7), 3938–3954. https://doi.org/10.1021/ACSCATAL.2C00090/ASSET/IMAGES/LARGE/CS2C00090_0008.JPEG

Fogler S. (2004). *Elements of Chemical Reaction Engineering* (Third edition).

Gaies, B., Nakhli, M. S., & Sahut, J. M. (2022). What are the effects of economic globalization on CO2 emissions in MENA countries? *Economic Modelling*, *116*, 106022. https://doi.org/10.1016/J.ECONMOD.2022.106022

Gallucci, F., Fernandez, E., Corengia, P., & van Sint Annaland, M. (2013). Recent advances on membranes and membrane reactors for hydrogen production. *Chemical Engineering Science*, *92*, 40–66. https://doi.org/10.1016/J.CES.2013.01.008

Gallucci, F., Medrano, J., Fernandez, E., Melendez, J., van Sint Annaland, M., & Pacheco-Tanaka, D. (2017). Advances on High Temperature Pd-Based Membranes and Membrane

Reactors for Hydrogen Purifcation and Production. *Journal of Membrane Science and Research*, *3*(3), 142–156. https://doi.org/10.22079/JMSR.2017.23644

Gobina, E. N., Oklany, J. S., & Hughes, R. (1995). Elimination of Ammonia from Coal Gasification Streams by Using a Catalytic Membrane Reactor. *Industrial and Engineering Chemistry Research*, *34*(11), 3777–3783. https://doi.org/10.1021/IE00038A014/ASSET/IE00038A014.FP.PNG_V03

Green ammonia | Royal Society. (n.d.). Retrieved October 28, 2022, from https://royalsociety.org/topics-policy/projects/low-carbon-energy-programme/green-ammonia/

Guo, J., & Chen, P. (2017). Catalyst: NH3 as an Energy Carrier. *Chem*, *3*(5), 709–712. https://doi.org/10.1016/J.CHEMPR.2017.10.004

Gutiérrez Martinéz, R. (2022). *An experimental investigation on hydrogen production from ammonia decomposition in packed bed palladium membrane reactor*.

HOME-UN Climate Change Conference (COP26)-Glasgow 2021. (n.d.). Retrieved October 26, 2022, from https://ukcop26.org/

Hughes, R. (2001). Composite palladium membranes for catalytic membrane reactors. *Membrane Technology*, *2001*(131), 9–13. https://doi.org/10.1016/S0958-2118(01)80152-X

ISO - Standards. (n.d.). Retrieved October 28, 2022, from https://www.iso.org/standards.html

Itoh, N., Oshima, A., Suga, E., & Sato, T. (2014). Kinetic enhancement of ammonia decomposition as a chemical hydrogen carrier in palladium membrane reactor. *Catalysis Today*, *236*(PART A), 70–76. https://doi.org/10.1016/J.CATTOD.2014.02.054

Ji, G., Yao, J. G., Clough, P. T., da Costa, J. C. D., Anthony, E. J., Fennell, P. S., Wang, W., & Zhao, M. (2018). Enhanced hydrogen production from thermochemical processes. *Energy & Environmental Science*, *11*(10), 2647–2672. https://doi.org/10.1039/C8EE01393D

Kulkarni, S. R., Velisoju, V. K., Tavares, F., Dikhtiarenko, A., Gascon, J., & Castaño, P. (2022). Silicon carbide in catalysis: from inert bed filler to catalytic support and multifunctional material. *Https://Doi.Org/10.1080/01614940.2022.2025670*. https://doi.org/10.1080/01614940.2022.2025670

Lamb, K. E., Dolan, M. D., & Kennedy, D. F. (2019a). Ammonia for hydrogen storage; A review of catalytic ammonia decomposition and hydrogen separation and purification. *International Journal of Hydrogen Energy*, *44*(7), 3580–3593. https://doi.org/10.1016/J.IJHYDENE.2018.12.024

Lamb, K. E., Dolan, M. D., & Kennedy, D. F. (2019b). Ammonia for hydrogen storage; A review of catalytic ammonia decomposition and hydrogen separation and purification. *International Journal of Hydrogen Energy*, *44*(7), 3580–3593. https://doi.org/10.1016/J.IJHYDENE.2018.12.024

Liguori, S., Iulianelli, A., Dalena, F., Pinacci, P., Drago, F., Broglia, M., Huang, Y., & Basile, A. (2014). Performance and long-term stability of Pd/PSS and Pd/Al2O3 membranes for hydrogen separation. *Membranes*, *4*(1), 143–162. https://doi.org/10.3390/membranes4010143

Lucentini, I., Garcia, X., Vendrell, X., & Llorca, J. (2021). Review of the Decomposition of Ammonia to Generate Hydrogen. *Industrial and Engineering Chemistry Research*, *60*(51), 18560–18611. https://doi.org/10.1021/ACS.IECR.1C00843/ASSET/IMAGES/LARGE/IE1C00843_0007.JPEG

MathWorks. (n.d.). *How GlobalSearch and MultiStart Work - MATLAB & Simulink - MathWorks Italia*. Retrieved October 11, 2022, from https://it.mathworks.com/help/gads/how-globalsearch-and-multistart-work.html

Melendez, J., Fernandez, E., Gallucci, F., van Sint Annaland, M., Arias, P. L., & Pacheco Tanaka, D. A. (2017). Preparation and characterization of ceramic supported ultra-thin (~1 μm) Pd-Ag membranes. *Journal of Membrane Science*, *528*, 12–23. https://doi.org/10.1016/J.MEMSCI.2017.01.011

Pal, N., Agarwal, M., Maheshwari, K., & Solanki, Y. S. (2020). A review on types, fabrication and support material of hydrogen separation membrane. *Materials Today: Proceedings*, *28*, 1386–1391. https://doi.org/10.1016/J.MATPR.2020.04.806

Perego, C., & Peratello, S. (1999). Experimental methods in catalytic kinetics. *Catalysis Today*, *52*(2–3), 133–145. https://doi.org/10.1016/S0920-5861(99)00071-1

Pérez-Ramírez, J., Berger, R. J., Mul, G., Kapteijn, F., & Moulijn, J. A. (2000). The six-flow reactor technology: A review on fast catalyst screening and kinetic studies. *Catalysis Today*, *60*(1–2), 93–109. https://doi.org/10.1016/S0920-5861(00)00321-7

Perry's Chemical Engineers' Handbook. (2008).

Poto, S., Vico van Berkel, D., Gallucci, F., & Fernanda Neira d'Angelo, M. (2022). Kinetic modelling of the methanol synthesis from CO2 and H2 over a CuO/CeO2/ZrO2 catalyst: The role of CO2 and CO hydrogenation. *Chemical Engineering Journal*, *435*. https://doi.org/10.1016/J.CEJ.2022.134946

Prasad, V., Karim, A. M., Arya, A., & Vlachos, D. G. (2009a). Assessment of overall rate expressions and multiscale, microkinetic model uniqueness via experimental data injection: Ammonia decomposition on Ru/γ-Al 2O 3 for hydrogen production. *Industrial and Engineering Chemistry Research*, *48*(11), 5255–5265. https://doi.org/10.1021/IE900144X/ASSET/IMAGES/LARGE/IE-2009-00144X_0007.JPEG

Prasad, V., Karim, A. M., Arya, A., & Vlachos, D. G. (2009b). Assessment of overall rate expressions and multiscale, microkinetic model uniqueness via experimental data injection: Ammonia decomposition on Ru/γ-Al 2O 3 for hydrogen production. *Industrial and Engineering Chemistry Research*, *48*(11), 5255–5265. https://doi.org/10.1021/IE900144X/ASSET/IMAGES/LARGE/IE-2009-00144X_0007.JPEG

Rahman, F., Rehman, S., & Abdul-Majeed, M. A. (2012). Overview of energy storage systems for storing electricity from renewable energy sources in Saudi Arabia. *Renewable and Sustainable Energy Reviews*, *16*(1), 274–283. https://doi.org/10.1016/J.RSER.2011.07.153

Rosen, M. A., & Koohi-Fayegh, S. (2016). The prospects for hydrogen as an energy carrier: an overview of hydrogen energy and hydrogen energy systems. *Energy, Ecology and Environment*, *1*(1), 10–29. https://doi.org/10.1007/S40974-016-0005-Z/FIGURES/5

Satterfield, N. C. (1996). *Heterogeneous Catalysis in Industrial Practice: Vol. Second Edition*.

Schüth, F., Palkovits, R., Schlögl, R., & Su, D. S. (2012). Ammonia as a possible element in an energy infrastructure: catalysts for ammonia decomposition. *Energy & Environmental Science*, *5*(4), 6278–6289. https://doi.org/10.1039/C2EE02865D

Srifa, A., Okura, K., Okanishi, T., Muroyama, H., Matsui, T., & Eguchi, K. (2017). Hydrogen production by ammonia decomposition over Cs-modified Co3Mo3N catalysts. *Applied Catalysis B: Environmental*, *218*, 1–8. https://doi.org/10.1016/J.APCATB.2017.06.034

Sun, S., Jiang, Q., Zhao, D., Cao, T., Sha, H., Zhang, C., Song, H., & Da, Z. (2022). Ammonia as hydrogen carrier: Advances in ammonia decomposition catalysts for promising hydrogen production. *Renewable and Sustainable Energy Reviews*, *169*. https://doi.org/10.1016/J.RSER.2022.112918

Tamaru, K. (1988). A “New” General Mechanism of Ammonia Synthesis and Decomposition on Transition Metals. *Accounts of Chemical Research*, *21*(2), 88–94. https://doi.org/10.1021/AR00146A007/ASSET/AR00146A007.FP.PNG_V03

Tsai, W., Vajo, J. J., & Weinberg, W. H. (1985). Inhibition by hydrogen of the heterogeneous decomposition of ammonia on platinum. *Journal of Physical Chemistry*, *89*(23), 4926–4932. https://doi.org/10.1021/J100269A009/ASSET/J100269A009.FP.PNG_V03

Wang, W., Olguin, G., Hotza, D., Seelro, M. A., Fu, W., Gao, Y., & Ji, G. (2022). Inorganic membranes for in-situ separation of hydrogen and enhancement of hydrogen production from thermochemical reactions. *Renewable and Sustainable Energy Reviews*, *160*, 112124. https://doi.org/10.1016/J.RSER.2022.112124

Yun, S., & Ted Oyama, S. (2011). Correlations in palladium membranes for hydrogen separation: A review. *Journal of Membrane Science*, *375*(1–2), 28–45. https://doi.org/10.1016/J.MEMSCI.2011.03.057

Zançat, S. (2020). *Ammonia decomposition in a packed bed membrane reactor: A computational and experimental study*.

Zhang, J., Xu, H., & Li, W. (2005). Kinetic study of NH3 decomposition over Ni nanoparticles: The role of la promoter, structure sensitivity and compensation effect. *Applied Catalysis A: General*, *296*(2), 257–267. https://doi.org/10.1016/J.APCATA.2005.08.046

Zhang, Z., Liguori, S., Fuerst, T. F., Way, J. D., & Wolden, C. A. (2019). Efficient Ammonia Decomposition in a Catalytic Membrane Reactor to Enable Hydrogen Storage and Utilization. *ACS Sustainable Chemistry and Engineering*, *7*(6), 5975–5985. https://doi.org/10.1021/ACSSUSCHEMENG.8B06065/SUPPL_FILE/SC8B06065_SI_001.PDF

Zheng W., Zhang, J., Hengyong, A. E., Ae, X., & Li, W. (2007). NH 3 Decomposition Kinetics on Supported Ru Clusters: Morphology and Particle Size Effect. *Catalysis Letters*. https://doi.org/10.1007/s10562-007-9237-z

Zheng, W., Zhang, J., Xu, H., & Li, W. (2007). NH3 decomposition kinetics on supported Ru clusters: Morphology and particle size effect. *Catalysis Letters*, *119*(3–4), 311–318. https://doi.org/10.1007/S10562-007-9237-Z/FIGURES/9

Websites

https://www.alfa.com/it/catalog/044575/ (last access 1st November 2022)

https://arenha.eu/content/ammonia-dehydrogenation (last access 3rd December 2022)

https://www.manualslib.com/manual/1236923/Varian-Cp-4900-Micro-Gc.html?page=47#manual (last access 15th October 2022)

https://ukcop26.org/ (last access 26th October 2022)

https://www.iso.org/standards.html (last access 21st April 2022)

https://it.mathworks.com/help/gads/how-globalsearch-and-multistart-work.html (last access 12nd October 2022)

Appendix

Operative condition investigated on the kinetic study and results.

runs	T [°C]	P_{in} [bar]	P_{out} [bar]	Inlet flowrate [l_N/min] He	NH_3	H_2	N_2
1	400	1.45	1.35	0.8	0.2	0	0
2	425	1.42	1.32	0.8	0.2	0	0
3	450	1.41	1.32	0.8	0.2	0	0
4	475	1.44	1.32	0.8	0.2	0	0
5	500	1.47	1.33	0.8	0.2	0	0
6	400	3.05	3	0.8	0.2	0	0
7	425	3.07	3	0.8	0.2	0	0
8	450	3.05	3	0.8	0.2	0	0
9	475	3.06	3	0.8	0.2	0	0
10	500	3.1	3	0.8	0.2	0	0
11	400	4.57	4.5	0.8	0.2	0	0
12	425	4.55	4.5	0.8	0.2	0	0
13	450	4.57	4.5	0.8	0.2	0	0
14	475	4.56	4.5	0.8	0.2	0	0
15	500	4.56	4.5	0.8	0.2	0	0
16	400	1.3	1.22	0.6	0.15	0	0
17	400	1.52	1.41	1	0.25	0	0
18	450	3.07	3	0.6	0.15	0	0
19	450	3.07	3	1	0.25	0	0
20	500	4.83	4.5	0.6	0.15	0	0
21	500	4.57	4.5	1	0.25	0	0
22	400	1.42	1.3	0.9	0.1	0	0
23	400	1.38	1.28	0.6	0.4	0	0
24	450	3.06	3	0.6	0.4	0	0
25	450	3.03	3	0.9	0.1	0	0
26	500	4.58	4.5	0.9	0.1	0	0
27	500	4.55	4.5	0.6	0.4	0	0
28	400	1.4	1.3	0.7	0.2	0.1	0
29	400	1.37	1.28	0.6	0.2	0.2	0
30	450	3.01	3	0.7	0.2	0.1	0
31	450	3.02	3	0.6	0.2	0.2	0
32	500	4.55	4.5	0.7	0.2	0.1	0
33	500	4.54	4.5	0.6	0.2	0.2	0
34	400	1.45	1.35	0.7	0.2	0	0.1
35	400	1.47	1.38	0.6	0.2	0	0.2
36	450	3.06	3	0.7	0.2	0	0.1
37	450	3.05	3	0.7	0.2	0	0.2
38	500	4.55	4.5	0.7	0.2	0	0.1
39	500	4.55	4.5	0.7	0.2	0	0.2

Molar composition in the outlet stream			
He	NH3	H2	N2
0.7987	0.1679	0.0190	0.0028
0.7849	0.1605	0.0329	0.0058
0.7735	0.1476	0.0516	0.0102
0.7588	0.1300	0.0744	0.0152
0.7414	0.1114	0.1020	0.0214
0.7921	0.1696	0.0186	0.0028
0.7875	0.1638	0.0292	0.0050
0.7771	0.1524	0.0456	0.0087
0.7651	0.1368	0.0674	0.0136
0.7470	0.1178	0.0933	0.0195
0.8000	0.1717	0.0155	0.0019
0.7881	0.1656	0.0273	0.0046
0.7800	0.1545	0.0431	0.0081
0.7721	0.1400	0.0628	0.0125
0.7509	0.1223	0.0874	0.0181
0.7954	0.1654	0.0232	0.0036
0.7965	0.1732	0.0160	0.0020
0.7736	0.1453	0.0536	0.0105
0.7802	0.1578	0.0401	0.0074
0.7428	0.1110	0.1006	0.0212
0.7561	0.1301	0.0778	0.0160
0.8808	0.0817	0.0153	0.0018
0.6019	0.3715	0.0227	0.0035
0.5790	0.3440	0.0560	0.0111
0.8659	0.0688	0.0369	0.0068
0.7722	0.0479	0.0692	0.0141
0.5540	0.2972	0.1085	0.0227
0.7097	0.1882	0.1084	-0.0010
0.6074	0.1973	0.2153	-0.0017
0.7027	0.1794	0.1207	0.0019
0.6024	0.1928	0.2219	0.0002
0.6780	0.1527	0.1557	0.0103
0.5917	0.1725	0.2435	0.0063
0.6618	0.1665	0.0193	0.1154
0.5379	0.1650	0.0189	0.2191
0.6465	0.1478	0.0459	0.1235
0.5237	0.1460	0.0456	0.2254
0.6244	0.1214	0.0838	0.0806
0.5043	0.1210	0.0836	0.1412